# Structural basis of haptoglobin-haemoglobin scavenging by CD163

Xu Zhou

Magdalen College

Department of Biochemistry

University of Oxford

This dissertation is submitted for the degree of

*Doctor of Philosophy*

October 2024

Supervisor: Professor Matthew Higgins

# Abstract

Haemoglobin (Hb) is essential for oxygen transport in vertebrates. However, when it is released from red blood cells, its haem group becomes reactive and must be tightly regulated to prevent its toxicity. Haptoglobin (Hp) acts as the first line of defence by scavenging Hb in the serum. Humans produce three major Hp phenotypes, the dimeric Hp 1-1 as well as the multimeric Hp 2-1 and 2-2. After complexing with Hb, the scavenger receptor CD163 of macrophages mediates the endocytosis of the haptoglobin-haemoglobin complex (HpHb), resulting in its detoxification. Here, I present the structural basis of HpHb scavenging by CD163. Cryogenic electron microscopy reveals that CD163 forms dimers and trimers, with the protomers collectively binding to a single 'head' of HpHb in an asymmetric fashion. The receptor primarily interacts with Hb but also contacts Hp. Uptake experiments demonstrate that this allows CD163 to mediate preferential uptake of HpHb, while Hb is internalised at a lower rate. Spheres of atomic density are present at both the ligand binding and multimerisation interfaces, and these are attributed to calcium. Indeed, biophysical assays show that calcium ions are critical for ligand binding. Mutational studies demonstrate that while monomeric CD163 can scavenge the multimeric Hp(2-2)Hb, uptake of the dimeric Hp(1-1)Hb and Hb is impaired compared to the wild-type receptor, suggesting that receptor multimerisation evolved to facilitate uptake of lower affinity ligands. I also present the cryo-electron microscopy structure of unliganded CD163. In the dimeric form, CD163 exhibits an 'arm-to-arm' contact, suggesting a potential regulatory mechanism. These results provide novel insights into the molecular mechanisms governing HpHb scavenging, shedding light on how CD163 selects its ligand and highlighting the important roles of calcium and multimerisation.

# Acknowledgements

I would like to thank the entire Higgins lab, my friends and family who supported me for the duration of the DPhil.

I am particularly grateful to Matt. We make a fantastic duo. We had countless fruitful discussions about the project, culminating in the work presented here. Without a collaborator, we made significant intellectual contributions to this extensive project, which led to the understanding of this important receptor. But Matt was not just invested in my success as a doctoral candidate; he always offered his advice about career and life, which I deeply appreciate. I hope to find a postdoctoral mentor as exceptional as he is.

I would like to highlight Hannah's organisation skills as our lab manager, which made it possible for me to perform experiments whenever I wanted to. I would like to express my gratitude to Sean Burnap and David Staunton, who performed mass photometry and SEC-MALLS, respectively. Furthermore, I would like to extend my gratitude to Vasiliki and Bobby for introducing me to FACS and for discussing how to perform the uptake experiments with me. I thank Ian for providing the Flp-In 293 system. I appreciate the experimental advice from Nawsad, Abhishek, Alex, Sam and Brendan, particularly when I was inexperienced in the lab. Teaching Dara was a privilege; she demonstrated the potential of the next generation of scientists. Poy and Kuang-Ting became cherished friends throughout the years, who kindly introduced me into their cultures. I am deeply thankful to Brian who worked long hours with me and was my gym buddy after work.

I am grateful to the friends I have made throughout my time in Oxford, and I look forward to meeting you again in your new paths. I would especially like to thank my close friend, Tom, who not only gave extensive advice about the uptake experiment but is also a brother to me and reminds me of why we conduct biomedical research. We want to help the people.

Lastly, Mum and Dad, thank you for everything; I would not be here without you.

## Table of contents

**Abstract** ..... **II**

**Acknowledgements** ..... **III**

**List of tables** ..... **X**

**List of figures** ..... **XI**

**List of abbreviations** ..... **XV**

**1. Introduction** ..... **1**

1.1 Mechanisms of ligand uptake into mammalian cells ..... 1

1.1.1 Overview of different types of endocytosis ..... 2

1.1.2 Non-selective endocytosis ..... 2

1.1.2.1 Phagocytosis ..... 2

1.1.2.2 Macropinocytosis ..... 3

1.1.2.3 Caveolae ..... 4

1.1.3 Selective endocytosis ..... 4

1.2 Molecular mechanisms of clathrin-mediated endocytosis ..... 4

1.3 Scavenger receptors ..... 8

1.3.1 Diversity and classes of scavenger receptors ..... 8

1.3.2 Class I scavenger receptors ..... 10

1.4 CD163 in physiology ..... 11

1.4.1 The CD163-haptoglobin pathway of haemoglobin detoxification ..... 12

1.4.2 Other haem detoxification pathways ..... 13

1.4.3 Structure of haemoglobin ..... 13

1.4.4 Structure and oligomerisation states of haptoglobin ..... 15

1.4.5 Predicted model of CD163 on its own and its binding mode with haptoglobin-haemoglobin ..... 17

1.5 Other functions of CD163 ..... 19

1.5.1 CD163 and bacterial infections ..... 19

1.5.2 CD163 as the intracellular receptor of Arteriviruses ..... 20

1.5.2.1 Uptake of porcine reproductive and respiratory syndrome virus ..... 20

1.5.2.2 Spillover potential of simian haemorrhagic fever virus and role of CD163 ..... 21

1.5.3 Interaction with tumour necrosis factor-related weak inducer of apoptosis. 22

1.6 Aims of this project ..... 22

**2. Material and methods ..... 24**

2.1 Molecular cloning by Gibson assembly ..... 24

2.1.1. Synthetic genes ..... 24

2.1.2 Constructs used for expression of CD163 in mammalian cells ..... 24

2.1.3 Primer design and polymerase chain reaction (PCR) ..... 25

2.1.4 Agarose gel electrophoresis, gel extraction and Gibson assembly ..... 25

2.1.5 Transformation of *E. coli* DH5α and MAX Efficiency Stbl2 ..... 26

2.1.6 DNA purification using Miniprep and Maxiprep Kits ..... 26

2.2 Protein expression and purification ..... 27

2.2.1 Transfection of Expi293F cells with various constructs of CD163 and HpSP 27

2.2.2 Protein purification using the C-tag column ..... 28

2.2.3 Gel filtration of purified proteins ..... 28
2.2.4 Assembly and purification of Hp(1-1)Hb and CD163-HpHb complexes ..... 29
2.2.5 SDS-PAGE ..... 29
2.2.6 Fluorescent labelling of proteins ..... 30
2.3 Biophysical analysis ..... 31
2.3.1 Surface plasmon resonance (SPR) ..... 31
2.3.2 Microscale thermophoresis (MST) ..... 33
2.3.3 Mass photometry (MP) ..... 35
2.3.4 Size exclusion chromatography coupled with multi angle laser light scattering (SEC-MALLS) ..... 36
2.4 Cryogenic electron microscopy ..... 37
2.4.1 Sample preparation, grid freezing and data collection ..... 38
2.4.2 Data processing ..... 40
2.4.2.1 Pre-processing ..... 40
2.4.2.2 2D classification ..... 41
2.4.2.3 3D reconstruction and refinement ..... 42
2.4.3 Model building and refinement ..... 43
2.5 Uptake assays ..... 44
2.5.1 Design of CD163-GFP fusion in vector providing hygromycin-resistance ..... 44
2.5.2 Generation of stable HEK293TRex cells expressing CD163 and its mutants. 45
2.5.3 Direct uptake of fluorescently labelled Hp(1-1)Hb and Hp(2-2)Hb ..... 47
2.5.4 Uptake of fluorescently labelled Hp(2-2)Hb in the presence of competitors 48
2.5.5 Quantification of uptake ..... 48

**3. Structures of dimeric and trimeric CD163 in complex with haptoglobin-haemoglobin ..... 49**

3.1 Summary ..... 49

3.2 Purification of haptoglobin-haemoglobin ..... 50

3.2.1 Purification of haemoglobin from lysed erythrocytes ..... 50

3.2.2 Production of the serine protease domain of haptoglobin and formation of its complex with haemoglobin ..... 51

3.2.3 Formation of a haptoglobin phenotype 1-1 complex with haemoglobin ..... 53

3.3 Purification of a CD163-haptoglobin-haemoglobin complex ..... 53

3.3.1 Design of the CD163 expression constructs ..... 53

3.3.2 Expression and purification of CD163 ..... 55

3.3.3 Formation of a complex of CD163 and Hp(1-1)Hb ..... 56

3.3.4 Formation of a complex of CD163 and HpSPHb ..... 58

3.4 Structural characterisation of CD163-Hp(1-1)Hb using cryo-EM ..... 60

3.4.1 An initial low-resolution reconstruction of CD163-Hp(1-1)Hb ..... 60

3.4.2 Structural analysis of CD163-HpSPHb via cryo-EM ..... 64

3.4.3 High-resolution structures of CD163-Hp(1-1)Hb ..... 67

3.5 Discussion ..... 75

**4. Molecular mechanisms of haptoglobin-haemoglobin scavenging by CD163 ..... 77**

4.1 Summary ..... 77

4.2 The binding of CD163 to a single ‘head’ of HpHb ..... 78

4.2.1 Formation of a Hp(2-2)Hb complex ..... 78

4.2.2 Characterisation of ligand specificity using surface plasmon resonance spectroscopy ..... 80
4.2.3 Assessment of the binding of Hb and Hp to CD163 by microscale thermophoresis ..... 83
4.2.4 Analysis of CD163-Hp(1-1)Hb and CD163-HpSPHb complexes using mass photometry ..... 84
4.2.5 Comparison of uptake efficiencies for various HpHb ligands ..... 86
4.3 Calcium-mediated multimerisation ..... 89
4.3.1 Calcium ions at the inter-protomeric interface ..... 89
4.3.2 The effect of calcium on the multimerisation of CD163 ..... 90
4.3.3 Design of a CD163 'monomer mutant' and its binding and uptake of HpHb . 94
4.3.4 The importance of multimerisation for the uptake of Hb and Hp(1-1)Hb ..... 98
4.4 Calcium-mediated ligand binding ..... 99
4.5 Discussion ..... 102
**5. Discovery and characterisation of an 'arm-to-arm' contact in unliganded CD163 ..... 104**
5.1 Summary ..... 104
5.2 Cryo-EM structures of unliganded CD163 ..... 104
5.3 Comparison of the ligand binding and inter-protomeric interfaces in the 'arms' of CD163 ..... 112
5.4 Mutations in the 'arms' of CD163 and their effects on ligand binding and uptake ..... 115

5.5 Discussion ..... 119

**6. Conclusions and future directions ..... 122**

6.1 Mechanisms of ligand selectivity ..... 122

6.2 Coordination of ligand binding and release with environment conditions ..... 123

6.3 Future directions ..... 125

**References ..... 127**

**Appendix: Constructs and primers ..... 144**

# List of tables

Table 1: Setup of MST experiments.. ..... 35

Table 2: Proteins used for MP, their concentrations and the buffers they were suspended in. ..... 36

Table 3: Cryo-EM data collection, refinement and validation statistics for dimeric and trimeric CD163-Hp(1-1)Hb. ..... 74

Table 4: SPR-derived dissociation constants ($K_D$) for the interactions between wild-type CD163 and Hp(1-1)Hb or HpSPHb.. ..... 82

Table 5: Summary of SEC-MALLS results for CD163 alone. ..... 92

Table 6: Summary of SEC-MALLS data for CD163 with Hp(1-1)Hb. ..... 94

Table 7: Cryo-EM data collection, refinement and validation statistics for unliganded dimeric CD163 as well as data collection statistics for unliganded trimeric CD163... 111

Table 8: Summary of all interface residues in the 'arms' of unliganded CD163 dimer, liganded CD163 dimer and trimer, as determined by PDBePISA. ..... 112

Table 9: All expression constructs used in this dissertation and the primers used to clone them. ..... 144

# List of figures

Figure 1: Overview of different phases in clathrin-mediated endocytosis and the proteins involved. ..... 5

Figure 2: Crystal structure of µ2-subunit of adaptor protein AP2 bound to the endocytosis signal peptide of trans-Golgi network integral membrane protein TGN38 (Owen & Evans, 1998, PDB: 1BXX).. ..... 6

Figure 3: Schematic overview of selected classes of scavenger receptors introduced in this thesis. ..... 9

Figure 4: Ribbon diagram of mouse macrophage receptor with collagenous structure (MARCO) SRCR domain (PDB: 2OY3, Ojala et al., 2007).. ..... 11

Figure 5: Crystal structure of human, oxygenated Hb (Shaanan, 1983).. ..... 14

Figure 6: Structure of porcine HpHb. ..... 16

Figure 7: Schematic illustration depicting abundant haptoglobin complexes detected within different human phenotypes. ..... 17

Figure 8: AlphaFold2 prediction of human CD163 (Uniprot Q86VB7). ..... 18

Figure 9: Predictions of a CD163-HpHb complex as seen in Andersen et al., 2012. ..... 19

Figure 10: Schematic illustrating SPR.. ..... 32

Figure 11: Purification of haemoglobin..... 50

Figure 12: Purification of HpSPHb..... 52

Figure 13: Formation of Hp(1-1)Hb..... 53

Figure 14: DeepTMHMM prediction (Hallgren et al., 2022) of transmembrane topology for human CD163.. ..... 54

Figure 15: Purification of CD163 by SEC.. ..... 56

Figure 16: Complex formation of CD163-Hp(1-1)Hb. ..... 57

Figure 17: Formation of CD163-HpSPHb. ..... 59

Figure 18: Micrographs of grids prepared before and after optimisation of blotting time and concentration.. ..... 61

Figure 19: Cryo-EM analysis of CD163-Hp(1-1)Hb.. ..... 62

Figure 20: Preliminary map and model of the CD163-Hp(1-1)Hb complex. ..... 64

Figure 21: Cryo-EM analysis of CD163-HpSPHb. ..... 66

Figure 22: Low-resolution map of CD163-HpSPHb (green) superimposed onto the map of CD163-Hp(1-1)Hb (grey)..... 67

Figure 23: Data processing pipeline for CD163-Hp(1-1)Hb imaged on Titan Krios.. ..... 69

Figure 24: Statistics of the trimeric and dimeric CD163-Hp(1-1)Hb maps..... 70

Figure 25: Structure of trimeric CD163 bound to Hp(1-1)Hb. ..... 71

Figure 26: Structure of the CD163 dimer bound to Hp(1-1)Hb..... 73

Figure 27: Formation of Hp(2-2)Hb.. ..... 79

Figure 28: Purification of Avi-tagged CD163.. ..... 80

Figure 29: SPR analysis of interactions between wild-type CD163 and various ligands.. ..... 81

Figure 30: MST responses showing the binding of CD163 to Hb (●) and Hp (▲).. ..... 83

Figure 31: MP spectra for unliganded CD163 (A), Hp(1-1)Hb (B), HpSPHb (C), CD163-Hp(1-1)Hb (D) and CD163-HpSPHb (E).. ..... 85

Figure 32: FACS sorting of cells transfected with CD163-GFP and selected in hygromycin.. ..... 87

Figure 33: Uptake of Hp(1-1)Hb and Hp(2-2)Hb by CD163+ cells and untransfected cells (negative control).. ..... 88

Figure 34: Uptake of fluorescently labelled Hp(2-2)Hb in the presence of various competitors. ..... 89

Figure 35: Close-up view of the inter-protomeric 'base' between chains B and C of trimeric CD163-Hp(1-1)Hb..... 90

Figure 36: MP spectra for CD163 alone and CD163 with Hp(1-1)Hb in the presence of either 2.5 mM $CaCl_2$ or 5 mM EDTA. ..... 91

Figure 37: SEC-MALLS traces for unliganded CD163..... 92

Figure 38: SEC-MALLS analysis of CD163 in the presence of Hp(1-1)Hb. ..... 93

Figure 39: Generation of CD163 'monomer mutant'.. ..... 95

Figure 40: Binding and uptake results for CD163-R809T.. ..... 97

Figure 41: MST curves for the interactions between CD163-WT or CD163-R809T and Hb.. ..... 98

Figure 42: Uptake of fluorescent Hp(2-2)Hb in the presence of competitors by cell expressing CD163-R809T.. ..... 99

Figure 43: Close-up view of the interface between Hp(1-1)Hb and the A-chain of CD163, as observed in the structure of dimeric CD163-Hp(1-1)Hb. ..... 100

Figure 44: SPR sensorgrams to assess interactions between Hp(1-1)Hb and CD163-WT or CD163-R809T in calcium-free or low pH buffers.. ..... 101

Figure 45: Schematic illustration depicting differences between the scavenging capabilities of CD163-WT and CD163-R809T.. ..... 102

Figure 46: Data processing workflow for unliganded CD163. ..... 106

Figure 47: Statistics and map of the unliganded CD163 trimer. ..... 107

Figure 48: Statistics, volume and model of the unliganded CD163 dimer.. ..... 109

Figure 49: Close-up view of the N-terminal SRCR domains within the ‘arms’ showing selected hydrogen bonds (A), salt bridges (B) and hydrophobic interactions (C) mediating the inter-protomeric interaction. ..... 110

Figure 50: Surface diagram of CD163 in the unliganded CD163 dimer, as well as liganded CD163 dimer and trimer. ..... 114

Figure 51: Close-up view of N284 in the unliganded CD163 dimer (A) and the liganded CD163 trimer (B). ..... 116

Figure 52: Purification and SPR analyses of CD163-G351W (A) and -QGE284-286NGT (B).. ..... 117

Figure 53: Evaluation of the Hb binding affinity of CD163-QGE284-286NGT using MST. ..... 118

Figure 54: Uptake of fluorescent Hp(2-2)Hb by stable HEK293 cells expressing CD163-WT and -QGE284-286NGT as well as untransfected cells. ..... 119

Figure 55: Schematic illustration conceptually depicting complexes between CD163 and various ligands, including Hp(1-1)Hb, Hp(2-2)Hb, Hb and unconjugated HpSP.... 123

# List of abbreviations

| | |
|---|---|
| AP2 | Assembly polypeptide 2 |
| BAR | Bin-Amphiphysin-Rvs |
| BSA | Bovine serum albumin |
| CCP | Complement control protein |
| CME | Clathrin-mediated endocytosis |
| CR | Complement-type repeat |
| Cryo-EM | Cryogenic electron microscopy |
| Cryo-ET | Cryogenic electron tomography |
| CTF | Contrast transfer function |
| CV | Column volume |
| CXCL16 | C-X-C motif chemokine ligand 16 |
| CXCR6 | C-X-C motif receptor 6 |
| DAMPs | Danger-associated molecular patterns |
| DQE | Detective quantum efficiency |
| EDTA | Ethylenediaminetetraacetic acid |
| EM | Electron micrscopy |
| FBS | Fetal bovine serum |
| FCHo | Fer/Cip4 homology domain-only |
| FRT | Flippase-recognition target |
| FSC | Fourier Shell Correlation |
| GP | Glycoprotein |
| Hb | Haemoglobin |
| HBS | HEPES-buffered saline |
| HSC70 | Heat shock cognate 70 |
| Hp | Haptoglobin |
| HpHb | Haptoglobin-haemoglobin |
| Hpx | Haemopexin |
| IEX | Ion-exchange chromatography |
| IL6 | Interleukin-6 |

| | |
|---|---|
| IMAC | Immobilised metal-ion affinity chromatography |
| LDV | Lactate dehydrogenase-elevating virus |
| LPS | Lipopolysaccharide |
| MARCO | Mouse macrophage receptor with collagenous structure |
| MBS | MES-buffered saline |
| MST | Microscale thermophoresis |
| MP | Mass photometry |
| NMR | Nuclear magnetic resonance |
| PCR | Polymerase chain reaction |
| PISA | Protein Interfaces, Surfaces and Assemblies |
| PRRS | Porcine reproductive and respiratory syndrome |
| PRRSV | Porcine reproductive and respiratory syndrome virus |
| RAP | Receptor-associated protein |
| RBCs | Red blood cells |
| ROS | Reactive oxygen species |
| SAXS | Small-angle X-ray scattering |
| SEC | Size-exclusion chromatography |
| SEC-MALLS | Size exclusion chromatography coupled with multi angle laser light scattering |
| SHFV | Simian haemorrhagic fever virus |
| SPR | Surface plasmon resonance |
| SRCR | Scavenger receptor cysteine-rich |
| SR-PSOX | Scavenger receptor that binds phosphatidylserine and oxidised lipids |
| SP | Serine protease |
| SPA | Single particle analysis |
| TAE | Tris-Acetate-EDTA |
| TbHpHbR | *Trypanosoma brucei* haptoglobin-haemoglobin receptor |
| TWEAK | Tumour necrosis factor-related weak inducer of apoptosis |
| WASP | Wiskott-Aldrich syndrome protein |

# 1. Introduction

## 1.1 Mechanisms of ligand uptake into mammalian cells

Compartmentalisation is crucial for the survival of living organisms and cells. Mammalian cells achieve compartmentalisation using lipid bilayers composed of amphipathic phospholipids. Embedded within the bilayer are, among other molecules, sterols and integral membrane proteins while peripheral proteins and saccharides are attached the membrane. To enable exchange with their surroundings, membranes are selectively permeable: they enable the uptake of desired nutrients and agents but leave out unwanted particles.

Small, hydrophobic molecules can generally pass the membrane via diffusion because of the predominantly hydrophobic nature of the lipid bilayer. While water can diffuse across the membrane at a slower rate, large hydrophilic molecules and larger particles in general are unable to enter the cell via diffusion. They require more specialised mechanisms for cell entry. These mechanisms can be categorised into two groups.

The first group includes mechanisms that allow the molecules to directly enter the cytoplasm from the extracellular space through membrane proteins. These include the use of active and passive transport systems. Active transporters include ion pumps and cotransporters that transfer molecules across the membrane against the concentration gradient. Ion pumps rely on energy derived from ATP hydrolysis, while cotransporters utilise an electrochemical potential difference. Passive transport systems include ion channels and small molecule transporters that move molecules along the concentration gradient without requiring energy input.

The second group involves the uptake of particles through vesicular routes, including through endocytosis. This is a process that is essential for internalising larger molecules that cannot pass through the membrane. This pathway is particularly relevant to the

protein central to this dissertation and will be examined in greater detail in the following sections.

### 1.1.1 Overview of different types of endocytosis

During endocytosis, a portion of the plasma membrane engulfs extracellular particles and fluid as it forms a trafficking vesicle. As a result, the engulfed material is internalised. Endocytosis plays a critical role in many physiological processes including nutrient uptake, cell signalling, detoxification and regulation of cell membrane composition. In addition, endocytic routes can be hijacked by pathogens to enter the cell.

There are different mechanisms underlying endocytosis, characterised by morphology, molecule to be transported and the intracellular proteins involved in coat vesicle formation (Doherty & McMahon, 2009). For the purposes of this dissertation, the mechanisms are divided into two groups: selective endocytic pathways and non-selective pathways. It should be noted that this distinction is primarily a concept. Further research might reveal that the underlying mechanisms could belong to both categories. Intracellular proteins enabling endocytosis might be found to be used by both groups.

### 1.1.2 Non-selective endocytosis

Non-selective endocytosis is a mechanism that is independent of an interaction resulting in increased internalisation of a specific cargo or receptor. This type of endocytosis can facilitate the uptake of a wide range of cargo. Mechanisms include phagocytosis, macropinocytosis and caveolae-mediated endocytosis.

#### 1.1.2.1 Phagocytosis

Phagocytosis is defined as uptake of particles larger than 0.5 μm (Rabinovitch, 1995). It is triggered by a variety of cargo on the surface of the phagocyte, and the morphology of the membrane-bound structure formed is therefore cargo-shaped (Doherty & McMahon, 2009). Literature distinguishes between professional and non-professional phagocytes. Professional phagocytes include primarily innate immune cells, such monocytes, macrophages, dendritic cells and granulocytes that engulf pathogens, apoptotic cells

and cell debris (Gordon, 2016). When taking up pathogens, professional phagocytes use acidification, enzymes and, in the case of granulocytes, toxic substances to neutralise the pathogen. Innate immune cells release pro-inflammatory cytokines to respond to the infection while dendritic cells present fragments from the pathogen for recognition by adaptive immune cells. The function of professional phagocytes is not only limited to pathogen clearance. Osteoclasts, cells originating from monocytes/macrophages, contribute to tissue remodelling by resorbing bone (Teitelbaum, 2000). Furthermore, professional phagocytes take up apoptotic cells preventing the release of inflammatory molecules from inside the cells (Nagata, 2018).

Non-professional phagocytes do not specialise in phagocytosis but can take up larger particles. Examples include endothelial cells that remove particulates from circulation, maintaining blood homeostasis, and Sertoli cells that take up aberrant sperm cells.

#### 1.1.2.2 Macropinocytosis

Like phagocytosis, macropinocytosis is also a mechanism leading to the internalisation of larger particles (> 0.2 μm). Unlike phagocytosis, however, macropinocytosis is not triggered by receptor interactions in the extracellular space but by activation of receptor tyrosine kinases (Kay, 2021). This causes actin polymerisation at the cell membrane, which in turn leads to ruffled membrane extensions engulfing extracellular fluid and the formation of a macropinosome (Kerr & Teasdale, 2009).

Cancer cells, including cultured cancer cells, perform macropinocytosis to take up nutrients from the surroundings (Lewis, 1937). Macropinocytosis allows them to gain a selective advantage by obtaining an additional source of amino acids. Non-cancerous cells, particularly macrophages and immature dendritic cells, also perform macropinocytosis (Kay, 2021). The function of macropinocytosis in this case is to display antigens on MHC class I and II molecules and present them to CD8+ and CD4+ T cells, respectively. While macropinocytosis acts to protect the host from pathogens, it can also be abused by the latter. Large viruses, such as vaccinia and Ebola, primarily rely on macropinocytosis for cell entry (Helenius, 2018). They mimic an apoptotic cell by

exposing a phosphatidylserine on their viral envelopes activating receptor tyrosine kinases and triggering macropinocytosis.

#### 1.1.2.3 Caveolae

Caveolae enable another non-selective endocytic mechanism. Caveolae are small invaginations that are found on most mammalian cells (Doherty & McMahon, 2009). They are caused by the expression of caveolin1, which multimerises into a disk and inserts into the plasma membrane. Structural studies suggested that caveolin1 does not induce a continuous curvature on the membrane but the disks it forms stabilise a side of a polyhedral caveolae (Porta et al., 2022).

How caveolae lead to endocytosis is not fully understood because cargo designated for caveolae-mediated endocytosis can be taken up through different routes. From a functional perspective, caveolae are thought to be involved in regulating lipid composition because of the ability of caveolin1 to interact with lipids and cholesterol. In addition, caveolae are proposed to facilitate transcytosis across the vascular barrier.

### 1.1.3 Selective endocytosis

Mechanisms of selective endocytosis rely on a defined interaction between a protein mediating endocytosis by inducing or forming a vesicle coat and a receptor, resulting in its increased uptake. Clathrin-mediated endocytosis (CME) is among the most common pathways of endocytosis and the best-studied route of selective endocytosis. CME is crucial for the function of the receptor at the centre of this dissertation. Therefore, its molecular mechanisms will be presented in detail in the following section.

## 1.2 Molecular mechanisms of clathrin-mediated endocytosis

CME is a universal mechanism shared by all eukaryotic cells and is defined by uptake of particulates from the extracellular space into clathrin-coated vesicles (McMahon & Boucrot, 2011). Functions of CME are diverse and include neurotransmission, signal transduction as well as receptor and receptor-complex internalisation. CME is

particularly relevant for direct receptor uptake, for example of epidermal growth factor receptor (Huang et al., 2004). Moreover, it is crucial for receptor-mediated uptake of physiological substrates, like lipids (by low-density lipoprotein receptor, Anderson et al., 1977) and iron (by transferrin receptor, Motley et al., 2003). The individual stages of the formation of a clathrin-coated vesicle, which are nucleation, receptor selection, coat assembly, vesicle scission and uncoating, are schematically displayed in Figure 1 and are described below.

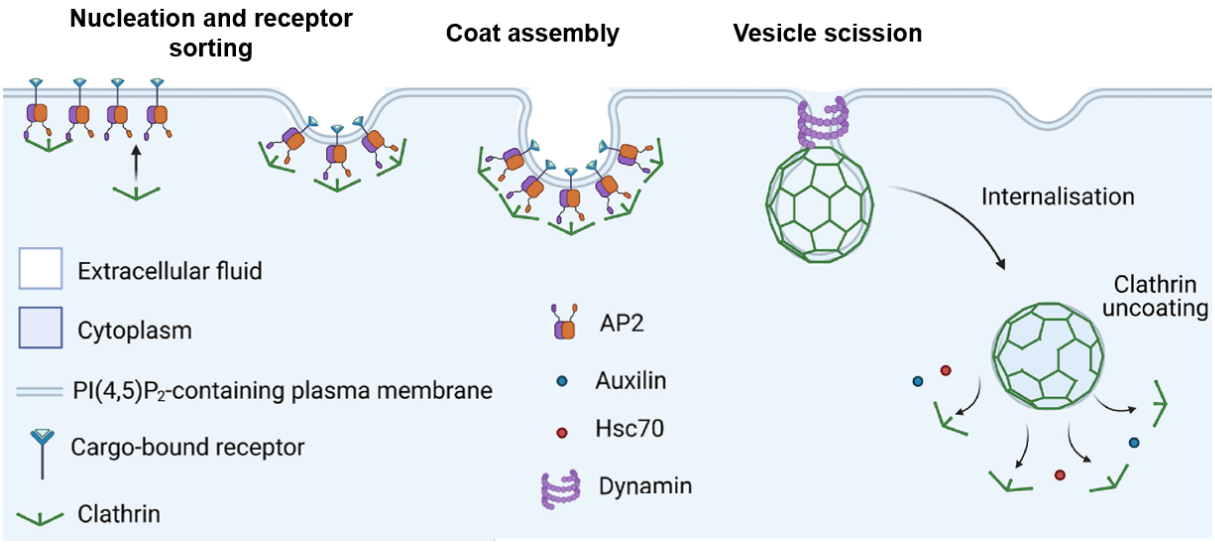


Figure 1: Overview of different phases in clathrin-mediated endocytosis and the proteins involved. The figure is adapted from S. M. Smith & Smith, 2022.

Nucleation creates an initial invagination at the plasma membrane. The mechanism has not been fully elucidated. Furthermore, the exact role of the receptor to be internalised in promoting nucleation is not exactly understood. Proving a causal relationship between receptor and nucleation is difficult because many receptors and receptor-complexes can be endocytosed in one vesicle (Kaksonen & Roux, 2018). However, endocytosis can be concentrated at a specific active region of the plasma membrane hinting at the possibility that certain membrane areas can promote nucleation.

It has been established that the membrane sculpting Fer/Cip4 homology domain-only proteins 1 and 2 (FCHo 1, -2) are part of a complex, called nucleation module, initially recruited to the plasma membrane to induce curvature (Henne et al., 2010). The adaptor protein called assembly polypeptide 2 (AP2) is thought to also be part of the complex but

this has been disputed (McMahon & Boucrot, 2011). Scaffolding proteins assemble at the nucleation module, enabling the formation of a coat at a later stage of CME.

Selective endocytosis in CME is enabled by interactions between cytosolic domains of receptors and adaptor proteins including members of the nucleation module. These interactions concentrate receptors at the endocytosis site and lead to them being selectively load into the forming vesicle. AP2 is a protein essential to receptor selection and is a hetero-tetramer composed of an α-, a β2-, a μ2- and a σ2-subunit (Traub, 2009).

The μ2-subunit of AP2 has two dedicated pockets to accommodate the tyrosine and the hydrophobic residue φ of the endocytosis signal YXXφ (Owen & Evans, 1998). This sequence is also part of the protein at the centre of this dissertation, and the complex structure of the motif with AP2 is shown in Figure 2.

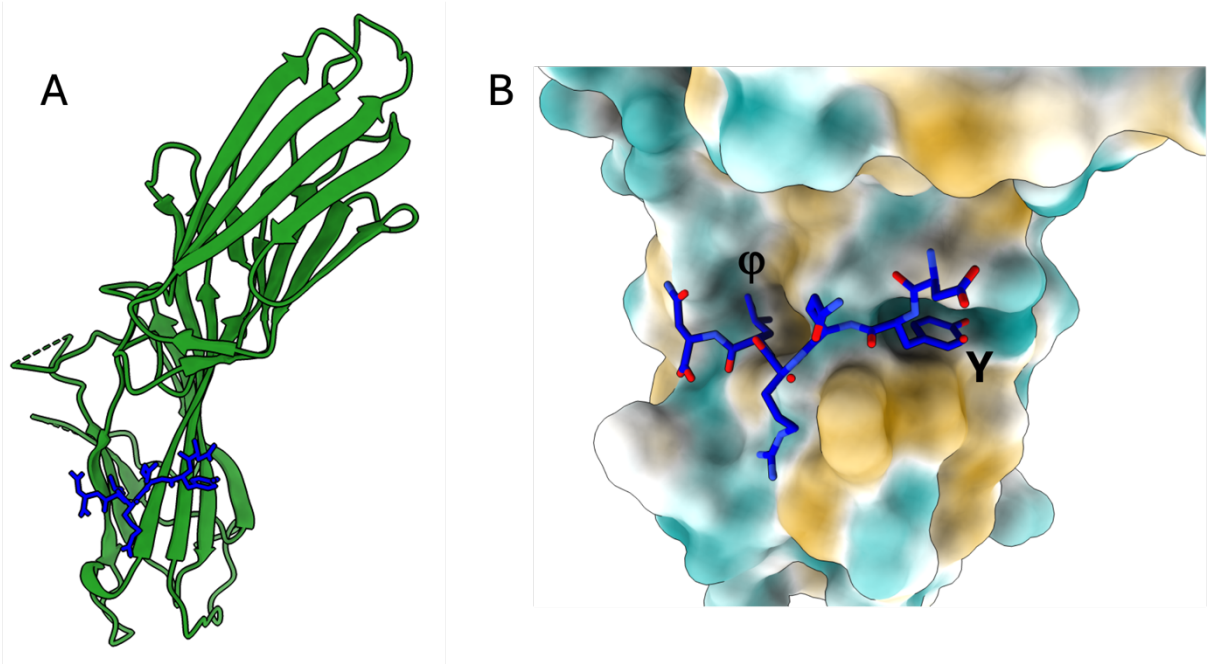


Figure 2: Crystal structure of μ2-subunit of adaptor protein AP2 bound to the endocytosis signal peptide of trans-Golgi network integral membrane protein TGN38 (Owen & Evans, 1998, PDB: 1BXX). A) Overview of the entire complex visible in the crystal structure. B) Close-up view of the peptide bound to AP2. The surface of AP2 is coloured by hydrophobicity. Surfaces in yellow display hydrophobic regions whereas those in blue show hydrophilic areas. ChimeraX 1.15 was used to depict the structure.

In addition, the σ2-subunit of AP2 recognises the acidic dileucine motif [DE]XXXL[LI][1] of transmembrane domains (Kelly et al., 2008). Upon receptor recognition and binding of the plasma membrane component phosphatidylinositol 4,5-bisphosphate, AP2 undergoes a conformational change revealing its clathrin-binding site, which enables coat formation (Kelly et al., 2014). AP2 is not the only receptor-sorting protein. Others relevant in CME include those that sort ubiquitinated receptors, GPCRs and integrins (Traub, 2009).

Coat assembly is a factor driving membrane curvature. Clathrin, a central component in CME, consists of three heavy and three light chains forming a triskelion (Kaksonen & Roux, 2018). This structure can polymerise by binding other triskelia. On the plasma membrane, the polymerisation and expansion of the clathrin coat causes membrane bending and the formation of a budding vesicle. Actin polymerisation also contributes to this process. Wiskott-Aldrich syndrome (WASP) family members facilitate this by recruiting proteins to the vesicle formation site ultimately connecting actin filaments with the clathrin coat (Sirotkin et al., 2005; Sun et al., 2006). The coordinated action of actin polymerisation and clathrin coat formation generates energy to further promote membrane curvature.

Vesicle scission is dependent on Bin-Amphiphysin-Rvs (BAR) domain proteins including endophilin and amphiphysin (Ringstad et al., 1999; Takei et al., 1999) that have a crescent shape and bind to strongly curved membrane (Peter et al., 2004). They recruit dynamin, a multimeric GTPase, to the neck of the budding vesicle. Dynamin multimerises forming a helical structure around the neck of vesicle and, upon GTP hydrolysis, tightens around the neck leading to vesicle scission (Hinshaw & Schmid, 1995; Sweitzer & Hinshaw, 1998). Removal of the clathrin coat is initiated by auxilin, a protein that binds to both clathrin and dynamin as well as engages heat shock cognate 70 (HSC70, Ungewickell et al., 1995). HSC70 interacts with clathrin and undergoes conformational changes upon

[1] The brackets indicate that either one of the two amino acid residues within them can fulfil the role required by the motif.

ATP hydrolysis (Sousa et al., 2016). These conformational changes exert force on the clathrin coat causing it to disassemble.

Overall, these temporally and spatially coordinated events lead to the successful internalisation of a selected set of receptors via CME.

## 1.3 Scavenger receptors

Having explored the mechanism of receptor-selective uptake, the extracellular domains of receptors along with ligands binding to them are presented. These ligands become internalised as a result of receptor engagement. A dedicated superfamily of transmembrane proteins, the scavenger receptors, use this mechanism to transfer molecules from the extracellular space into cells.

### 1.3.1 Diversity and classes of scavenger receptors

The first scavenger receptor identified was the molecule responsible for the internalisation of low-density lipoprotein (Brown et al., 1979). Ever since, it has been established that scavenger receptors are, from a structural point of view, incredibly diverse (Canton et al., 2013, Figure 3). They all serve their purpose by binding a molecule leading to its cellular uptake. This enables them to fulfil a wide range of functions, including cargo transport, detoxification, pathogen clearance and cell signalling.

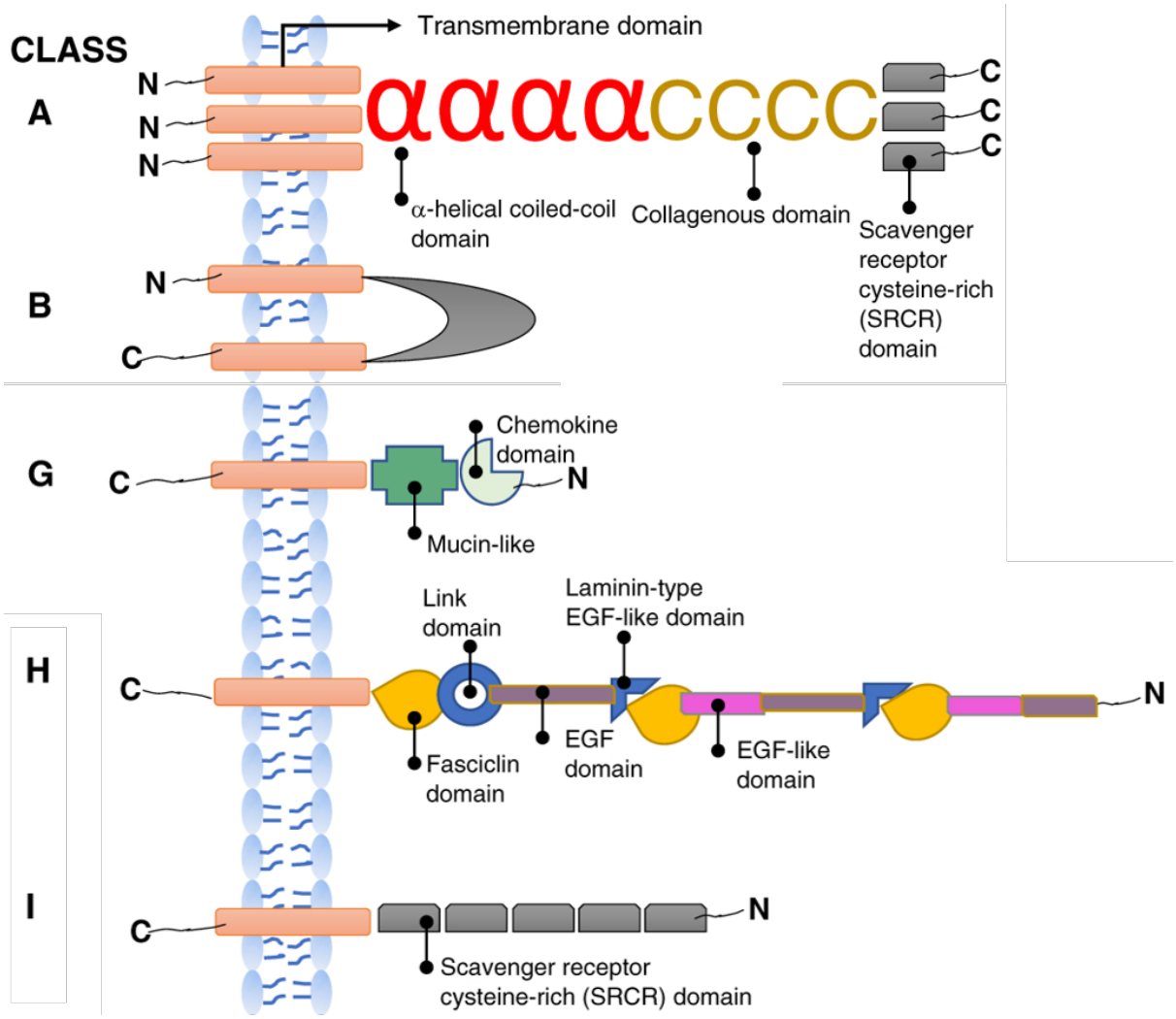


Figure 3: Schematic overview of selected classes of scavenger receptors introduced in this thesis. The figure is adapted from Alquraini & El Khoury, 2020.

Canton et al. describe at least 14 types of domains shared among the scavenger receptors. Based on the preference and arrangement of the domains, the scavenger receptors can then further be grouped into at least 8 classes (PrabhuDas et al., 2014). While scavenger receptors can vary significantly in size, they usually only contain one transmembrane domain and have a short cytoplasmic region. The following sections aim at providing an overview of a few distinctive classes of scavenger receptors.

Class A members were the first to be recombinantly expressed and contain one scavenger receptor cysteine-rich (SRCR) domain as well as at least one collagen domain (Alquraini & El Khoury, 2020). They are mainly produced by innate immune cells and bind to many danger-associated molecular patterns (DAMPs).

Class B receptors are particularly relevant for lipid transport. They are different from other scavenger receptors due to them having both an N-terminal and a C-terminal transmembrane helix. They are additionally remarkable because they can fulfil their physiological function of ligand transfer without the need of endocytosis. Structural studies on class B members of the CD36 superfamily showed that they possess a large hydrophobic tunnel within their ectodomain, which facilitates the transport of cholesterol esters to the membrane (Hsieh et al., 2016; Neculai et al., 2013).

The scavenger receptor that binds phosphatidylserine and oxidised lipids (SR-PSOX) is the only member of class G and is expressed by macrophages and myocytes (Sheikine & Sirsjö, 2008). Its extracellular motif is unique among scavenger receptors in that it harbours a chemokine domain. Upon proteolytic cleavage, the receptor becomes C-X-C motif chemokine ligand 16 (CXCL16), which can engage with CXC receptor 6 (CXCR6) mediating T-cell migration towards the chemokine.

### 1.3.2 Class I scavenger receptors

Class I is of particular interest for this dissertation. Its members contain a series of scavenger receptor cysteine-rich (SRCR) domains followed by a transmembrane helix and a short cytoplasmic tail. The SRCR domain contains ca. 110 amino acid residues and is formed from two $\beta$-sheets surrounding an $\alpha$-helix (Hohenester et al., 1999). Crystal structures of SRCR domains of non-class I receptors showed $Mg^{2+}$- and $Ca^{2+}$-ions that bind to anionic patches of the SRCR domain and contribute to ligand binding (Ojala et al., 2007; Reichhardt et al., 2020, Figure 4). Regulation by bivalent ions has also been suggested for class I scavenger receptors (Madsen et al., 2004).

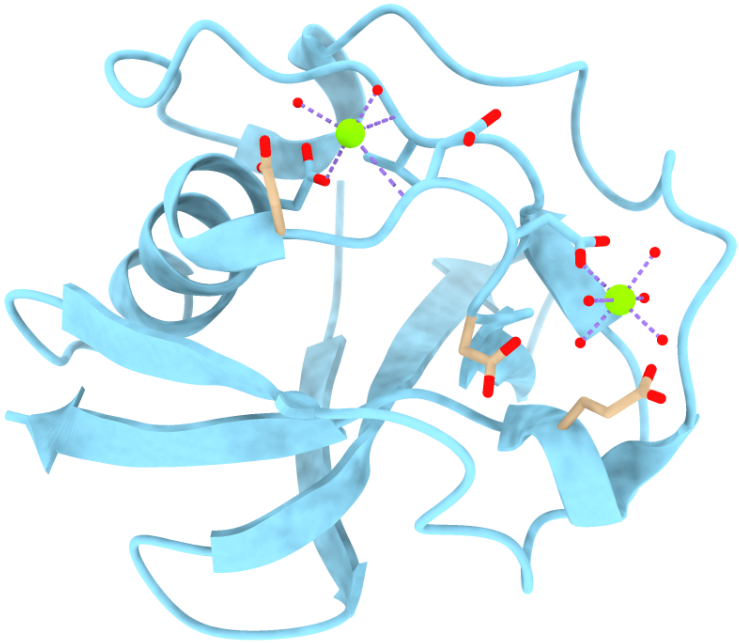

Figure 4: Ribbon diagram of mouse macrophage receptor with collagenous structure (MARCO) SRCR domain (PDB: 2OY3, Ojala et al., 2007). Magnesium ions coordinated by acidic residues and water are displayed in green.

The exact definition of class I receptors is controversial because this family has been only recently characterised. CD5, CD6 and CD163 are usually included in class I. CD5 and CD6 are B- and T-cell proteins that regulate immune cell signalling but can also recognise pathogen-associated molecular patterns (Aragón-Serrano et al., 2023; Berland & Wortis, 2002; Sarrias et al., 2007; Vera et al., 2009). Similarly, CD163 is a monocyte/macrophage protein that can both engage with pathogenic antigens and molecules produced by its host organism. CD163 is the focus of this thesis and will be discussed in detail in the following chapters.

## 1.4 CD163 in physiology

CD163 was at first identified as the M130 antigen, a 130 kDa protein from the spleen of a hairy cell leukaemia patient (Law et al., 1993). In 2001, its primary physiological function was elucidated: CD163 is the haptoglobin-haemoglobin (HpHb) scavenger (Kristiansen et al., 2001).

### 1.4.1 The CD163-haptoglobin pathway of haemoglobin detoxification

During intravascular haemolysis, haemoglobin (Hb) can be released from red blood cells (RBCs). Causes of intravascular haemolysis are diverse. They include genetic diseases (sickle cell disease, hereditary spherocytosis), infectious diseases (malaria, babesiosis) and acquired anaemias (blood transfusion reaction, Rh disease, Rother et al., 2005). While many of the diseases have devastating effects beyond Hb release, cell-free Hb is itself harmful to the body. Notably, Hb binds to nitric oxide, which is a second messenger regulating vasodilation. Furthermore, the positively charged iron of the haem group is highly reactive, binds to phospholipids and catalyses the production of reactive oxygen species (ROS) from lipid hydroperoxides that are already present on the cell membrane (Carlsen et al., 2005; Kumar & Bandyopadhyay, 2005). Therefore, regulation of released Hb is critical.

Mammals have evolved multiple lines of defence against released Hb. The first one is mediated by haptoglobin (Hp) and the macrophage receptor CD163. Hp acts in first instance by binding cell-free Hb, dissociated into the $\alpha\beta$-dimers, in serum using a picomolar interaction. The importance of Hp is highlighted by its abundance in plasma at a concentration of 0.3 to 3 mg/ml (Levy et al., 2009). Hp binding increases the rigidity of Hb and protects Hb residues susceptible to oxidation (Andersen et al., 2012) until it reaches its destination. It is particularly noteworthy that Hp protects the CD163-binding region of Hb preserving its receptor recognition ability. Next, the surface protein CD163 on alternatively-activated M2 macrophages binds HpHb. Due to an YXXφ[2] motif in its cytoplasmic region, CD163 along with HpHb is constitutively endocytosed (C. A. Schaer et al., 2006).

From there, HpHb is enzymatically degraded in the lysosome and haem is first broken down to biliverdin and iron (Thomsen et al., 2013) catalysed by the haem oxygenase. It is then reduced to the water-insoluble bilirubin (Gourley, 1997). This product is conjugated

[2] In CD163, the motif is specifically YREM.

to glucuronic acid in the liver to increase its hydrophilicity and finally secreted in bile. Unlike Hb and Hp, CD163 is recycled back to the cell membrane in the meantime (C. A. Schaer et al., 2006).

Macrophage uptake of HpHb upregulates cytokine expression, including the expression interleukin-6 (IL6), which in turn increase production of haptoglobin in hepatocytes and CD163 on macrophages.

### 1.4.2 Other haem detoxification pathways

The serum protein haemopexin (Hpx) and scavenger receptor CD91 together complement the Hp-CD163 system. When haem is released from met-Hb (Hb with $Fe^{3+}$) during severe haemolysis, Hpx acts by directly binding haem in a sub-picomolar interaction (Tolosano & Altruda, 2002). Structural studies have showed that Hpx contains two β-propeller domains between which the haem group binds (Paoli et al., 1999). The iron is directly coordinated by two histidine residues, thereby controlling its reactivity. Once the Hpx-haem complex reaches CD91 (Hvidberg et al., 2005), this complex becomes internalised, and the haem is degraded in the lysosome. In contrast to CD163, CD91 is not just expressed by macrophages but also by hepatocytes. Like Hp, the expression of Hpx is also induced by IL6 (Tolosano & Altruda, 2002).

Once the haem-binding capacities of Hpx are exhausted, Hb is filtered by the kidneys and damages them in the process, and the iron is stored as haemosiderin (A. Smith & McCulloh, 2015). If the kidneys' absorbance ability is saturated, haemoglobinuria occurs at which point devastating effects of Hb toxicity would have manifested. The CD163-Hp pathway of Hb detoxification is the major focus of this dissertation, and its components are introduced in detail in the following.

### 1.4.3 Structure of haemoglobin

Hb, being the component to be detoxified, is at the centre of the pathway. It was among the first proteins to be structurally elucidated. Max Perutz and colleagues started publishing structures of Hb from 1964. A horse deoxyhaemoglobin crystal structure is

among the oldest structures of the PDB and shows Hb to be composed of a tetramer (Bolton & Perutz, 1970). The tetramer itself is comprised of two α- and two β-subunits, with each α-subunit interacting with two β-subunits and each β-subunit in contact with both α-subunits[3]. The non-covalent interactions between the subunits are extensive and include hydrophobic interactions, hydrogen bonds and salt bridges. A high-resolution crystal structure of human, oxygenated Hb is depicted in Figure 5.

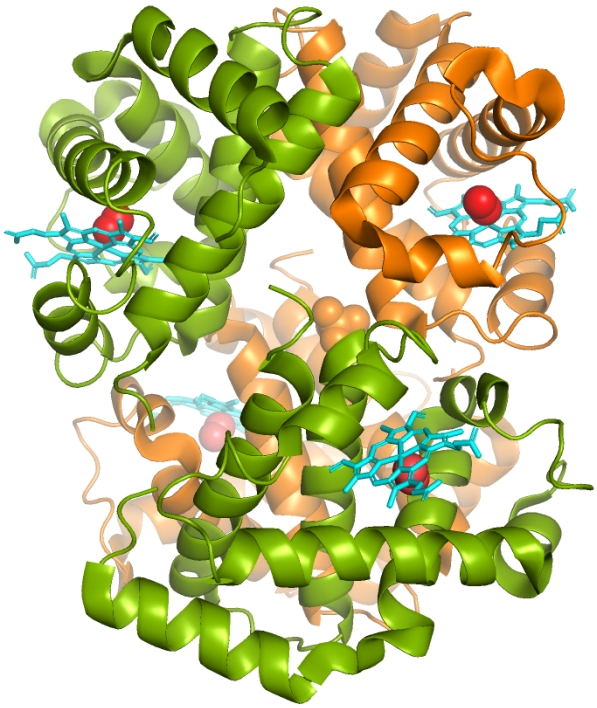

Figure 5: Crystal structure of human, oxygenated Hb (Shaanan, 1983). α- and β-chains are shown in orange and green, respectively. PDB: 1HHO is displayed using PyMOL 2.5.2.

Each subunit adopts a globular globin fold, characterised by eight α-helices connected through short loops. The human α- and β-globin chains are 142 and 147 residues long, respectively. In Hb, each chain harbours a haem-binding pocket. When comparing oxygenated and deoxygenated Hb, one striking difference is the position of the iron atom in the porphyrin ring. In deoxy-Hb, the iron atom is coordinated by four nitrogen atoms of the ring and a globin histidine residue. However, the iron atom is not in the plane of the porphyrin ring. In oxygenated Hb, $Fe^{2+}$ is in the plane of the porphyrin ring, coordinated by

[3] In deoxyhaemoglobin, there is a salt bridge between the two α-chains.

an oxygen molecule on one side and a globin histidine residue on the other (Shaanan, 1983).

Upon oxygen binding in one subunit, the iron-coordinating histidine residue and the α-helix it is part of are repositioned. This shift induces a conformational change throughout the molecule, leading to the movement of the iron atoms in other subunits towards the plane of the porphyrin ring (Perutz, 1970). Overall, oxygen binding in one subunit increases the affinity of other subunits for oxygen, a mechanism known as cooperative effect.

Although the haem groups are bound in dedicated pockets in their respective subunits, they are still exposed enough to facilitate oxygen binding. Therefore, Hb cannot prevent the iron's toxicity on its own.

### 1.4.4 Structure and oligomerisation states of haptoglobin

Hp is a multimeric protein. In its simplest form, the 1-1 phenotype, Hp is organised as a dimer, characterised by the swapping of a β-strand in a region defined by two complement control protein (CCP) domains (Andersen et al., 2012). The crystal structure shows multiple disulphide bridges in the CCP dimer region indicating the constitutive nature of the dimer. The C-terminal end of the CCP domain marks the beginning of a serine protease (SP) domain, which is proteolytically inactive. Only the SP domain engages in interacting with the αβ-dimer of Hb. The high affinity of the HpHb complex (ca. 1 pM) is explained by an extensive network of hydrogen bonds, ionic and hydrophobic interactions between the interacting proteins. It should be noted that the interaction interface between Hp and Hb is more extensive than within the two Hb dimers favouring HpHb complex formation. Overall, the existence of a HpHb crystal structure suggests that this complex is rigid. The structure is depicted in Figure 6.

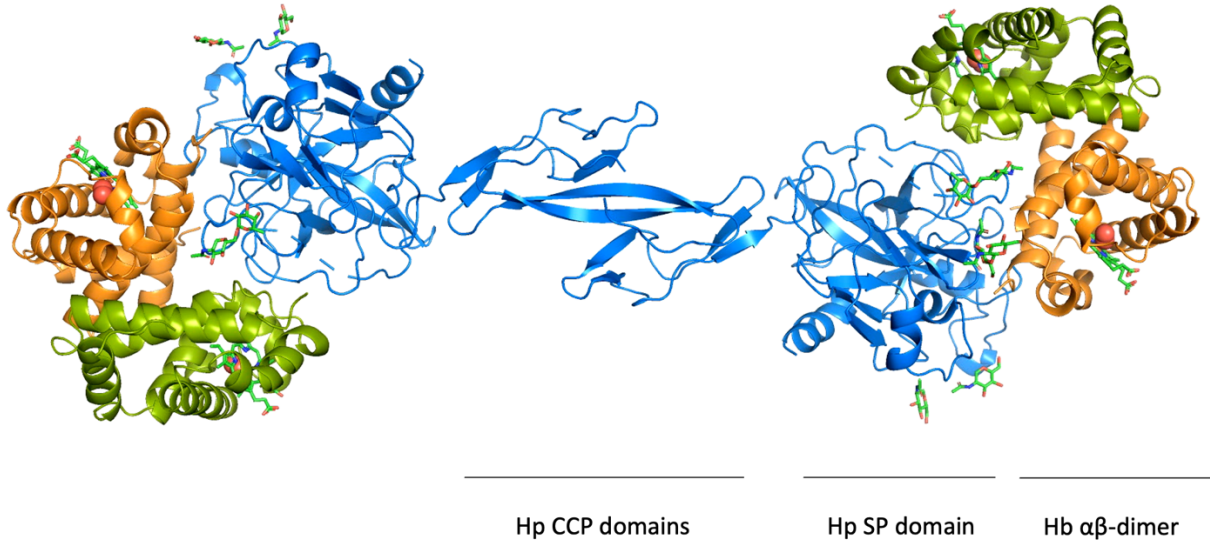


Figure 6: Structure of porcine HpHb. Hp is indicated in blue whereas the Hb α- and β-subunits are displayed in orange and green, respectively. PDB: 4F4O is depicted using PyMOL 2.5.2.

Humans have three phenotypes of Hp, which dominate in different geographies. In addition to 1-1, there are the 2-1 and 2-2 phenotypes. 1 and 2 refer to different alleles for Hp, with 1 encoding Hp with a single CCP domain and 2 containing two CCP domains. Having a single *Hp2* copy in the genome causes Hp to form oligomers bigger than dimers (Figure 7). They can range from a trimer to large oligomers (Tamara et al., 2020). While Hp(2-2) is of circular nature, Hp(2-1) becomes a linear oligomer. It was previously shown that Hp(2-2)Hb binds to CD163 at a higher affinity than its dimeric counterpart (Kristiansen et al., 2001) presumably due to an avidity effect.

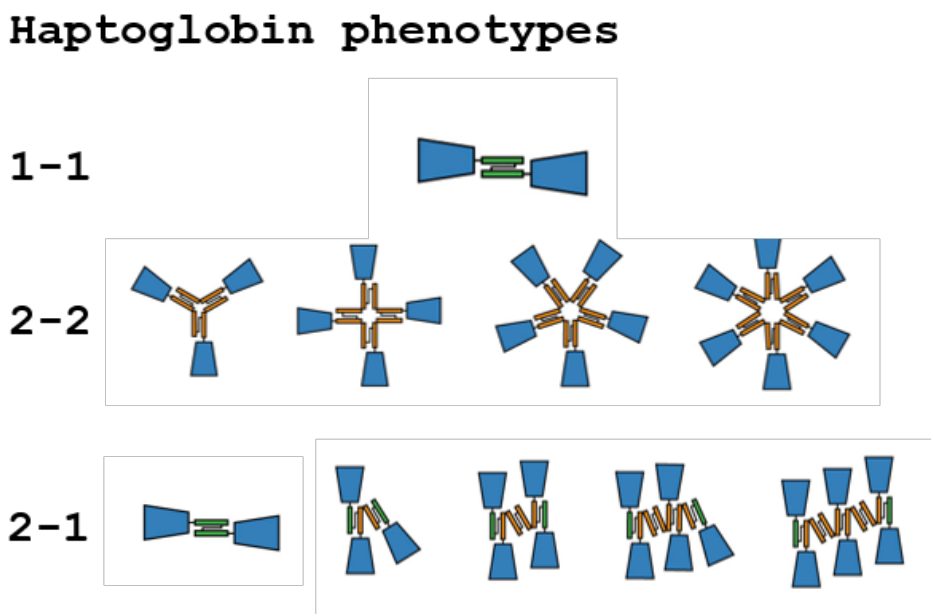


Figure 7: Schematic illustration depicting abundant haptoglobin complexes detected within different human phenotypes. The figure is adapted from Tamara et al., 2020. The SP domains are shown as blue trapezoids while the CCP domains of Hp1 and Hp2 are shown in green and orange, respectively.

It should be noted that both Hp1 and Hp2 are synthesised as a pre-protein that is cleaved by the complement C1r-like protein. This generates an α- and a β-chain, which correspond to the CCP and SP domain, respectively (Andersen et al., 2017; Wicher & Fries, 2004). The two chains are still connected via a disulphide bond. While Hp(2-2) was tested in functional experiments, Hp(1-1)Hb was the main protein to be studied due to its homogeneity.

### 1.4.5 Predicted model of CD163 on its own and its binding mode with haptoglobin-haemoglobin

AlphaFold2 (Jumper et al., 2021) provides a high-confidence prediction of human CD163 (Figure 8). It suggests a large ectodomain comprised of a chain of nine SRCR domains, a transmembrane helix and a short, disordered cytoplasmic tail. Notably, the N-terminal four SRCR domains are predicted to be sequentially ordered in a chain whereas the five C-terminal SRCR domains are clustered into a compact arrangement. Notably, CD163 contains an RSSR motif in the extracellular region and can be cleaved from the cell

surface (Etzerodt et al., 2013). However, the exact function of soluble CD163 is currently still under investigation (Møller et al., 2012).

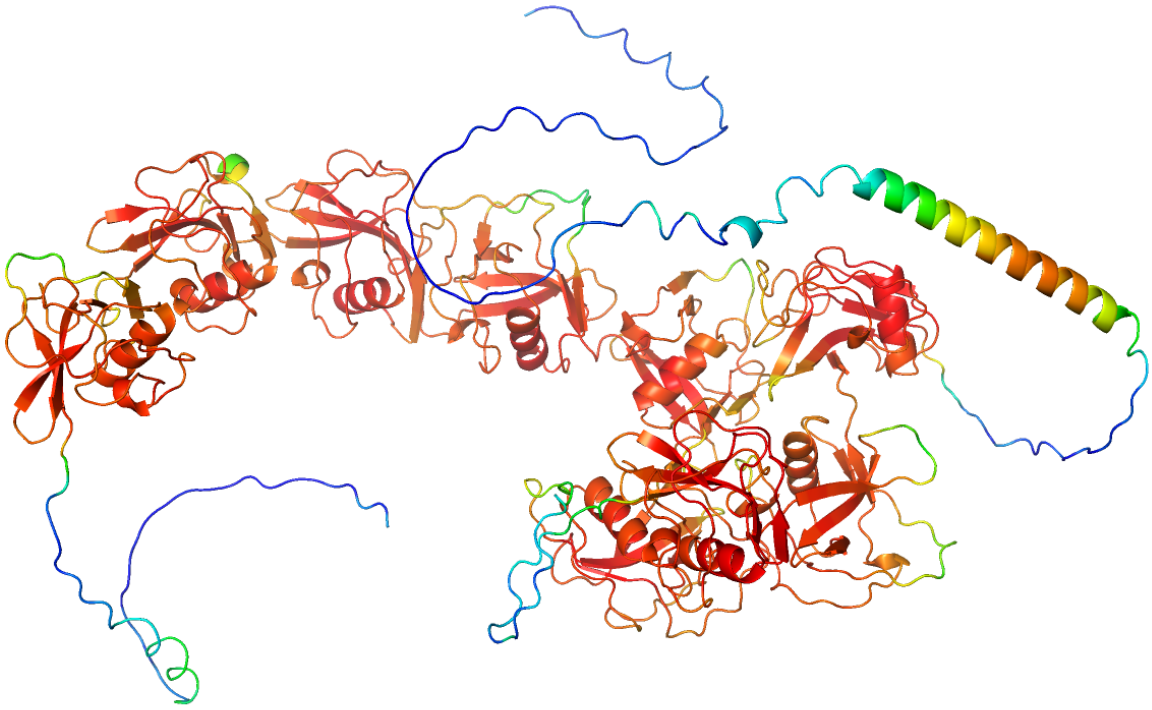

Figure 8: AlphaFold2 prediction of human CD163 (Uniprot Q86VB7). Colour indicates confidence of prediction, with red being most confident and blue least confident. The model was displayed using PyMOL 2.5.2.

Multiple studies aimed at predicting how CD163 binds to HpHb. In one such study, truncations of CD163 were generated, and the first five N-terminal SRCR domains alone can interact with HpHb (Madsen et al., 2004). In that same paper, they show that CD163 binding to HpHb is highly pH- and $Ca^{2+}$-dependent. Binding improved as pH and $Ca^{2+}$-concentration reached serum conditions. Moestrup's group later identified a loop within the SP domain of Hp (HpSP) that is responsible for HpHb interaction (Nielsen et al., 2006). Moreover, Moestrup's laboratory published a small-angle X-ray scattering (SAXS) envelope showing that N-terminal domains of CD163 primarily interact with Hp (Andersen et al., 2012). Using this envelope, the authors predicted that two molecules of CD163 can each interact with one protomer within the Hp(1-1)Hb dimer (Figure 9).

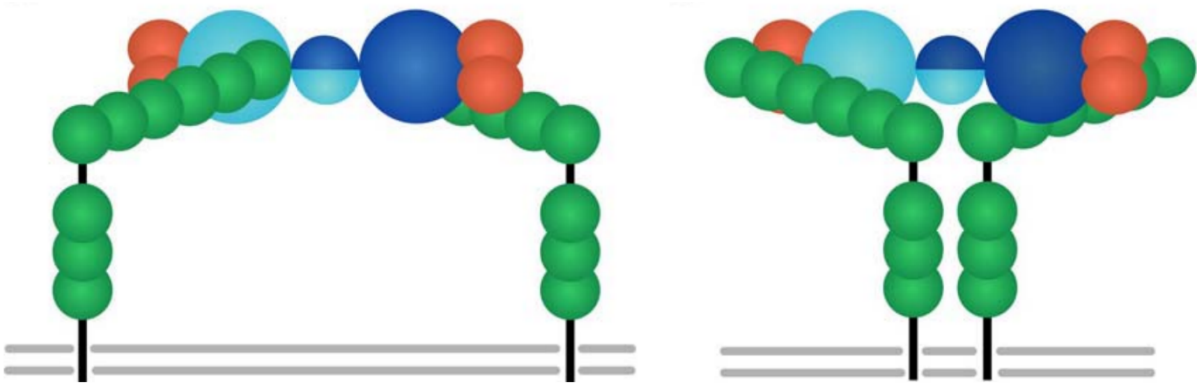

Figure 9: Predictions of a CD163-HpHb complex as seen in Andersen et al., 2012. Two copies of membrane-inserted CD163 with SRCR domains (green) are proposed to each bind one protomer of Hp (blue). Hb is displayed in orange.

This model suggests that CD163 predominantly interacts with Hp, which contrasts a study conducted by a different group of authors. In it, HEK293 cells transfected with CD163 were shown to take up both HpHb and Hb (D. J. Schaer et al., 2006). Furthermore, this study demonstrated that the Hb β-chain affected HpHb uptake indicating that Hb harbours the CD163 binding site. Therefore, there is a lack of clarity about how CD163 binds to its ligand.

## 1.5 Other functions of CD163

While the main physiological function of CD163 is to act as the Hb scavenger receptor, it also plays significant roles in infectious diseases. On the one hand, it may play a role in defending against bacteria whereas, on the other hand, it is exploited by a group of Arteriviruses as a viral receptor.

### 1.5.1 CD163 and bacterial infections

In a 2009 study, CD163 was demonstrated to directly bind Gram-positive and –negative bacteria with SRCR domain 2 strongly mediating the interaction (Fabriek et al., 2009). Additionally, the macrophage model cell line THP-1 significantly upregulates the expression of pro-inflammatory cytokines when transfected with CD163 highlighting the role of CD163 in recognising bacteria and defending against them.

A function for the shedded, soluble version of CD163 was suggested in the context of immunity against bacteria. Upon recognising *S. aureus*, CD163 is shed from the monocyte membrane and binds to fibronectin on the bacteria cell wall. Soluble CD163 opsonises the bacterium enhancing phagocytosis (Kneidl et al., 2012). CD163 shedding is not only limited by Gram-positive bacteria. Lipopolysaccharide (LPS) is also capable of causing CD163 cleavage from the cell membrane (Hintz et al., 2002; Weaver et al., 2006), although its exact effects requires further investigation.

### 1.5.2 CD163 as the intracellular receptor of Arteriviruses

Porcine reproductive and respiratory syndrome virus (PRRSV) and simian haemorrhagic fever virus (SHFV) belong to the family of Arteriviruses, which are enveloped, positive-sense, single-stranded RNA viruses. PRRSV and SHFV have been consistently found to use CD163 as receptor for viral entry, and the underlying mechanisms will be explored in the following.

A recent study has suggested that another Arterivirus family member, the lactate dehydrogenase-elevating virus (LDV) also requires CD163 for infection suggesting that hijacking CD163 is a common mechanism among Arteriviruses (Shaw et al., 2023).

#### 1.5.2.1 Uptake of porcine reproductive and respiratory syndrome virus

Porcine reproductive and respiratory syndrome (PRRS) was first described in the late 1980s and has since spread to most countries with a pig farming industry in Europe, North America and Asia (Nathues et al., 2014; Shi et al., 2010). This disease causes severe respiratory symptoms in young pigs and induces pre-mature stillbirth in sows during later stages of pregnancy (Rossow, 1998). It is an economically devastating disease in agriculture with an annual financial burden of more than 500 million US dollars in the US alone (Neumann et al., 2005). A potential vaccine could be an effective strategy to prevent PRRS transmission.

The PRRSV envelope proteins are particularly interesting in the context of viral entry. The major envelope proteins M and glycoprotein 5 (GP5) are critical to produce functional

virions and are disulphide-linked (Dokland, 2010). They enable viral attachment and internalisation by mediating interactions with heparan sulphate and sialoadhesin (Delputte et al., 2005). Additionally, the minor envelope proteins (GP2, GP3, GP4) form a heterotrimeric complex that interacts with CD163 and potentially with the GP5-M protein complex (Das et al., 2010).

CD163 plays a crucial role in the life cycle of PRRSV. Without CD163 expression, the viruses remain coated and cannot escape into the cytoplasm (Calvert et al., 2007; Vanderheijden et al., 2003). CD163 further defines the tropism of PRRSV towards porcine macrophages, as transfection of CD163 in different cell types enables infection. Further evidence of the importance of CD163 was generated using transgenic pigs. Pigs with a CD163 knockout are immune to PRRSV (Yang et al., 2018).

When investigating which SRCR domains mediate viral entry, Van Gorp et al. discovered that while the four N-terminal domains were dispensable, the five C-terminal domains were crucial for infection. Interestingly, domains six to nine could be replaced by corresponding domains in CD163-L1 whereas domain five could not. CD163-L1 originates from a duplication of the CD163 gene (Moeller et al., 2012). The five C-terminal SRCR domains of CD163-L1 share up to 75 % sequence identity with CD163. The importance of domain 5 in CD163 is additionally highlighted by genetically engineered pigs with a deletion in SRCR domain 5 that are resistant to PRRSV (Wang et al., 2019).

Elucidating the structure of CD163 is important because it might shed light on why the N-terminal domains behave differently than the C-terminal domains in PRRSV infection.

#### 1.5.2.2 Spillover potential of simian haemorrhagic fever virus and role of CD163

Another Arterivirus family member, the simian haemorrhagic fever virus (SHFV), also relies on CD163 for infection. This virus causes fatal haemorrhagic fever in primates with outbreaks in macaques reported since the 1960s (Wahl-Jensen et al., 2016). Recent publications showed that CD163 acts as a receptor facilitating viral infection (Caì et al., 2015; Warren et al., 2022). Surprisingly, even human CD163 enabled SHFV infection and

replication in transgenic, human cell lines. Considering that humans are immunologically naïve to Arteriviruses and that humans engage with primates (Paige et al., 2014), this means that a spillover of SHFV onto humans is possible.

Interestingly, CD163 was again necessary as the endocytic receptor. Understanding how the receptor functioned at conditions of the endosome might provide mechanistic insights into how SHFV exploits CD163 for infection.

### 1.5.3 Interaction with tumour necrosis factor-related weak inducer of apoptosis

In addition to previously mentioned functions of CD163, it has also been demonstrated to interact with the cytokine called 'tumour necrosis factor-related weak inducer of apoptosis' (TWEAK, Bover et al., 2007). Like CD163, TWEAK can exist both as a membrane-bound receptor as well as a soluble protein. While the transmembrane protein Fn14 binds to membrane-bound TWEAK, CD163+ macrophages interact with and take up soluble TWEAK. This affects plasma TWEAK concentrations with implications in heart and kidney diseases and diabetes mellitus (Moreno et al., 2009; Ratajczak et al., 2022). In addition, soluble CD163 binds to soluble TWEAK inhibiting its ability to activate Fn14-mediated Notch signalling with direct implications for muscle cell growth and tissue regeneration (Akahori et al., 2015).

## 1.6 Aims of this project

Overall, CD163 is an important protein in physiology and in pathology. Its primary physiological function is to scavenge HpHb. Our understanding of how CD163 scavenges HpHb is, however, limited. There are particularly three areas of questions.

Firstly, we do not conclusively know which part of the ligand the receptor interacts with. If CD163 mainly binds to Hp, as suggested, it remains to be answered how it prevents serum Hp uptake and how it distinguishes between different Hp phenotypes. If CD163 predominately interacts with Hb, would direct Hb uptake be possible? Secondly, we do

not understand why CD163 releases its ligand in the endosome. While pH- and $Ca^{2+}$-concentration decrease have been implicated as the driving factors, their mechanisms are not known. Calcium ions could be directly involved at the ligand-receptor interface. Thirdly, mechanisms by which the activity of CD163 is regulated are not known.

To answer all the research questions above, I elucidated the cryogenic electron microscopy (cryo-EM) structures of CD163 on its own and in complex with HpHb. To validate the structural insights and make hypotheses building on the structures, I conducted mutational studies along with biophysical and functional experiments under both serum and endosome conditions and developed a cellular uptake assay.

# 2. Material and methods

## 2.1 Molecular cloning by Gibson assembly

Gibson assembly was the only cloning strategy used in this dissertation. This method requires fragments with an overlap that are digested with a 5' exonuclease. After annealing of the fragments, a polymerase then restores the removed nucleotides, and a DNA ligase re-establishes the covalent bonds generating a plasmid that can be used for transformation.

### 2.1.1. Synthetic genes

Synthetic genes were ordered from GeneArt. For human CD163, residues 46-1050 (Uniprot Q86VB7-1) were used. For uptake experiments, a synthetic gene comprised of transmembrane and cytoplasmic domain of CD163 (Uniprot Q86VB7-1, residues 1051 - 1156) fused to a GSG-linker and GFP (Uniprot P42212, residues 2 – 238) was ordered. All residues were reverse translated into cDNA optimised for expression in human cells. The 'single-headed', human HpSP cloned into an expression vector was already available in the laboratory.

### 2.1.2 Constructs used for expression of CD163 in mammalian cells

A detailed list of all constructs used for expression of CD163, along with the primers and vectors used to clone them, is shown in the Appendix.

Generally, for recombinant protein expression and purification, the ectodomain of CD163 and its mutants were produced. All ectodomain constructs were cloned along with a C-tag (De Genst et al., 2010) into pHLsec (Addgene plasmid #99845, Aricescu et al., 2006). To immobilise CD163 for downstream experiments, an Avi-tag (Fairhead & Howarth, 2015) was inserted into CD163's ectodomain construct between the ectodomain and the C-tag using the Q5 mutagenesis kit (NEB), ensuring presentation which matches the orientation found on the membrane surface.

While the ecto-domain of CD163 was used as a recombinant protein for structural and biophysical studies, the full-length version of CD163 was expressed for uptake experiments because the cytoplasmic region of CD163 is required for endocytosis (C. A. Schaer et al., 2006). Generally, for uptake experiments, pcDNA5/FRT/TO (originally obtained from Thermo Scientific) was used. To enable constitutive expression of CD163 in stable HEK293TRex cells, the tetracycline operator was removed by amplifying pcDNA5/FRT/TO using primers that flanked the operator.

### 2.1.3 Primer design and polymerase chain reaction (PCR)

All primers used in this thesis contain a 25 bp overlap with the expression plasmid upstream of the gene of interest. The overlap with the gene of interest was designed to be sufficiently long to facilitate an annealing temperature of 60 - 66 °C according to Thermo's Tm calculator.

Due to the length of gene of CD163 and the length of the expression vectors, KOD Xtreme Hot Start DNA Polymerase (Merck) was used to amplify the desired fragments with the overlaps.

### 2.1.4 Agarose gel electrophoresis, gel extraction and Gibson assembly

Following PCR, the amplified fragments were purified and verified via agarose gel electrophoresis and gel extraction. A 1 % agarose gel was made in Tris-Acetate-EDTA (TAE)-buffer, cast onto an agarose gel cassette and run using TAE-buffer. Agarose, tris-base, acetic acid and EDTA were purchased from Sigma-Aldrich. The PCR products were mixed with 6 x Gel Loading Dye (NEB) and loaded onto the gel. After performing electrophoresis for 40 min at 120 V, the gels were imaged on iBright (Thermo Scientific), and bands of expected size were excised. dsDNA yield was quantified by measuring UV absorbance at 260 nm using DS-11 (DeNovix).

For each Gibson assembly, 300 ng of gene fragment was added to 100 ng of destination vector, topped up to 5 µl using MQ water and mixed with 5 µl of 2 x Gibson Assembly Master Mix (NEB). The reaction took place at 50 °C for 30 min for two fragment assembly

and 60 min for assembly of more than two fragments. The resulting product was either stored at – 20 °C or used directly for transformation.

### 2.1.5 Transformation of *E. coli* DH5α and MAX Efficiency Stbl2

Compared to conjugation and transduction, amplifying DNA in bacteria in a laboratory setting via transformation is most convenient. During this process, competent cells take up DNA from the environment through the cell membrane.

Generally, Gibson-assembled DNA fragments were heat-shock transformed into a recombinase-defective *E. coli* strain called MAX Efficiency Stbl2 Competent Cells (Thermo Scientific). Cells were thawed on ice, 1.5 µl of the Gibson Assembly product was added to 50 uL of cells and the mixture was incubated for 30 min on ice. After a 30 s heat shock at 42 °C in a water bath, cells were cooled for 2 min on ice. The cells were then subjected to out-growth in 950 uL of SOC media (NEB) for 1 h at 37 °C. Cells were then centrifuged, resuspended in 100 uL of SOC media and plated onto LB agar plates with 100 µg/ml carbenicillin (Fisher Scientific). All plasmids used in this dissertation have carbenicillin resistance.

Due to the size of CD163, cloned plasmids required Sanger sequencing using 4-5 primers. Instead, plasmids were quality-controlled using Nanopore sequencing (provided by Source Biosciences). Plasmids with desired sequences were then used to transform a less expensive *E. coli* strain DH5α (Thermo Scientific) using the same protocol for large scale DNA preparation.

### 2.1.6 DNA purification using Miniprep and Maxiprep Kits

Sequence-verified DNA was amplified in a large scale for downstream usage. If more than 20 µg of DNA was needed, PureLink HiPure Plasmid Maxiprep Kit (Thermo Scientific) was used to extract DNA. Otherwise the QIAprep Spin Miniprep Kit (Qiagen) was employed. Both kits were used according to the manufacturer's protocols. This involved lysis of bacteria using an alkaline buffer, that was neutralised and applied onto a DNA-binding column, where the DNA was washed and eluted into TE-buffer.

## 2.2 Protein expression and purification

CD163, its mutants and HpSP were recombinantly produced in Expi293F cells whereas oxygenated haemoglobin was directly purified from fresh red blood cell lysate using size-exclusion chromatography (SEC). Haptoglobin (1-1 and 2-2) purified from human serum were commercially available (Sigma).

### 2.2.1 Transfection of Expi293F cells with various constructs of CD163 and HpSP

Transfection refers to the uptake of genetic material by mammalian cells. Physical, chemical and viral treatment are methods of introducing DNA into cells. A cationic, lipid-based reagent that binds to the negatively charged DNA and is taken up by cells enables an efficient and easy way of transfection.

In this dissertation, the ExpiFectamine 293 Transfection Kit (Thermo Scientific) was used. This kit requires a HEK293-derived suspension cell line called Expi293F provided by Thermo Fisher. Expi293F cells grow at 37 °C in a shaking incubator with 8 % $CO_2$, 70 % humidity. The cells were split every 3 – 4 days to a density of 0.8 Mio/ml. In our group, a stock of it was kindly maintained and provided at 1.5 million/ml on the day before transfection by our laboratory manager, Hannah Ivison.

To transfect 100 ml of culture, 100 µg of sterile-filtered DNA and 267 µl of ExpiFectamine were each incubated for 5 min at RT in 5 ml of Opti-MEM I reduced serum medium (Thermo Scientific). After that, the two mixtures were combined and incubated for 20 min at RT. This suspension was added to the culture, which was transferred to the shaking incubator overnight. 16 – 18 h post-transfection, 0.5 ml and 5 ml of Enhancers 1 and 2 were added, respectively. If the protein to be expressed contained an Avi-tag, sterile biotin was added to the culture at 0.1 mM final concentration. After another 5 days of culturing in the shaking incubator, the supernatant was harvested by centrifugation for 30 min at 7000 g, 16 °C.

### 2.2.2 Protein purification using the C-tag column

Overexpressed protein in the supernatant requires separation for downstream experiments. Orthogonal methods of chromatography can achieve a high purity of the protein of interest. Affinity chromatography is often the first approach used. Purification of a poly-histidine tagged protein on a NiNTA column is well established but, often leads to impure products due to non-specific electrostatic interactions. Therefore, a C-tag (De Genst et al., 2010) with the sequence of EPEA was fused to the C-terminus of all recombinant proteins. It was specifically captured using a nanobody binding it and eluted by disrupting the ionic interactions using $MgCl_2$.

Before purification, harvested supernatant was passed through a 0.22 µm bottle-top filter to remove potential contaminants blocking the CaptureSelect C-tagXL Affinity Matrix (Thermo Scientific). Meanwhile, 1 ml of resin was equilibrated in 10 column volumes (CV) of C-tag buffer (20 mM Tris pH 7.5, 150 mM NaCl). The filtered supernatant was next applied onto the matrix. Subsequently, the column was washed with 30 CV of C-tag buffer and eluted in 5 CV of C-tag elution buffer (20 mM Tris pH 7.5, 2 M $MgCl_2$).

Due to a small amount of protein evading capture, the column was re-equilibrated in C-tag buffer, and the flow-through was subjected to a second round of purification. The column was then washed with 30 CV of MQ water and stored in 10 CV of 20 % (v/v) ethanol.

### 2.2.3 Gel filtration of purified proteins

To obtain a greater purity of products, a second, orthogonal approach of chromatography was applied. Gel filtration is an ideal method due to its compatibility with buffer exchange for downstream analysis. This approach separates proteins based on their hydrodynamic radius with larger particles eluting first.

ÄKTA pure (cytiva) was used in the laboratory. The molecular weight of the protein of interest determined the gel filtration column to be used. HpSP was applied onto a

Superdex 75 Increase 10/300 GL column (cytica) whereas Hp(1-1) and its Hb complex were purified using a Superdex 200 Increase 10/300 GL column (cytica). Due to the multimeric nature of CD163, CD163 on its own and its complexes were separated on a Superose 6 Increase 10/300 GL column (cytica). To purify Hb, fresh RBC lysate (kindly provided by Poy Pholcharee) was directly applied on a HiLoad 16/600 Superdex 200 pg (cytiva).

After gel filtration, every protein used in this study was eluted in HBS with calcium (20 mM HEPES pH 7.5, 150 mM NaCl, 2.5 mM $CaCl_2$), aliquoted out and flash frozen in liquid nitrogen.

### 2.2.4 Assembly and purification of Hp(1-1)Hb and CD163-HpHb complexes

Hp phenotype 1-1 was purchased from Sigma-Aldrich. 2 mg of Hp was mixed with Hb at a 1:3 molar excess of Hb. Due to the extremely high affinity of Hp for Hb, the mixture was injected immediately onto a SEC column. To purify Hp(1-1)Hb, the corresponding mixture was applied on a Superdex 200 Increase 10/300 GL column (cytica).

CD163-Hp(1-1)Hb and CD163-HpSPHb were formed by mixing purified CD163 with excess Hp(1-1)Hb or HpSPHb and incubating at RT for 20 min. Due to the sizes of the complexes, the mixtures were then applied on a Superose 6 Increase 10/300 GL column (cytica).

### 2.2.5 SDS-PAGE

Bolt Bis-Tris Plus Mini Protein Gels, 4-12 % assembled onto a Mini Gel Tank (both Thermo Scientific) were used to run SDS-PAGE. 5 µl of purified protein was mixed in 15 µl of 4x NuPAGE LDS Sample Buffer (Thermo Scientific) supplied with 5 % beta-mercaptoethanol. Gels were run for 25 min at 220 V before being stained in Quick Coomassie Stain (Generon).

### 2.2.6 Fluorescent labelling of proteins

For MST and uptake experiments, fluorescently labelled binding partners of CD163 were required. Amine coupling is a convenient way of covalently attaching fluorophores onto proteins. All proteins have primary amines in the form of the N-terminus, and additionally proteins used in this study contain lysines. The structure of CD163-HpHb shows that particularly the lysines of Hb are critical for CD163 interaction. Therefore, Hb modification was avoided if possible. For all variants of HbHp complexes, Hp was initially labelled, the dye was then removed via buffer exchange, and a complex of Hp was formed in the presence of excess Hb.

Alexa Fluor 594 NHS Ester was used for uptake experiments whereas Alexafluor 647 NHS Ester (both Thermo Scientific) was used for MST. 1 mg of dye was dissolved in 100 µl of DMSO. In parallel, 100 µl of 1 M sodium bicarbonate was added to 4 mg of protein and the volume was topped up to 900 µl using PBS. Subsequently, the dissolved dye was mixed with the protein and incubated for 1 h at RT.

Unbound dye was removed using Zeba Spin Desalting Columns (7K MWCO, Thermo Scientific). To equilibrate the column, 300 µl of the desired buffer was added to the column and centrifuged at 1,500 g for 1 min for a total of three times. Afterwards, the labelled sample was applied onto the column and eluted by centrifugation at 1,500 g for 2 min. If needed, excess Hb was added to Hp, and the sample was buffer exchanged into HBS with calcium using gel filtration, aliquoted out, quantified and flash frozen in $N_2$ (l).

The protein concentration and the molar ratio of dye to protein was determined by measuring the sample's absorbance at the dye's emission maximum ($A_{max}$) and at 280 nm while using the formulas, correction factors and extinction coefficients ε provided by Thermo Scientific:

$$(1)\ [Labelled\ protein] = \frac{A_{280\,nm} - (A_{max} * correction\ factor)}{\varepsilon_{protein}},$$

$$(2)\ Molar\ ratio\ of\ dye\ to\ protein = \frac{A_{max}}{\varepsilon_{dye} * [labelled\ protein]}.$$

The molar extinction coefficients $\varepsilon_{dye}$ of Alexa Fluor 594 and 647 are 92,000 and 239,000 $M^{-1}cm^{-1}$, respectively. The correction factor at 280 nm accounts of absorbance by the dye itself at 280 nm and is 0.56 and 0.03 for Alexa Fluor 594 and 647, respectively. The protocol described above consistently leads to labelling of proteins with 3 to 4 molecules of dye attached.

## 2.3 Biophysical analysis

The purpose of all methods listed in this chapter is to detect, quantify and characterise protein-protein interactions, particularly between CD163 or its mutants and Hb or its complexes with Hp.

### 2.3.1 Surface plasmon resonance (SPR)

SPR relies on light excitation of surface plasmons at the interface of a metal and a liquid (Nguyen et al., 2015). The oscillation of the surface plasmons is influenced by the refractive index of that interface, which is dependent on proteins adsorbed on it. This interface wave affects the angle of the reflected incident light that is then detected and quantified (Figure 10). The response is directly proportional to the amount of the proteins adsorbed onto the metal surface (Frostell et al., 2013; Motsa & Stahelin, 2023).

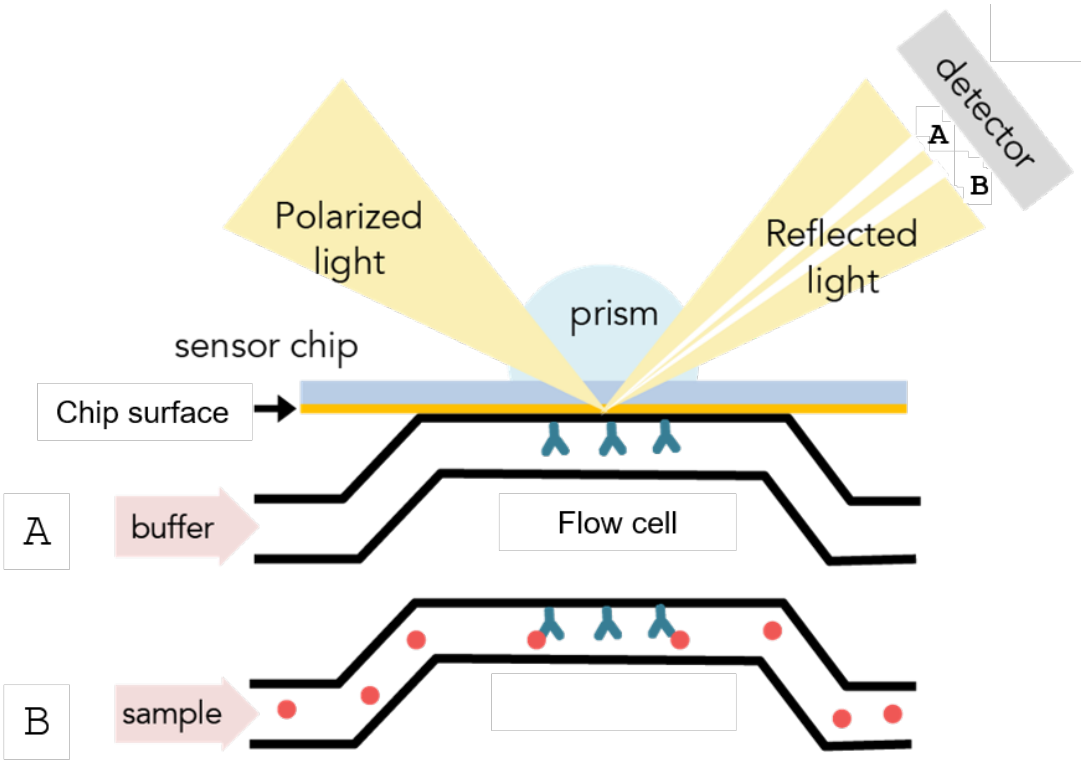


Figure 10: Schematic illustrating SPR. The figure is adapted from https://cmi.hms.harvard.edu/surface-plasmon-resonance. A) and B) depict differences in the angles of reflected light upon analyte binding to an immobilised protein on the chip surface.

In an SPR experiment, one protein (the ligand) is immobilised onto the surface of the SPR chip while its potential interaction partner (the analyte) is flown over it to probe any interactions. Typically, proteins can be covalently bound to an SPR chip using amine coupling. However, relevant proteins to be studied here turned out to be protein complexes (CD163 multimer, HpHb) that would dissociate upon exposure to acidic buffers required for immobilisation. Therefore, an Avi-tag (Fairhead & Howarth, 2015) was introduced to the C-terminus of CD163 constructs that was biotinylated during protein expression.

Cytiva's Biotin CAPture Kit provides a capture reagent that contains ssDNA conjugated to streptavidin. Upon binding complimentary ssDNA on the sensor chip, the biotinylated CD163 can then be immobilised onto the chip. After flowing the analyte, the chip is then regenerated using chaotropic reagents releasing the ssDNA-conjugate.

In this setup, the ligand was always Avi-tagged CD163 and its mutants, and the analytes were Hp(1-1)SP, Hp(2-2)Hb and HpSPHb. Prior to the run, both analyte and ligand were exchanged into SPR running buffer (20 mM HEPES pH 7.5, 150 mM NaCl, 2.5 mM $CaCl_2$, 0.005 % tween-20). The ligand was then diluted to 8 µg/ml whereas the analyte was diluted to 10 nM (Hp(1-1)Hb, Hp(2-2)Hb) and 20 nM (HpSPHb). Another seven 2-fold dilutions of the analyte were prepared. The capture reagent was diluted in an equal volume of SPR running buffer. The regeneration buffer was made by mixing stocks 1 and 2 at a 3:1 ratio.

SPR was performed on Biacore T200 SPR system (cytiva). During each cycle, the capture reagent was flown on both sample and reference cells of a sensor chip at 2 µl/min for 5 min. Afterwards the ligand was captured on the sample cell only for 160 s at 8 µl/min. The analyte was then flown onto both sample and reference cells for 3 min at 30 µl/min in high-performance mode, and dissociation was allowed to occur for 5 min. Finally, both sample and reference cells were restored by applying regeneration buffer for 80 s at 10 µl/min followed by a 100 s stabilisation period.

To demonstrate non-binding conditions, the SPR running buffer was switched to running buffer without calcium, or the HEPES was replaced with MES pH 6.0, or a MES buffer without calcium was used. Instead of a dilution series, a single injection of 10 nM Hp(1-1)Hb was conducted.

To obtain statistically relevant results, all SPR experiments were done in technical triplicates.

### 2.3.2 Microscale thermophoresis (MST)

Hp and Hb binding to CD163 could not be quantified by SPR because Hp showed high binding to the reference cell, and the binding of Hb to CD163 did not fit a 1:1 binding model. Therefore, these interactions required a different method of analysis. Furthermore, due to the nature of SPR, immobilised CD163 was concentrated on the sensor chip surface. Therefore, even the ‘monomer mutant’ of CD163 might behave as a

multimer on SPR. To validate SPR results, an immobilisation-independent, solution-based method was used.

MST was chosen for this study. During MST, laser light induces a temperature increase leading to movement of molecules out of areas exposed to the laser (Jerabek-Willemsen et al., 2014). This thermophoresis is dependent on the molar mass, charge and solvation energy of the particle, which will differ based on whether it is bound by an interaction partner. This technique requires fluorescently labelled proteins that are excited by the laser and send Stoke-shifted light to the detector. In a typical setup, 16 capillaries at constant fluorophore concentration with decreasing concentration of its binding partner in a two-fold dilution series are prepared. Each of the capillaries are individually excited, after which the emission is detected. If there is interaction between the fluorescent protein and its ligand, differences in thermophoresis of each sample can be used to derive binding parameters.

MST was performed on Monolith NT.115 (NanoTemper). Table 1 summarises conditions used for each MST measurement. It should be noted that the concentration of the fluorescent protein was adjusted to approximately match the estimated interaction $K_D$. This is why the affinity interaction between CD163-R809T and Hp(1-1)Hb was recorded at 40 nM fluorescent receptor, and a high LED power was used to compensate for the low dye concentration. After preparing the samples, they were incubated for 1 h at RT before a Monolith Capillary (NanoTemper) was inserted into each sample. Every interaction was characterised using technical triplicates.

Table 1: Setup of MST experiments. The concentrations provided are final concentrations of the fluorescent protein and concentrations of the unlabelled partner in the first and last capillary.

| Fluorescent protein | [Fluorescent protein] / nM | Unlabelled partner | [Unlabelled partner] / nM | LED power / % | MST power / % |
|---|---|---|---|---|---|
| Hb | 200 | CD163-WT | 24400-0.74 | 10 | 20 |
| Hp | 500 | CD163-WT | 37900-1.2 | 8 | 20 |
| Hb | 200 | CD163-R809T | 41500-1.3 | 10 | 20 |
| Hb | 200 | CD163-284NGT | 20800-0.64 | 10 | 20 |
| Hp(1-1)Hb | 40 | CD163-R809T | 4000-0.12 | 95 | 40 |

### 2.3.3 Mass photometry (MP)

To confirm the presence of multimers of CD163 alone and bound to Hp(1-1)Hb, a population-based method of characterising protein-protein interactions was required. Native mass spectrometry was not useful due to the presence of five N-glycans on CD163. The N-glycans would have caused sample heterogeneity leading to mass spectra that cannot be deconvoluted.

MP seemed to be an ideal approach. A low concentration sample (10 – 100 nM) is applied on a glass cover slip (Sonn-Segev et al., 2020; Young et al., 2018). Particles gradually adsorb onto the glass, with some particles also detaching from it. The dynamic process of particle adsorption onto the glass cover is monitored using a microscope and recorded as a movie. A sample containing proteins of known masses with multiple oligomeric states can be used as a standard for a contrast-to-mass calibration curve. This allows unknown masses of particle mixtures to be determined and displayed as histograms.

Sean Burnap at the Kavli Institute of Nanoscience at Oxford kindly performed MP measurements with my samples and assistance. A concentrated sample was diluted to achieve the following final gasket concentrations (Table 2). All samples were recorded on TwoMP (Refeyn) for 1 min, and the gasket volume was 20 µl. All measurements were

conducted in triplicates, and the most representative replicate was chosen for presentation. Sean Burnap analysed the data using Discover$^{MP}$ (Refeyn).

Table 2: Proteins used for MP, their concentrations and the buffers they were suspended in.

| Sample | Concentrations | Buffer components |
|---|---|---|
| CD163WT alone | 17.7 nM | 20 mM HEPES pH 7.5, 150 mM NaCl, 2.5 mM $CaCl_2$ |
| CD163WT alone | 17.7 nM | 20 mM HEPES pH 7.5, 150 mM NaCl, 5 mM EDTA |
| Hp(1-1)Hb alone | 14 nM | 20 mM HEPES pH 7.5, 150 mM NaCl, 2.5 mM $CaCl_2$ |
| HpSPHb alone | 9.7 nM | 20 mM HEPES pH 7.5, 150 mM NaCl, 2.5 mM $CaCl_2$ |
| CD163WT + Hp(1-1)Hb | 87 nM CD163WT, 30 nM Hp(1-1)Hb | 20 mM HEPES pH 7.5, 150 mM NaCl, 2.5 mM $CaCl_2$ |
| CD163WT + Hp(1-1)Hb | 30 nM CD163WT, 9.7 nM Hp(1-1)Hb | 20 mM HEPES pH 7.5, 150 mM NaCl, 5 mM EDTA |
| CD163WT + HpSPHb | 75 nM CD163WT, 24 nM Hp(1-1)Hb | 20 mM HEPES pH 7.5, 150 mM NaCl, 2.5 mM $CaCl_2$ |
| CD163R809T alone | 34 nM | 20 mM HEPES pH 7.5, 150 mM NaCl, 2.5 mM $CaCl_2$ |
| CD163R809T + Hp(1-1)Hb | 50 nM (each protein) | 20 mM HEPES pH 7.5, 150 mM NaCl, 2.5 mM $CaCl_2$ |

### 2.3.4 Size exclusion chromatography coupled with multi angle laser light scattering (SEC-MALLS)

SEC-MALLS was used to compliment MP findings, including analysis of the dimer-trimer equilibrium and the validity of R809T to disrupt CD163 multimerisation. In SEC-MALS, sample components are initially separated according to their hydrodynamic radii on a

SEC column. The separated particles are then passed through a MALLS detector, which measures the refractive index change in solution and the distribution of light scattered at various angles to determine the molar mass and heterogeneity of an analyte (Some et al., 2019).

SEC-MALLS samples were usually prepared with 0.4 mg/ml CD163 in 100 µl final volume. Complexes with HpHb were composed of 0.08 mg/ml Hp(1-1)Hb. Typical running buffer was HBS with calcium but was switched to HBS without calcium, MBS with calcium and MBS without calcium to demonstrate calcium- and pH-dependence of multimersation and ligand binding. In experiments showing a concentration-dependent increase in trimer population, the concentration of CD163WT was gradually increased (0.4, 0.7, 1.4, 2.7 mg/ml). To show that R809T prevents multimerisation, samples at 0.4 and 2.7 mg/ml were prepared. Samples were made in duplicates or triplicates and given to the department's biophysics facility manager, David Staunton, who kindly performed the experiments on Dawn Heleos (Wyatt Technology).

## 2.4 Cryogenic electron microscopy

A structure was required to provide crucial information about the CD163-HpHb complex. There are three main structural methods: nuclear magnetic resonance (NMR) spectroscopy, X-ray crystallography and cryo-EM. Large proteins tumble slow in solution and exhibit fast relaxation causing peaking broadening in NMR. The sizes of the either CD163 or HpHb are above 100 kDa, which makes structural studies using NMR incredibly difficult. Crystallography is possible for large protein complexes and was attempted before significant progress was made using cryo-EM. The cryo-EM structure of CD163 would subsequently show that crystallising CD163 would have been improbable because CD163 is heterogeneous and forms dimers and trimers in a concentration-dependent manner. Furthermore, the N-terminal domains of CD163, particularly in the trimer, are highly flexible, further impeding crystallisation.

There are three main approaches in cryo-EM: 2D-crystallography, single-particle analysis (SPA) and cryo-electron tomography (cryo-ET). In each method, the sample is irradiated

with an electron beam at cryogenic conditions within a microscope. 2D-crystallography relies on the formation of a 2D crystal. Because of that, this technique is inferior to SPA, which does not require crystallisation. In SPA, software assigns particles from different 2D projections into 2D- and 3D classes. SPA was chosen over cryo-ET because the complexes could be assembled *in vitro*. Cryo-ET would require extensive sample preparation but could provide insights into how CD163 on a cell surface binds to and internalises HpHb.

### 2.4.1 Sample preparation, grid freezing and data collection

During SPA, a thin layer of purified protein or protein complex is vitrified in liquid ethane. Sample purity is crucial as contaminants might dominate the 2D classes. Liquid ethane freezes water significantly quicker than liquid nitrogen, preventing the formation of ice crystals. Ice crystals diffract electrons significantly, degrading image quality. Furthermore, formation of crystalline ice might affect proteins as they are surrounded by a hydration shell.

Another challenge of cryo-EM is the air-water interface. Proteins at that interface might denature. Furthermore, particles often prefer a specific orientation relative to the air-water interface restricting the range of particle orientations seen on a recorded micrograph.

Sample thickness also needs optimisation as samples too thin often force proteins out of the centre of a grid hole and induce preferred orientation. Ice layers too thick increase scattering of electrons on the way to the detector and worsen the signal-to-noise ratio. After sample application on the grid, it is then blotted before plunge-frozen in liquid ethane. The blotting time and force are important parameters to control ice thickness.

Sample concentration was also varied to obtain grid holes showing consistent, dense but not overlapping particle distribution. Complex concentration did not linearly correlate with particle density as the CD163 complexes preferably attached onto the carbon film. Complexes were only visible in the holes after saturation of the carbon film. In this study,

the correlation between sample concentration and particle density in grid holes was also rather irreproducible. Therefore, each grid was screened individually prior to data collection.

On the day of sample freezing, aliquots of CD163 and Hp(1-1)Hb were thawed and mixed together with at least 5-times molar excess of Hp(1-1)Hb, and the complex was purified on the Superose 6 Increase 2.3/300 (cytiva). This excess was initially chosen because CD163-HpHb could be easily separated from excess HpHb, and complexes of CD163-HpHb without unbound components can be isolated. It would later turn out that this step was crucial as the CD163-HpHb complex stoichiometry was 3:1 and 2:1, respectively.

A Vitrobot Mark IV (Thermo Scientific) was used for sample application and plunge freezing. An initial screening session showed visible particles on Quantifoil R 1.2/1.3 Cu 300 grids, which is why sample preparation on these grids was initially optimised. Standard copper grids were selected because they are mechanically stable, cheap and do not have a continuous carbon support film. The support film often decreases the contrast of particles and the resolution of the final volume.

Grids containing CD163-HpHb complexes frozen at 0.04 – 1.3 mg/ml and blotted for 1.5 – 8 s were clipped to enable loading by the microscope's autoloader. These grids were screened on FEI Talos Arctica (200 kV emission gun, Falcon 4 direct electron detector (DED, Thermo Scientific). Sample concentration did not consistently correlate with particle density in the grid holes. This is particularly true for grids frozen at different sessions. Therefore, grids that were imaged for an overnight or multi-day collection were screened individually beforehand. Increases in blotting time did usually lead to thinner ice, and the optimal blotting time was determined to be between 2.5 and 4 s.

For overnight data collection of CD163-HpHb on the Arctica, a complex at 0.13 mg/ml was pipetted onto a Quantifoil R 1.2/1.3 Cu 300 grid with a blot time of 8 s and blot force of - 2 before being submerged in liquid ethane and stored in liquid nitrogen. Defocus values of -2.7 to – 0.8 µm were chosen, and dose and pixel size were set to 29.98 $e^-/Å^2$ and 1.2 Å, respectively. For a 6-day collection of CD163-HpHb on FEI Titan Krios (300 kV

emission gun, Gatan K3 DED and energy filter), 1.3 mg/ml complex were pipetted on three Quantifoil R 1.2/1.3 Cu 300 grids at a blot time of 2.5, 3.5 and 4 s, respectively. Here, defocus values of -2.0 to – 0.4 µm, a dose of 41.68 $e^-/Å^2$ and a pixel size 0.832 Å were used.

In addition to the CD163-HpHb complex, the structure of unbound CD163 was also of interest. A volume of the CD163-HpHb indicated that apo-CD163 would exhibit the triangular base without evidence of the ligand bound. For a 2-day collection of CD163 on its own on the Titan Krios, 1.3 mg/ml of sample was applied onto copper grids at a blot force of 7 for 2.5 s. Defocus values between – 1.8 and – 0.6 µm, an electron dose of 42.82 $e^-/Å^2$ and a pixel size of 0.832 Å were chosen.

## 2.4.2 Data processing

The workflow of generating a 3D protein complex structure from collected images is described. A graphical overview of how each protein complex was processed is depicted in the corresponding Results Chapter.

### 2.4.2.1 Pre-processing

Pre-processing refers to all processing steps before 2D classification can take place. It includes motion correction, contrast transfer function (CTF) estimation, particle picking and extraction.

After obtaining and importing the micrographs, the first step was to motion correct each micrograph. Motion during acquisition was caused by mechanical drift of the grid against the stage and by the beam (X. Li et al., 2013). In a 2020 paper, Thorne proposed that the beam allows the sample to release tension built up during vitrification. To enable motion correction, every micrograph was captured as a collection of multiple frames, which were aligned to a reference frame and then combined. Another aspect of motion correction is dose-weighting (Zivanov et al., 2019), in which later frames are down-weighted to account for radiation damage caused by the electron beam. In this dissertation, motion correction was performed using SIMPLE 3.0 (Caesar et al., 2020)

because this software allowed correction to be run while data was still being acquired on the microscope.

Micrographs were collected in defocus to increase the contrast of particles against their surroundings. Defocus introduces intentional differences in the focal plane positions of the sample, enhancing contrast by making particle edges more distinguishable from the background. However, defocus (along with spherical aberrations) affects phase and amplitude of the electron's wave function, ultimately affecting resolution. CTF estimation is necessary to account for these parameters using mathematical methods.

Moreover, sample thickness is usually inhomogeneous across the grid hole with ice being thinnest at the centre. This variation in thickness further complicates image analysis by introducing differences in depth of focus across the micrograph. To address this, CTF estimation was applied on patches of micrographs (Zivanov et al., 2018). This job, like most other processing jobs, was done in CryoSPARC v4.2-4.4 (Punjani et al., 2017).

There were three particle picking jobs that were considered initially. Blob picking identifies particles with a Gaussian distribution of intensity without the need of prior knowledge about the complex's shape or size. Manual picking is an interactive job, where users pick particles of defined size on the micrograph themselves. Template picking requires a series of 2D templates (which can be generated from a 3D map) to guide the picking job. Since structural information of CD163 was initially unknown, blob picker was used to find initial particles that were extracted and 2D-classified. These 2D classes or 2D classes from initial 3D volumes were used to re-pick using template picker to find rare views of the complex.

#### 2.4.2.2 2D classification

2D classification is particularly useful for providing an overview of all picked particles. Furthermore, it allows particles corresponding to the complex of interest to be distinguished from contaminant 'particles'. During initial stages of classification in CryoSPARC (Punjani et al., 2017), particles are assigned to classes randomly, after which

particles become allocated to classes based on similarity. At the end of each round of assigning particles to 2D classes, the 2D classes receive an update based on particles allocated during that round. After a set number of particles have been classified (e.g. 100,000), the final round begins in which all remaining particles are aligned onto previously defined 2D classes.

After a job of 2D classification had been completed, 2D classes resembling the complex of interest were selected and used for further processing whereas junk particle classes was discarded. Usually, 2D classification was repeated several times before proceeding with reconstruction. During later rounds of classification, a mask was applied around the particle to focus the alignment specifically on signal originating from the complex.

2.4.2.3 3D reconstruction and refinement

To reconstruct, CryoSPARC uses Branch and Bound to find correct rotational and translational parameters of a 2D view (called pose, Punjani et al., 2017). Branch and Bound searches the parameter space to find the best alignment between 2D projections and a 3D model. Just as merging two different pictures produces a new image unlike the inputs, aligning a 2D view with wrong parameters on a 3D map would produce an image artefact. To find the right pose, therefore, requires iterative adjustments, minimising the image artefact between the 2D projection and a view of the 3D map. The second component of reconstruction is Stochastic Gradient Descent, a machine learning tool (Bottou, 2010) to further optimise the map. During Stochastic Gradient Descent the orientation of particles is iteratively refined by minimising the error in the reconstruction.

To determine resolution in cryo-EM, particles are randomly assigned into two groups prior to refinement. The two groups are independently refined and compared to each other. By determining the gold-standard Fourier Shell Correlation (FSC) curves, the resolution can be estimated. It is usually defined as the frequency at which a resolution-FSC plot reaches the FSC of 0.143 (Scheres & Chen, 2012). This is to reliably quantify the map's quality and to ensure that resolution is not overestimated.

An initial reconstruction enabled 3D refinement. During refinement, low-pass filtered maps were used as input. In heterogeneous refinement, particles were iteratively assigned to 3D classes, gradually improving resolution while re-assigning particles to different 3D maps. This step was always performed after *ab initio* reconstruction. Next, homogeneous and non-uniform refinement were run consecutively. Non-uniform refinement took regions of disorder into account during refinement and, as a result, usually improved resolution compared to homogeneous refinement (Punjani et al., 2020). This technique is particularly beneficial for flexible complexes, which CD163 and CD163-HpHb both are.

In the Titan Krios datasets of CD163-HpHb, non-uniform refinement was combined with the optimisation of per-particle defocus and CTF parameters to further boost resolution. Finally, the volume was sharpened using DeepEMhancer (Sanchez-Garcia et al., 2021). Cryo-EM maps were visualised using UCSF ChimeraX 1.15 (Meng et al., 2023).

### 2.4.3 Model building and refinement

The AlphaFold 2 (Jumper et al., 2021) prediction of human CD163 and an X-ray structure of human HpHb previously determined in the laboratory (Lane-Serff et al., 2014) were used as templates for model building. Overall, the structure of HpHb fitted into the EM density very well. While the Alphafold model of CD163 was not a perfect fit for the map, individual SRCR domains could still be rotated and translated into the corresponding densities that were then adjusted or re-built from there.

After initial models of the complexes were produced using Coot 0.9.8.8 (Emsley & Cowtan, 2004), real-space refinement was performed in Phenix 20.1 (Afonine et al., 2018). During real-space refinement, the global energy of the protein model is reduced, while empirically determined geometric constraints are refined. At the same time, the model-to-map fit is iteratively improved. Phenix accomplishes this by using simulated annealing to explore the conformational space and performing NQH-flips to correct side-chain orientations. Phenix also applies a rigid body fit to align the model into the map and uses local grid searches to optimise rotamer conformations.

Models were iteratively optimised in Coot and refined in Phenix until clash scores, Ramachandran and sidechain outliers reached desirable values according PDB's validation system. PDB uses clash scores to quantify the number of steric clashes per 1,000 atoms. In a 1963 publication, Ramachandran et al. described protein backbone dihedral angles that are usually observed. Outliers in lower resolution models are often wrong and were corrected. Side chain outliers refer to bond lengths and angles deviating from their optimal values and additional issues like incorrect chirality, planarity and improper rotamers.

PDBe's Protein Interfaces, Surfaces and Assemblies (PISA) software (Krissinel & Henrick, 2007) was employed for structural analysis, particularly to identify amino acid residues involved in interfaces between proteins.

## 2.5 Uptake assays

A ligand uptake assay is a direct method of functionally validating the structures. To accomplish that, detection of fluorescently labelled ligands of CD163 in cells via FACS was chosen because this approach demonstrates the ability of CD163, a scavenger receptor, to internalise ligands via endocytosis.

Performing uptake in transiently transfected cells did not lead to useful uptake data since transfected cells have pores that take up molecules, including the live-dead cell stain. Therefore, stable CD163+ HEK293TRex cells were generated and used for uptake. This following section describes the approaches used to generate, select and use the cells for uptake.

### 2.5.1 Design of CD163-GFP fusion in vector providing hygromycin-resistance

The Flip-In 293 system (Thermo Scientific) was used for this purpose and kindly provided by Ian Gibbs-Seymour. Its major advantage is that the transgene is integrated in a

transcriptionally active region of the host cell's genome. In contrast, randomly transfected cells will incorporate the gene in transcriptionally inactive regions leading to populations with variable gene expression levels.

An ideal vector would enable expression of CD163 controlled by a strong promoter and selection in a mammalian antibiotic. pcDNA5/FRT (Thermo Scientific), a part of the Flip-In system, provides the CMV immediate-early enhancer and promoter regulating the gene of interest. Furthermore, it confers resistance to hygromycin.

For this functional experiment, the full-length version of CD163 was required as the cytoplasmic region is relevant for uptake (C. A. Schaer et al., 2006). A C-terminal fusion of full-length CD163 and GFP efficiently took up HpHb (D. J. Schaer et al., 2006). The GFP allows FACS sorting of CD163+ cells and selective culturing of these cells. Furthermore, detecting the GFP and the fluorophore attached to HpHb at the same time enabled the correlation of HpHb uptake with CD163 expression. In contrast, using an antibody to label CD163 prior to FACS detection might not provide useful results because adherent HEK293 cells need to be trypsinised before FACS, causing degradation of CD163 and preventing antibody staining.

### 2.5.2 Generation of stable HEK293TRex cells expressing CD163 and its mutants

A Flp-In host cell line, which contains a genome-integrated start-codon, flippase-recognition target (FRT) site and zeocin-resistance gene, was kindly provided by Ian Gibbs-Seymour in the Department. Upon its exposure to a recombinase and pcDNA5, which itself contains an FRT site, the zeocin-resistance gene in the genome is replaced by a hygromycin resistance gene. Moreover, the CMV promoter-regulated CD163 gene becomes genome-integrated. Selecting transfected cells for hygromycin-resistance would therefore select for CD163 expression.

HEK293TRex cells were generally grown in high glucose DMEM with GlutaMAX, 10 % FBS and 1x penicillin/streptomycin (all Thermo Scientific). These cells require incubation at

37 °C, 5 % $CO_2$. To maintain a parental stock, 2 Mio cells were seeded into a 10 cm dish (Thermo Scientific) and split after 3 days. The parental was maintained in 15 µg/ml blasticidin and 100 µg/ml zeocin.

To generate stable cells, 360,000 cells were seeded in each well of a 6-well plate (Thermo Scientific) in media without blasticidin or zeocin. A well was needed for each construct and the untransfected negative control. After the cells reached 60 % confluency, media was replaced with fresh DMEM, and the transfection reagent was prepared. 250 µl of Opti-MEM reduced (Thermo Scientific) was mixed with 7.5 µl of TransIT-LT1 transfection reagent (Mirus Bio) and 2.5 µg of a 9:1 mixture of pOG44 and pcDNA5/FRT. (pOG44 encodes the recombinase.) After a 20 min incubation at RT, the mixture was added dropwise to the designated wells, and the cells were incubated for a day. Next, each well was trypsinised, and the cells were split into a 15 cm dish (Thermo Scientific) and incubated overnight. Starting from the following day, media was replaced with DMEM containing 15 µg/ml blasticidin S HCl (Gibco) and 100 µg/ml hygromycin B (VWR) every 2-3 days. Colonies usually appeared about 8 days after transfection, at which point the hygromycin concentration was lowered to 50 µg/ml to accelerate cell growth. Colonies were allowed to merge to obtain a confluent plate for FACS sorting.

To derive conclusions about effects of each mutant, cells transfected with each construct were sorted for high, uniform CD163 expression with consistent expression levels across all different constructs. On the day of sorting, cells on the 15 cm dishes were washed in 15 ml PBS and incubated in 10 ml trypsin-EDTA for 5 min at RT. After resuspending the cells in trypsin-EDTA, the cells were added to 10 ml DMEM with FBS to deactivate the trypsin. Following a 5 min centrifugation at 200 g, the cells were resuspended in 1.5 ml PBS and given to Vasiliki Tsioligka and Robert Hedley at the Dunn School's Flow Cytometry Facility who kindly sorted 1 – 2 million cells per construct using FACSAria Fusion (BD Biosciences). Subsequently, the cells were pelleted and resuspended in DMEM containing 15 µg/ml blasticidin S and 50 µg/ml hygromycin B. This mixture was used to inoculate a 10 cm dish, which was incubated at 37 °C. The cells were allowed to grow until they reached 80 % confluency, at which point they were ready for uptake experiments.

To verify that the correct transgene was incorporated into the designated cell lines, an aliquot of each cell line was subjected to genomic DNA extraction. To accomplish that, ca. 100,000 cells were mixed in 0.5 ml QuickExtract DNA Extraction Solution (Biosearch Technologies) by vortexing for 15 s. Subsequently, the cells were warmed up to 65 °C for 6 min, vortexed again for 15 s, and finally heated up to 98 °C for 2 min. The product was used for PCR amplification of amplicons less than 900 bp in length, which were used for Sanger sequencing.

### 2.5.3 Direct uptake of fluorescently labelled Hp(1-1)Hb and Hp(2-2)Hb

Direct uptake of Alexa Fluor 594-labelled Hp(1-1)Hb and Hp(2-2)Hb was used to compare uptake efficiencies between different stable cell lines and the untransfected negative control.

Uptake of Hp(1-1)Hb was evaluated in a time course experiment. A day before conducting the uptake experiment, 108,000 cells were seeded into wells of four 24-well plates (Thermo Scientific) in 1 ml DMEM with FBS but without blasticidin S or hygromycin B. On the day of experimentation, a mastermix containing 500 nM Alexa Fluor 594-labelled Hp(1-1)Hb was made in DMEM-HEPES (Thermo Scientific) with FBS. Each well was washed in 0.5 ml PBS, after which 400 µl of the mastermix was added to the designated wells and incubated at 37 °C for 0, 15, 30 or 60 min. Following incubation, the supernatant was discarded, and the cells were washed in 0.5 ml PBS, resuspended in 0.2 ml trypsin-EDTA and added to 0.6 ml DMEM with FBS. To thoroughly remove any ligand that is bound to the cell surface but not internalised, cells were subjected to two additional wash steps in 0.5 ml PBS. Afterwards, they were stained in the live-dead cell dye, DRAQ7 (abcam). Finally, GFP- and Alexa Fluor 594-fluorescence were detected using the 488 nm and 561 nm laser of the LSRFortessa X-20 Cell Analyzer (BD Biosciences).

For the uptake of Hp(2-2)Hb, a concentration titration experiment was performed. Unlike the time course format, this setup required multiple mastermixes, each containing Alexa

Fluor 594-labelled Hp(2-2)Hb in a two-fold serial dilution. The cells were incubated consistently at 37 °C for 30 min.

### 2.5.4 Uptake of fluorescently labelled Hp(2-2)Hb in the presence of competitors

Only the uptake of Hp(2-2)Hb was predominately and specifically mediated by CD163. The uptake of all other ligands was mainly caused by non-specific mechanisms, such as macropinocytosis performed by cultured cancer cells. To compare the CD163-mediated uptake efficiencies of different ligands, a competition assay was established. This assay followed the same protocol as the direct Hp(2-2)Hb uptake experiment, with only one difference: the mastermixes were prepared with 50 nM Alexa Fluor 594-labelled Hp(2-2)Hb and a two-fold serial dilution of the unlabelled competitor for each solution.

### 2.5.5 Quantification of uptake

While gating strategies can be used to define uptake and quantify the percentages of cells that have internalised the ligand, these methods are subjective and arbitrary. Therefore, the mean fluorescence intensity of all live, single cells in each sample was quantified using FlowJo v10.10 and directly plotted as a function of time or concentration.

# 3. Structures of dimeric and trimeric CD163 in complex with haptoglobin-haemoglobin

## 3.1 Summary

The main objective of this dissertation is to reveal how HpHb is scavenged by the macrophage receptor CD163 in atomic detail, by combining structural biology, biophysics and cell uptake assays. Structural methods considered for this project were X-ray crystallography and single-particle analysis in cryo-EM, which both required a pure protein sample.

I first established conditions to allow purification of Hp(1-1)Hb, Hp(2-2)Hb and HpSPHb and then produced pure and functional CD163. Constructs were designed for expression of the five N-terminal SRCR domains of CD163 intended for crystallography. For cryo-EM, an expression construct containing the entire ectodomain of CD163 was used to produce soluble, recombinant protein in Expi293F cells. The ectodomain of CD163 formed a high-affinity complex with Hp(1-1)Hb and HpSPHb, and the complex was purified for grid preparation.

Resolutions for a CD163-HpSPHb complex were limited by preferred orientation whereas the CD163-Hp(1-1)Hb complex was captured from multiple orientations, likely due to the effect of Hp(1-1)Hb on the overall shape of the complex. Reconstructions of CD163-Hp(1-1)Hb at 2.8 and 3.1 Å revealed the structural basis of HpHb scavenging and provided many surprising insights, including the multimeric assembly of CD163, the role of calcium and how HpHb binds.

## 3.2 Purification of haptoglobin-haemoglobin

### 3.2.1 Purification of haemoglobin from lysed erythrocytes

Obtaining functional, oxygenated Hb with iron in the ferrous ($Fe^{2+}$) state from a heterologous expression system is challenging. The haem group needs to be incorporated into the Hb subunits. Furthermore, the iron in the haem group is highly susceptible to becoming oxidised during a multi-day protein expression at 37 °C. Recombinant expression is further complicated by Hb being composed of two different globin chains.

Native Hb, however, can be obtained at a high yield and purity from red blood cells directly. Extracts from lysed red blood cells were available in the laboratory and directly applied on the HiLoad 16/600 Superdex 200 gel filtration column (Figure 11).

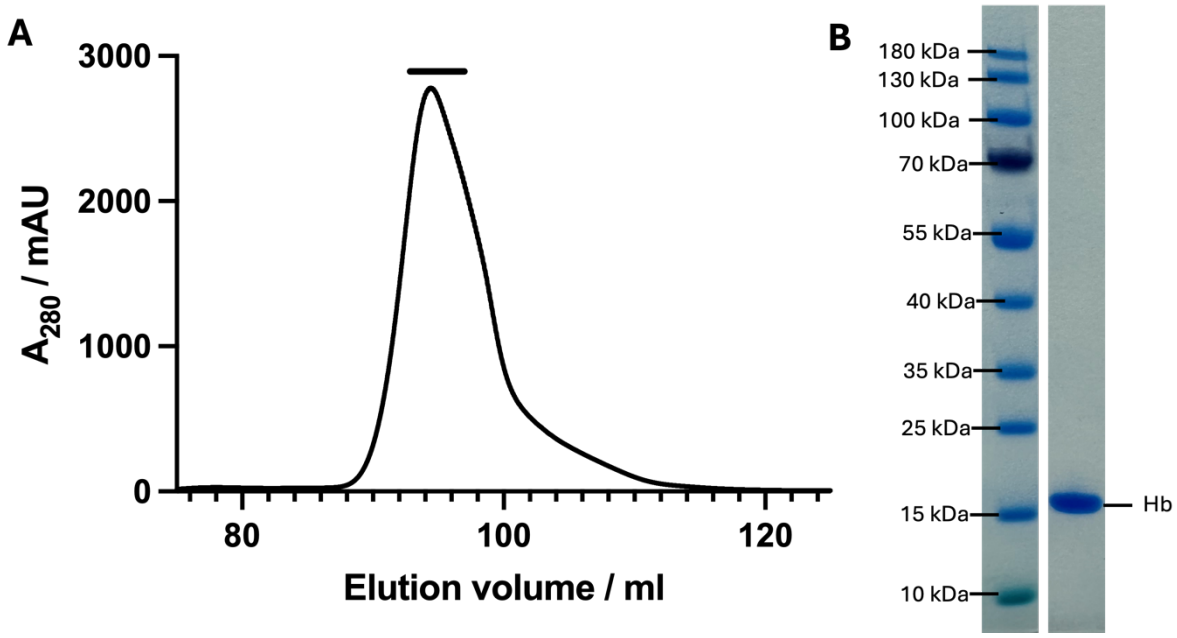


Figure 11: Purification of haemoglobin. A) SEC chromatogram between an elution volume of 75 and 125 ml. The black line indicates fractions pooled for further use. B) Reduced SDS-PAGE analysis of SEC-purified, diluted Hb. The expected molecular weight of Hb α- and β-chain are 15.2 and 15.9 kDa, respectively.

### 3.2.2 Production of the serine protease domain of haptoglobin and formation of its complex with haemoglobin

Hp protomers consist of an SP domain forming a 'head' structure and one or two CCP domains that multimerise through interactions with other Hp protomers. As described in Chapter 1.4.4, the Hp genotype determines whether an individual exhibits the Hp(1-1), Hp(2-2) or Hp(2-1) phenotype. While Hp(1-1) and Hp(2-2) were commercially available, HpSP, the part of Hp that exclusively binds to Hb (Andersen et al., 2012), was also required.

In contrast to natural Hp phenotypes, HpSP is monomeric. The monomeric ligand could be useful as structural characterisation of complexes at a 1:1 ratio could be advantageous. For instance, the crystal structure of the *Trypanosoma brucei* haptoglobin-haemoglobin receptor (TbHpHbR) was elucidated in complex with monomeric HpSP (Lane-Serff et al., 2014). The structure showed that TbHpHbR directly and exclusively interacts with HpSPHb. While this complex successfully crystallised, the inclusion of an additional CCP domain in the construct might have hindered crystallisation as it could have introduced more flexibility and size into the complex. In cryo-EM, HpSP might cause the CD163-bound complexes to have a different shape than the natural HpHb phenotypes, which could affect interactions with the air-water-interface and orientation bias.

A construct encoding HpSP was previously generated in the laboratory (Lane-Serff et al., 2014). To enable expression in mammalian cells, the gene along with a C-tag was cloned into pHLsec, which was used to transfect Expi293F cells. The C-tag is detected by a nanobody and usually leads to a purer product after affinity chromatography compared the polyhistidine tag. Pure HpSP was obtained by subjecting the cell supernatant to C-tag purification followed by SEC (Figure 12A).

As CD163 had previously been shown to interact strongly with HpHb and weakly or not at all with Hp or Hb (Kristiansen et al., 2001), complexes of various Hp constructs bound to

Hb were made to study the CD163-HpHb interaction, including HpSPHb complex. HpSPHb has approximately the same size as tetrameric Hb and cannot be separated from Hb using SEC. Therefore, HpSP was first purified on the Superdex 75 10/300 column (Figure 12A). Then it was mixed with an excess of Hb, applied onto a C-tag and then onto a Superdex 200 10/300 column. The final SEC elution showed a homogenous peak containing pure HpSPHb (Figure 12B and C).

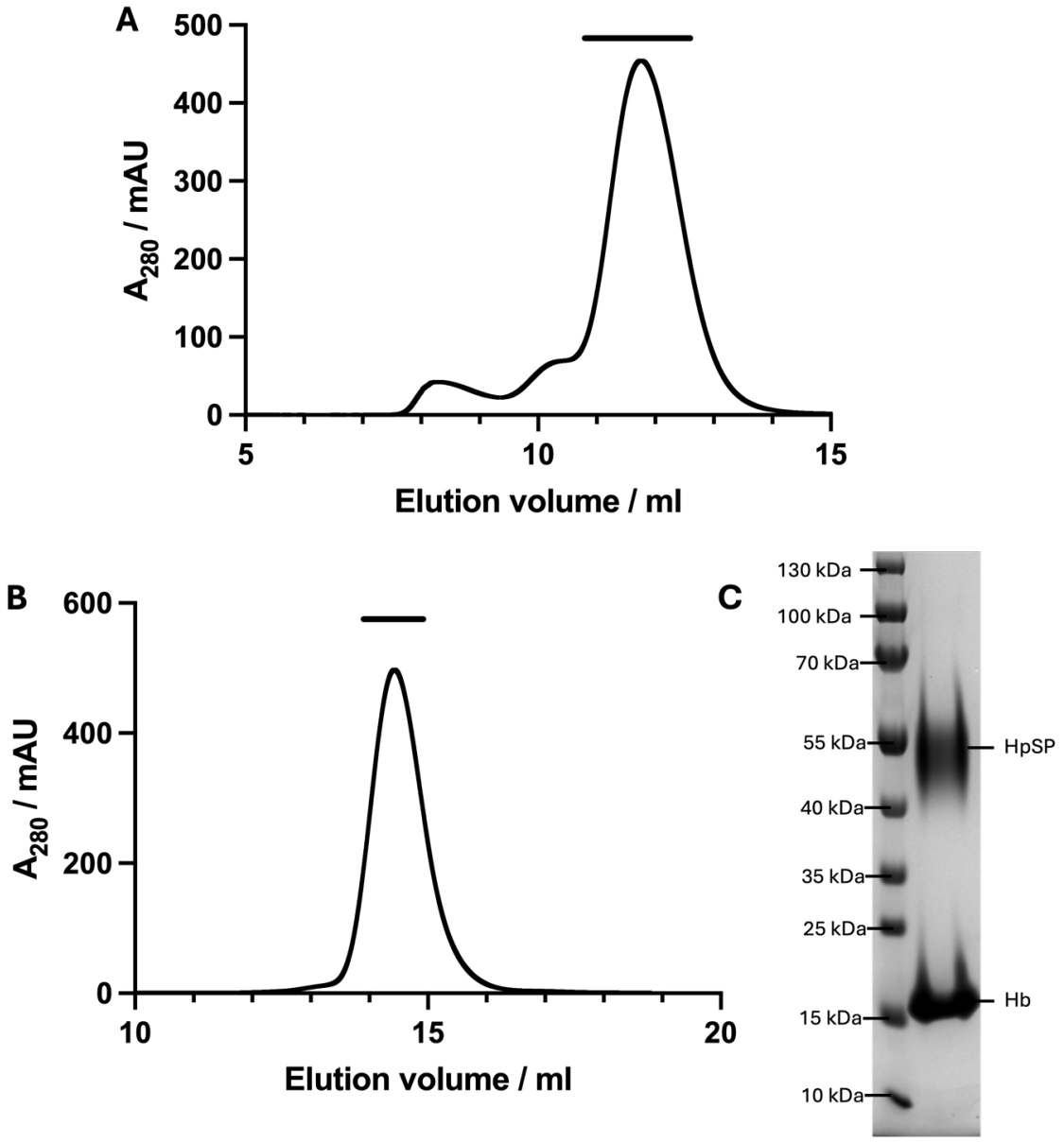


Figure 12: Purification of HpSPHb. A) and B) show the SEC chromatogram of C-tag purified HpSP and HpSPHb, respectively. The black bar above the elution profiles depicts collected fractions. C) Reduced SDS-PAGE gel of purified HpSPHb. The expected molar mass of HpSP is 29.9 kDa, which does not include four predicted N-linked glycans attached to the protein. The Hb $\alpha$- and $\beta$-chains weigh between 15 and 16 kDa.

### 3.2.3 Formation of a haptoglobin phenotype 1-1 complex with haemoglobin

Hp(1-1) is significantly larger than HpSP, which might be helpful as larger complexes have higher contrast in cryo-EM micrographs. Therefore, their complexes with Hb were formed as well. Initially, an excess of purified Hb was mixed with commercially available, lyophilised Hp(1-1). Due to the high affinity interaction between Hp and Hb, this complex formed immediately after mixing and could be directly applied on a HiLoad 16/600 Superdex 200 column. The elution profile shows two non-overlapping peaks with the first one containing pure Hp(1-1)Hb and the second consisting of excess Hb (Figure 13).

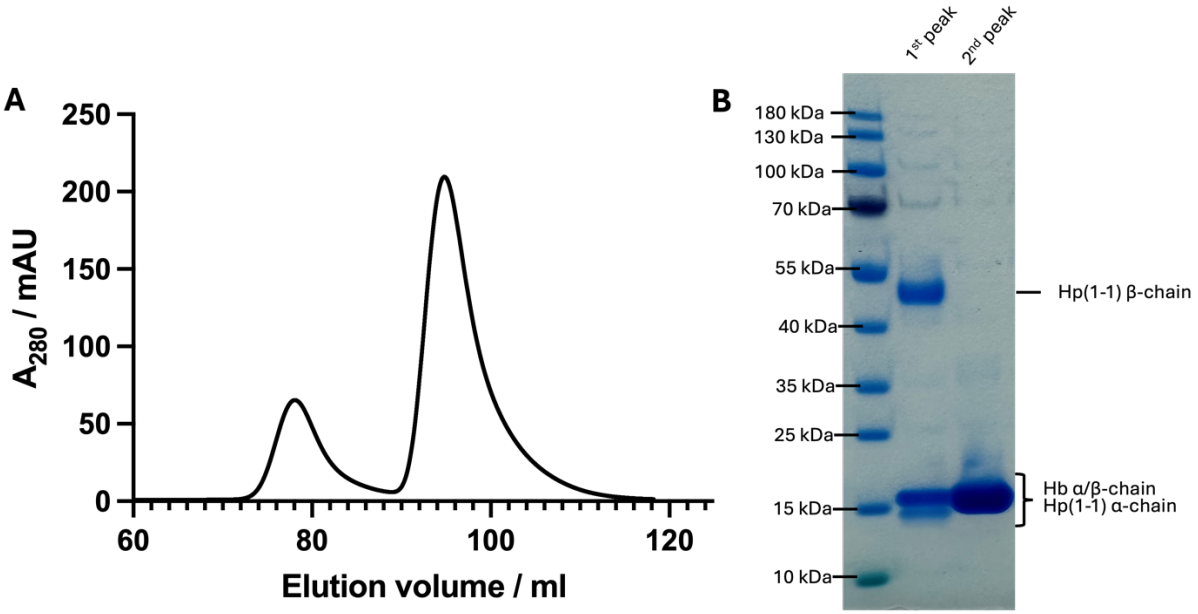


Figure 13: Formation of Hp(1-1)Hb. A) SEC chromatogram of a mixture containing Hp(1-1)Hb and excess Hb. B) Reduced SDS-PAGE analysis of first and second peak in SEC elution trace. The α- and β-chain of Hp(1-1) have a molecular weight of 15.9 and 27.3 kDa, respectively. The mass of the β-chain does not account for four N-linked glycans.

## 3.3 Purification of a CD163-haptoglobin-haemoglobin complex

### 3.3.1 Design of the CD163 expression constructs

Having obtained pure HpHb complexes, I next expressed and purified CD163. A previous publication described the production of the five membrane-proximal SRCR domains of CD163 (R. Li et al., 2018). The authors expressed the protein in *D. melanogaster*-derived

Schneider 2 cells and purified it using a combination of immobilised metal-ion affinity chromatography (IMAC), ion-exchange chromatography (IEX) and SEC.

However, a human protein can likely be expressed more effectively by human cells. Furthermore, the use of a more specific purification tag reliant on antibody or nanobody interaction could lead to a purer sample without the need of another step of chromatography. This could also increase the yield as additional steps in purification are associated with losses of protein. Therefore, expression of CD163 was attempted in Expi293F cells using the mammalian expression vector pHLsec. To obtain a pure sample, a C-tag, which is specifically detected by a nanobody, was fused to CD163 (De Genst et al., 2010).

To design the expression construct, the transmembrane topology was first assessed using DeepTMHMM (Hallgren et al., 2022), a webserver that employs a deep learning model to predict transmembrane architecture. For CD163, DeepTMHMM identified a short signal peptide followed by a 1,005-residue long ectodomain (Figure 14). At the C-terminus, a transmembrane helix and a short cytoplasmic region were predicted. Since the ectodomain is predicted to bind HpHb (Madsen et al., 2004), the boundaries predicted by TMHMM were used to guide the design of an ectodomain construct.

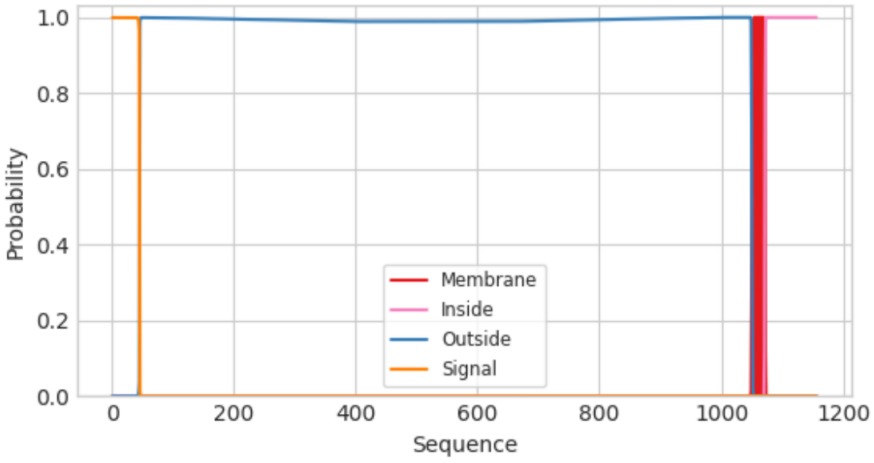


Figure 14: DeepTMHMM prediction (Hallgren et al., 2022) of transmembrane topology for human CD163. The image was directly sourced from the output of the webserver.

AlphaFold2 (Jumper et al., 2021) was used to further guide the design of the construct by precisely predicting domain boundaries. The prediction for CD163 (Figure 8) included

domain boundaries for the N- and C-terminal SRCR domains, which were used to define the first and last amino acid residues of the expression construct. This construct was codon-optimised for production in human cells.

For crystallography, the domain boundaries of the five N-terminal SRCR domains that were shown to bind to HpHb were predicted using AlphaFold2, and the SRCR1-5 construct was cloned into a mammalian expression vector. However, this was not progressed to purification as an initial cryo-EM reconstruction, using full-length CD163 showed that CD163 is composed of dimers and trimers and therefore heterogenous, which would make crystallisation unlikely. Therefore, the crystallography component of the project was not pursued.

### 3.3.2 Expression and purification of CD163

After transfection of Expi293F cells with the full-length CD163 ectodomain construct, and incubation for four days, the cell supernatant was subjected to C-tag purification. Due to the expected molar mass of CD163 at 109 kDa per protomer, the protein was then SEC-purified on a Superose 6 Increase 3.2/300 column. The protein mainly eluted as a homogenous peak (Figure 15) at a slightly earlier elution volume than expected based on mass standards and their elution volumes according to cytiva's manual for Superose 6 3.2/300. SDS-PAGE analysis, however, showed that the peak predominately contained a single protein at the expected molecular weight for CD163 (Figure 15).

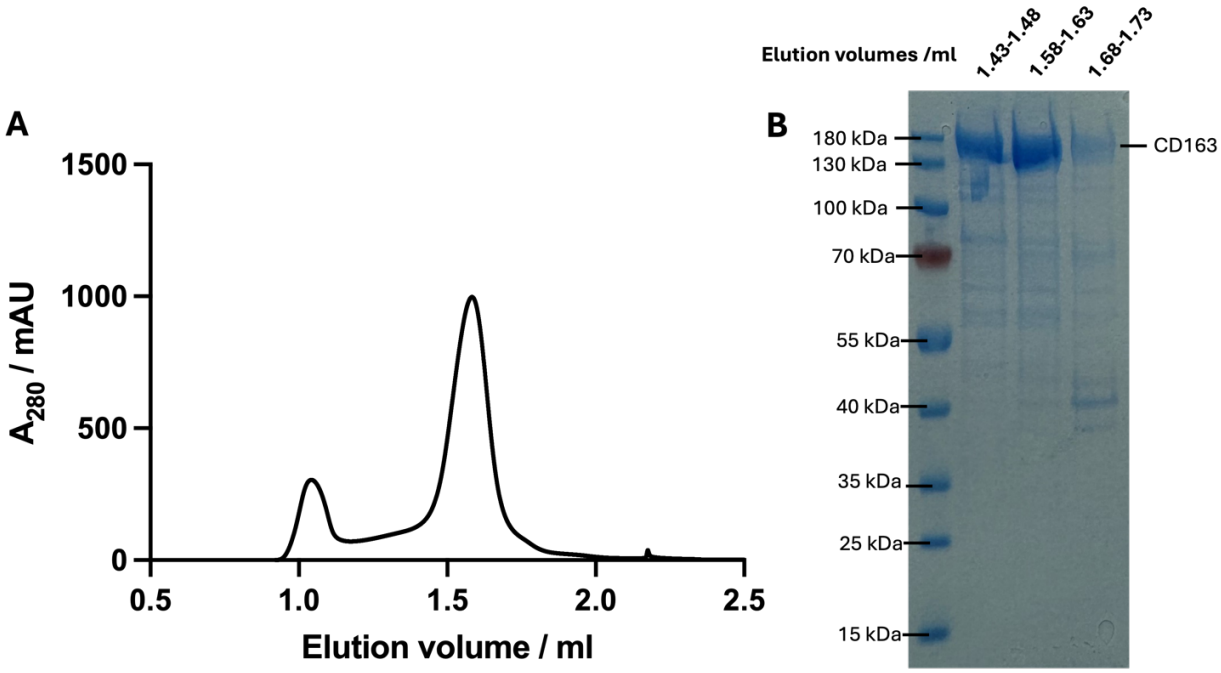


Figure 15: Purification of CD163 by SEC. A) and B) show the SEC chromatogram and a reducing SDS-PAGE gel, respectively. CD163 has an anticipated molar mass of 109 kDa, which does not include five predicted N-linked glycans.

### 3.3.3 Formation of a complex of CD163 and Hp(1-1)Hb

A direct way to validate the functionality of purified CD163 is to assess its binding to HpHb. SEC can be used to demonstrate complex formation since complexes have a larger hydrodynamic radius than their individual components, which would cause a peak shift towards earlier elution times. Furthermore, applying the sample on a SEC column would remove aggregated material, which has very large molecular weights, and uncomplexed components, which have molar masses smaller than the complex. The purified complex is also suitable for grid preparation in cryo-EM as the particles seen should predominately be the protein complex assuming it does not fall apart during plunge freezing.

Hp(1-1)Hb was tested at first because it was proven to bind to CD163 (Kristiansen et al., 2001) and it is homogenous in molecular weight, unlike Hp(2-2)Hb. An excess of Hp(1-1)Hb was mixed with CD163 and incubated for 20 min at RT before the sample was injected on a Superose 6 Increase 3.2/300 column. The SEC chromatogram displayed

two peaks, with the first containing CD163, the Hp α- and β-chains as well as the Hb α- and β-subunits (Figure 16). This peak is also shifted compared to the peak for CD163 alone (Figure 15). The second peak was comprised of mainly Hp and Hb with decreasing amounts of CD163 (Figure 16). Overall, this indicates that the first peak contained a complex of CD163 and Hp(1-1)Hb whereas the second corresponded to excess Hp(1-1)Hb.

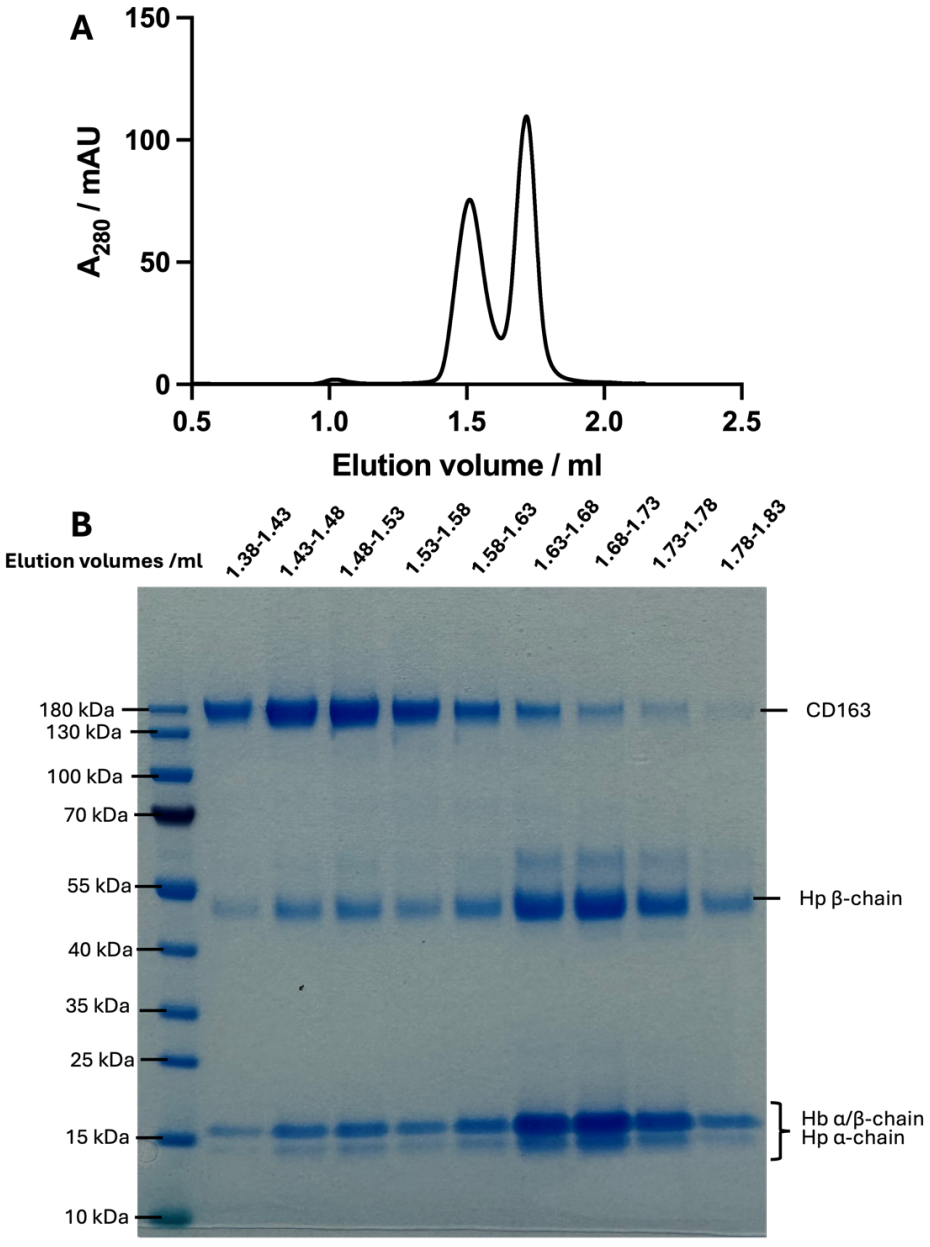


Figure 16: Complex formation of CD163-Hp(1-1)Hb. A) and B) correspond to the SEC chromatogram and a reducing SDS-PAGE gel, respectively. Elution volumes in ml of the analysed fractions are displayed above the respective lanes of the gel.

### 3.3.4 Formation of a complex of CD163 and HpSPHb

While a complex of CD163 and Hp(1-1)Hb is suitable for cryo-EM analysis, obtaining a second complex with a different shape could be beneficial if CD163-Hp(1-1)Hb shows preferred orientation, potentially due to its interaction with the air-water-interface. Considering that HpSP lacks the CCP domain and is monomeric, its complex with CD163 is likely to have a different shape than CD163-Hp(1-1)Hb.

CD163-HpSPHb was prepared in the same manner as CD163-Hp(1-1)Hb and subsequently subjected to SEC on a Superose 6 3.2/300 column. The sample eluted as two distinct peaks (Figure 17A). The first peak contained CD163, with traces of Hb and even smaller amounts of HpSP (Figure 17B). While affinity was initially considered a possible explanation, it was later determined that the likely cause was the stoichiometry of the complex, with a significantly larger mass of CD163 incorporated into the complex compared to its ligand. The second peak corresponded to excess HpSP.

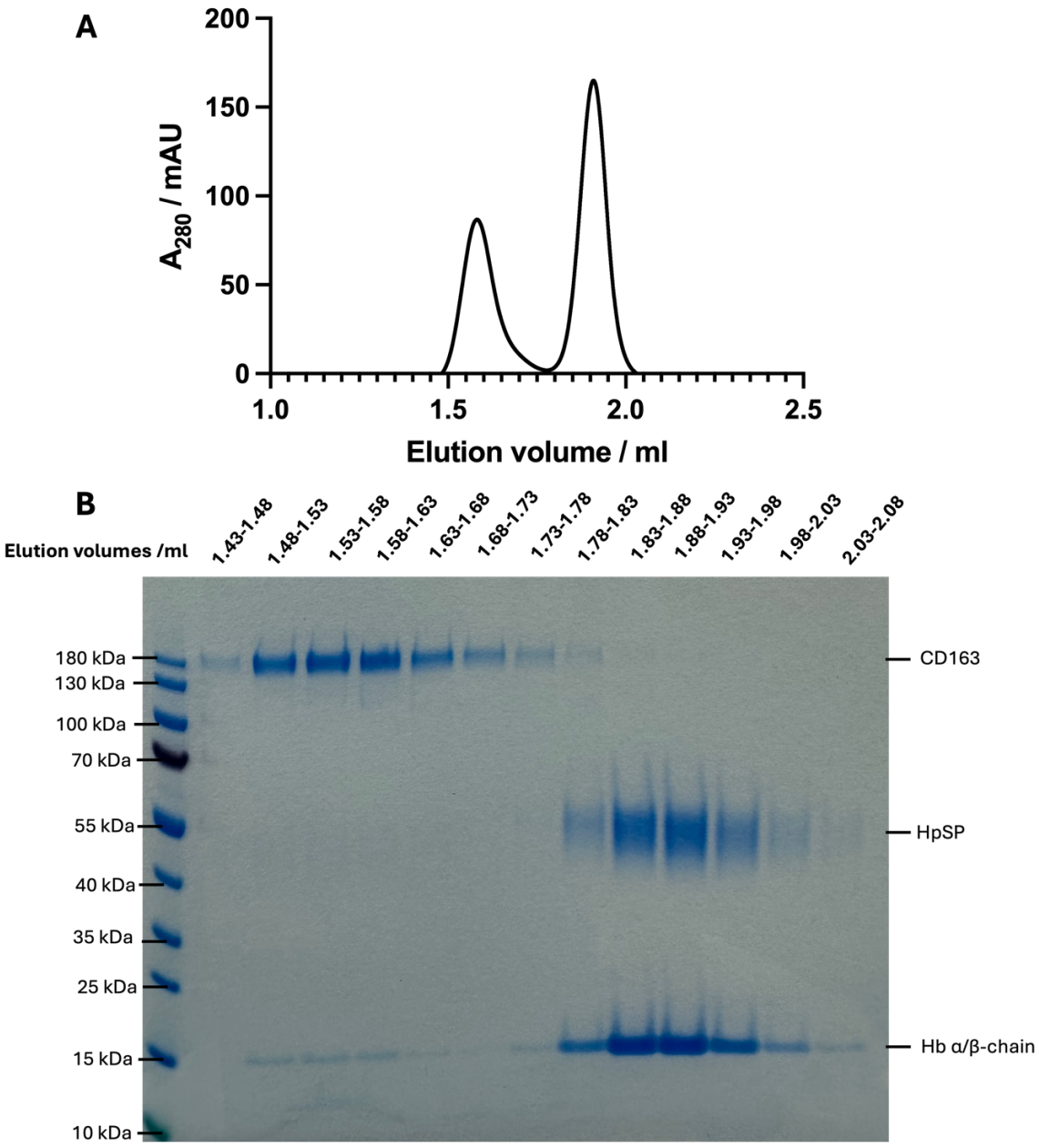


Figure 17: Formation of CD163-HpSPHb. A) SEC chromatogram for assembly of CD163 with excess HpSP. B) Reducing SDS-PAGE analysis of fractions from SEC.

## 3.4 Structural characterisation of CD163-Hp(1-1)Hb using cryo-EM

### 3.4.1 An initial low-resolution reconstruction of CD163-Hp(1-1)Hb

Having obtained a CD163-HpHb complex, the next goal was to elucidate its structure. Since CD163-Hp(1-1)Hb is larger than CD163-HpSPHb, the complex with Hp(1-1) was screened at first for cryo-EM grid production. In cryo-EM, large complexes scatter more electrons elastically, which produces a higher signal-to-noise contrast (Vinothkumar & Henderson, 2016). Additionally, large complexes are more likely to have a distinctive shape, which increases the probability that different projections can be observed, aiding classification and reconstruction. As a result, larger molecular assemblies require a less concentrated sample that is applied onto a grid. However, for the first screening session, the primary objective is to see particles. Therefore, 0.7 mg/ml CD163-Hp(1-1)Hb was applied onto grids, which is a high concentration for a complex exceeding 250 kDa (Vinothkumar & Henderson, 2016).

Particles were clearly visible in grid holes during the first screening session (Figure 18A). It is notable that these grids lacked a continuous carbon support, which is where particles often preferably adsorb. Interestingly, some of the particles appear to have the Hp(1-1)Hb 'dumbbell' shape (Andersen et al., 2012), suggesting that at least one component of the complex was being visualised. But the particles were excluded from the centre and forced towards the edges of the grid hole. This observation indicated that the ice layer, which is thinnest at the centre of a hole, was too thin to accommodate proteins in this region.

A key parameter that controls ice thickness is the blotting time, which is the duration for which the sample is blotted before being plunge frozen. Generally, shorter blotting times lead to grid holes with thicker ice. However, in this project this was not always true, which is why each grid was individually screened before data was acquired on the respective grids. Blotting time was optimised along with sample concentration to achieve optimal protein distribution at a high density without particle overlap (Figure 18B).

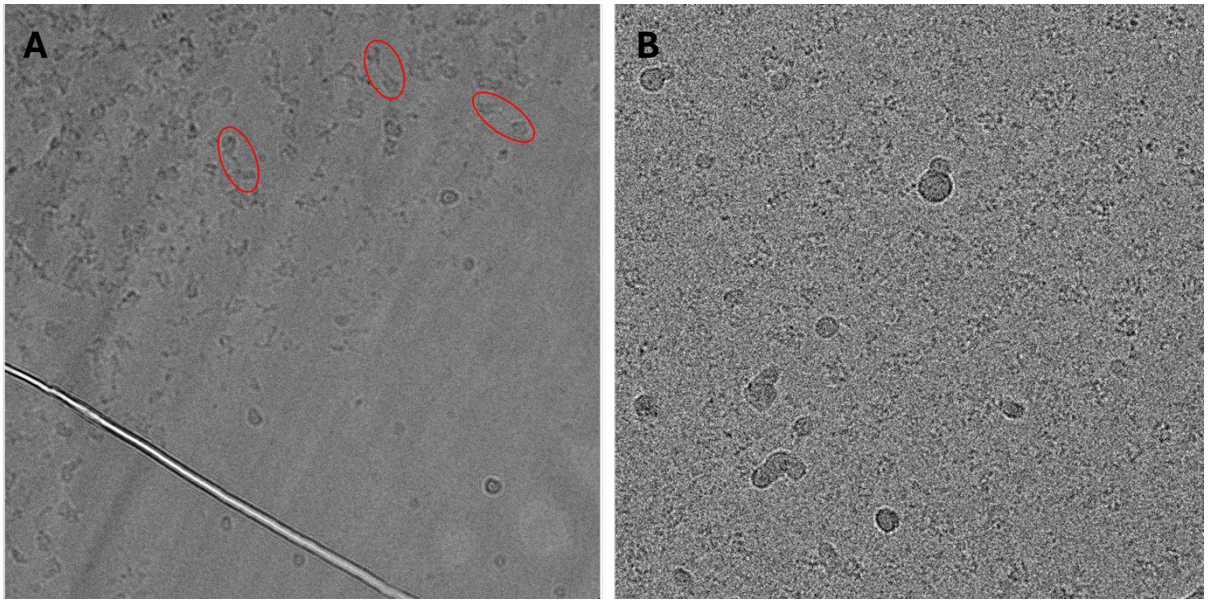


Figure 18: Micrographs of grids prepared before and after optimisation of blotting time and concentration. A) shows a Quantifoil R 1.2/1.3 Cu 300 grid frozen with 0.7 mg/ml CD163-Hp(1-1)Hb at a blotting time of 4 s and a blot force of – 2. Red circles highlight potential CD163-Hp(1-1)Hb complexes that have the Hp(1-1)Hb 'dumbbell' shape. B) depicts a Quantifoil copper grid frozen with 0.5 mg/ml complex at a blotting time of 8 s and a blot force of - 2.

An optimised grid (0.5 mg/ml complex, blotted for 8 s at a blot force of - 2) underwent overnight data collection on the Talos Arctica at a pixel size of 1.5 Å and a dose of 29.98 $e^-/Å^2$. 2,483 micrographs were motion-corrected using SIMPLE 3.0 while subsequent processing was done using CryoSPARC v4.2-4.4. Following CTF estimation using CTFFIND4, exposures with a CTF resolution fit below 15 Å were subjected to template picking using a template generated from a pilot data collection (Figure 19A). Afterwards, 1,200,607 particles were extracted and subjected to three rounds of 2D classification, retaining only 2D classes that resembled actual particles. The final 2D classes were characterised by a triangular shape with a strong density at the centre of each side (Figure 19B). A total of 362,381 particles were subjected to *ab initio* reconstruction. Of the three generated classes, one corresponded to an promising volume, potentially representing CD163-Hp(1-1)Hb. This volume resolved to 6.3 Å and was reconstructed from multiple projections (Figure 19C and D). The other two reconstructed volumes had a lower signal-to-noise ratio and only had partial features of the more promising map.

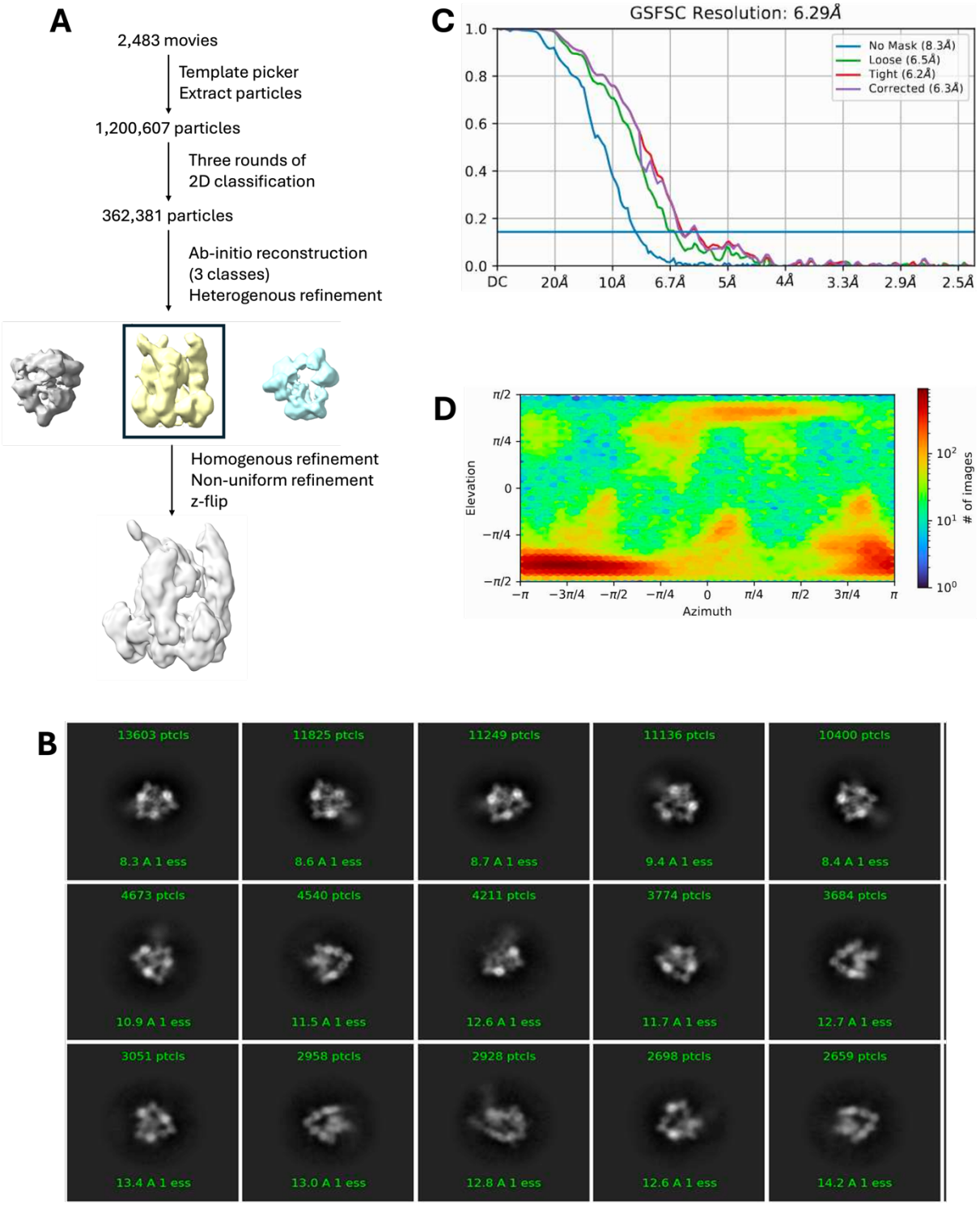


Figure 19: Cryo-EM analysis of CD163-Hp(1-1)Hb. A) Flow chart depicting the processing pipeline for CD163-Hp(1-1)Hb. B) Classes obtained in the final round of 2D classification. Only a selection is shown. C) Gold-standard FSC curve for final 3D map of the complex. D) Particle angular distribution during the last round of non-uniform refinement.

The 3D volume obtained after non-uniform refinement had a resolution sufficient to resolve α-helices of haemoglobin and individual SRCR domains (Figure 20A). This enabled the docking of the CD163 AlphaFold 2 model (Figure 8) as well as the structure of Hp(1-1)Hb (Andersen et al., 2012). Based on this docking, I developed a model that suggested the 3D volume has remarkable features with direct implications for how CD163 binds to Hp(1-1)Hb.

According to the model, CD163 forms a trimer with a triangular 'base' composed of the five C-terminal SRCR domains of each protomer (Figure 20B). Furthermore, the four N-terminal domains of the CD163 protomers form 'arms' that each interact with only one 'head' of Hp(1-1)Hb. This mode of binding is particularly surprising given that Hp(1-1)Hb is an asymmetric ligand (Andersen et al., 2012). The model further suggests that the C-terminal SRCR domains are membrane-proximal, implying that the triangular base is positioned directly above the cell membrane. The 'arms' are positioned in a way that they point away from the membrane and are free to scavenge the ligand from the extracellular space.

When decreasing the contour levels of the map, the second 'head' of the Hp(1-1)Hb dumbbell becomes visible (Figure 20C). Surprisingly, there is no evidence of another trimer of CD163 bound to the second 'head'. This could either be caused by the concentration of CD163 being too low, steric clashes of two CD163 trimers binding or the box sizes for particle extraction being too small, causing signal from the other 'head' to be removed.

While the preliminary volumes generated provided initial insights into the mechanism of HpHb scavenging by CD163, the structural details of the complex were not visible. Therefore, further cryo-EM analysis was conducted to ultimately produce a high-resolution reconstruction of CD163-HpHb.

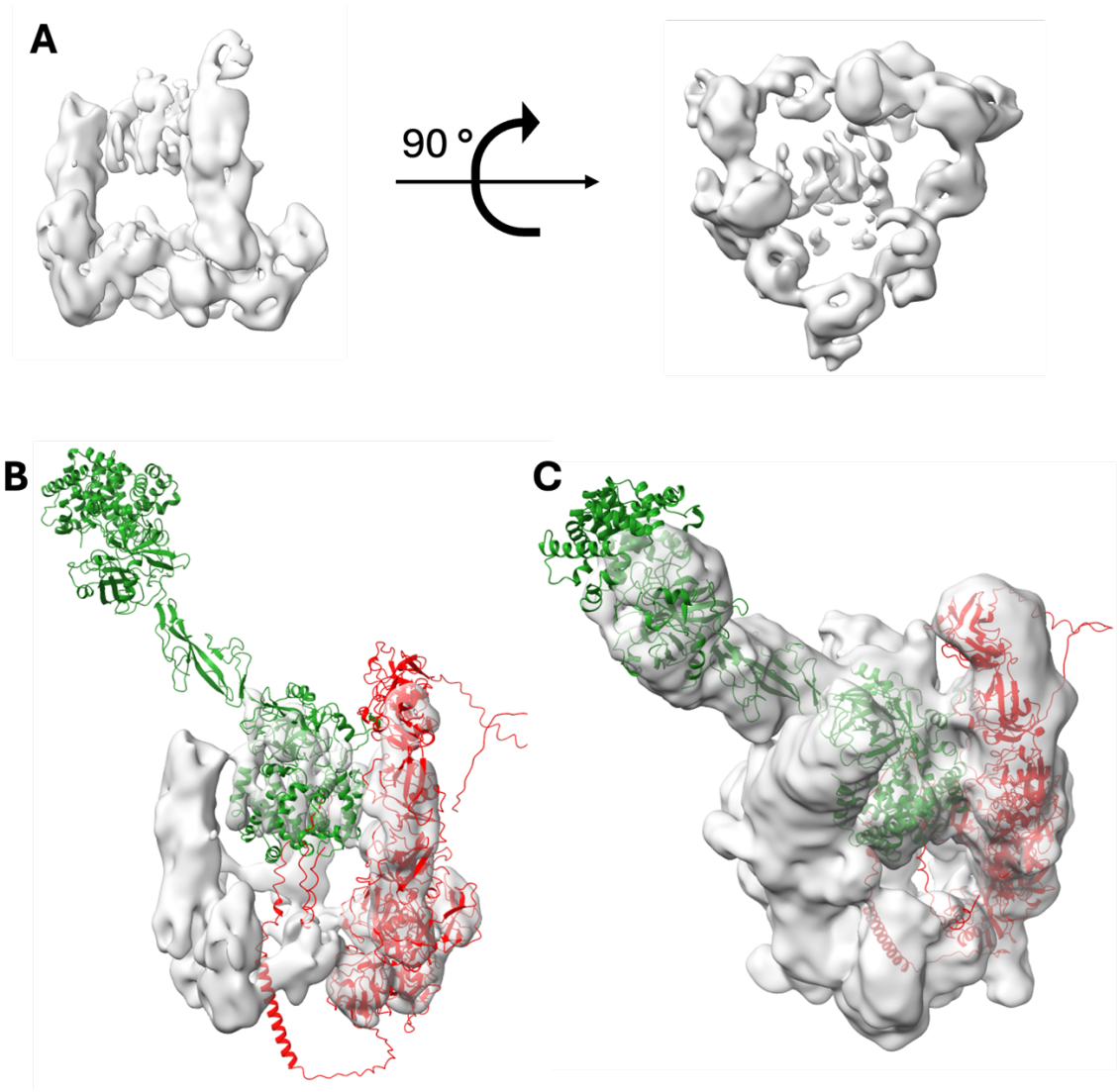


Figure 20: Preliminary map and model of the CD163-Hp(1-1)Hb complex. A) 6.3 Å volume of CD163-Hp(1-1)Hb obtained from an overnight collection on Talos Arctica. B) Volume with Hp(1-1)Hb structure (green) and AlphaFold2 prediction of CD163 (red) docked in. C) Volume at lower contour level showing the second Hp(1-1)Hb 'head' without a second CD163 bound to it.

### 3.4.2 Structural analysis of CD163-HpSPHb via cryo-EM

Although the map of CD163-Hp(1-1)Hb provided valuable structural insights, the reconstruction showed signs of preferred orientation (Figure 19D). Moreover, while the particles had a distinguishable 'dumbbell' shape when separated apart on the micrographs, 'heads' of different Hp(1-1)Hb molecules can be mistakenly grouped into the same particle when particles are close to each other. Conversely, the CD163-

HpSPHb particle is unlikely to suffer from the same issue, as the absence of the CCP domains prevents the dimerisation of Hp.

Optimal grids were obtained at 0.3 mg/ml CD163-HpSPHb and a blotting time of 3 s at a blot force of 7. An overnight collection on the Talos Arctica at a pixel size of 1.2 Å and a dose of 29.94 $e^-/Å^2$ yielded 2,004 movies. From there, 2,315,400 particles were picked using a template from a previous data collection and extracted (Figure 21A). After three rounds of 2D classification, 509,147 particles resembling a CD163 complex were selected for *ab initio* reconstruction (Figure 21B). Although all three classes showed the 'base' of the CD163 trimer, only one class displayed the 'arms' of CD163 along with a ligand bound. This class was subjected to non-uniform refinement. The resolution estimation provided by CryoSPARC at 5.2 Å is likely an under-estimation given the irregular shape of the gold-standard FSC curve (Figure 21C). It is notable that this complex had significant preferred orientation (Figure 21D).

This complex exhibited virtually the same global features as CD163-Hp(1-1)Hb with one notable exception: the density for the CCP domains of Hp(1-1)Hb is missing (Figure 22). This is expected due to the CCP domain being absent from HpSP. Aside from that, the overall architecture of this complex resembles that of CD163-Hp(1-1)Hb supporting the previous interpretation, including the trimerisation of CD163 at the 'base' and the asymmetric ligand binding using the 'arms'.

The absence of the CCP domains could also be the reason for the preferred orientation, as the interaction of the Hp(1-1) 'dumbbell' with the air-water-interface might lead to views of the complex from the side of the 'arms'. Since the CCP domains are absent, CD163-HpSPHb is primarily imaged from the perspective of the triangular base. Overall, these datasets demonstrated that CD163-Hp(1-1)Hb is a more suitable complex for an extended data collection because the complex is imaged from a wider range of views.

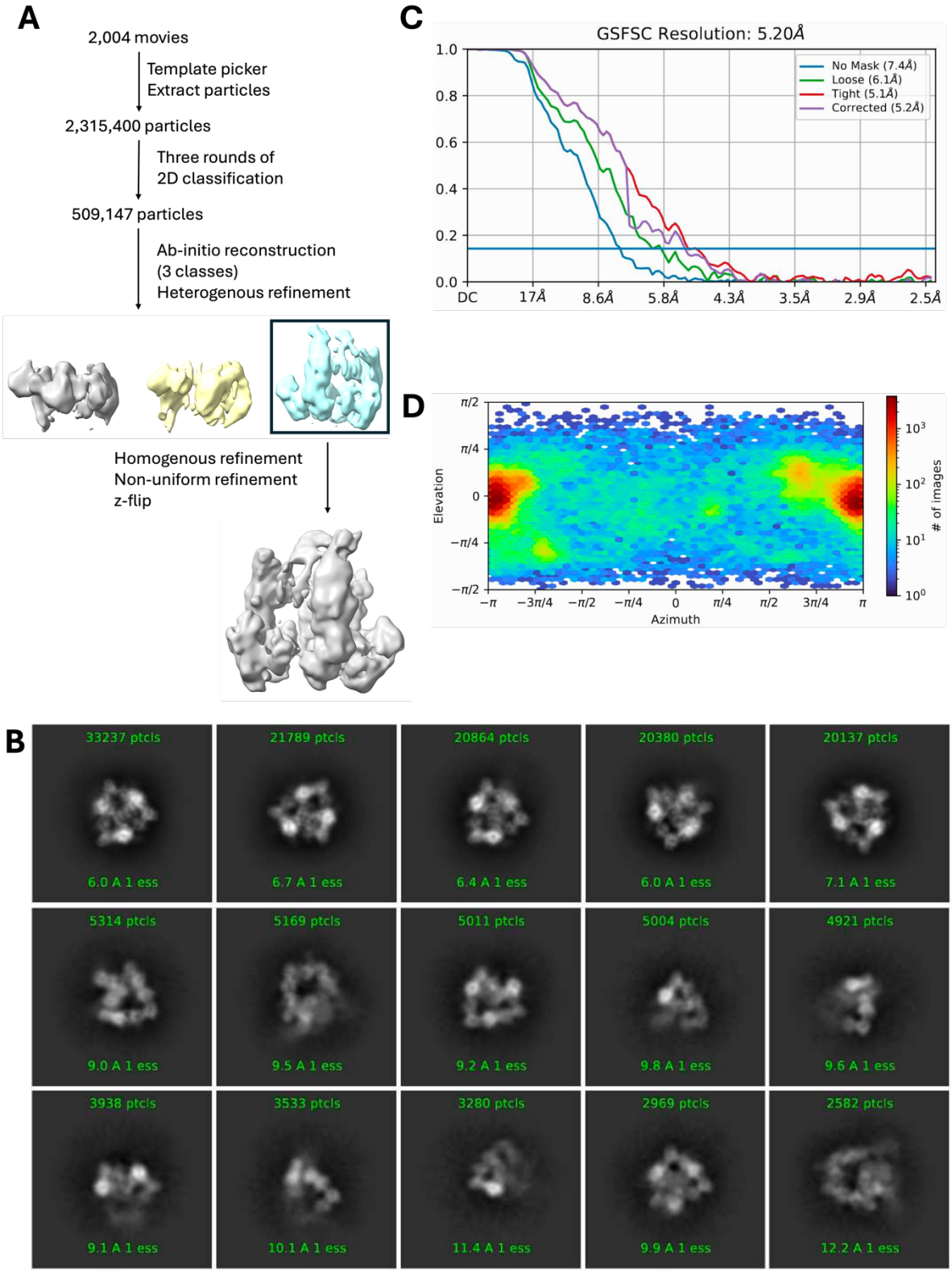


Figure 21: Cryo-EM analysis of CD163-HpSPHb. A) Processing pipeline for CD163-HpSPHb. B) Final 2D classes used for *ab initio* reconstruction. Only a selection is depicted. C) Resolution estimation of the final volume by CryoSPARC. D) Angular particle distribution during non-uniform refinement of the final map.

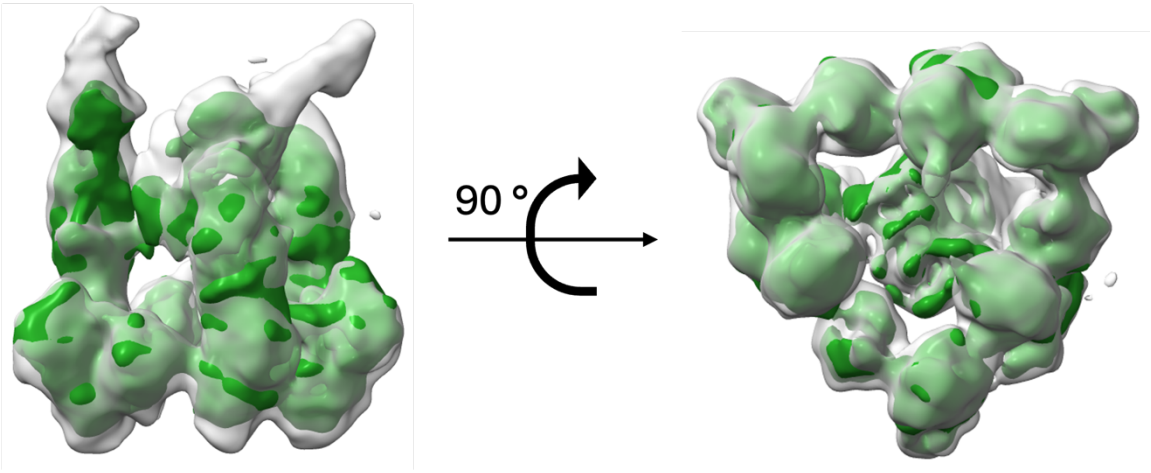


Figure 22: Low-resolution map of CD163-HpSPHb (green) superimposed onto the map of CD163-Hp(1-1)Hb (grey).

### 3.4.3 High-resolution structures of CD163-Hp(1-1)Hb

To obtain a higher resolution reconstruction of CD163-Hp(1-1)Hb, micrographs were collected on a more advanced microscope. The microscope Titan Krios has an energy filter to remove inelastically scattered electrons that would reduce the signal-to-noise ratio. The Krios additionally uses an acceleration voltage of 300 kV, in contrast to the Arctica's 200 kV, which according to the de Broglie equation (Broglie, 1925) enables a shorter electron wavelength. Since optical resolution is directly proportional to wavelength, shorter wavelengths unlock improved resolutions (Abbe, 1873).

The Krios is further equipped with a Cs image corrector reducing the spherical aberration of the objective lens. It uses the Gatan K3 Direct Detection Camera, which has a high detective quantum efficiency (DQE) facilitating movies to be captured at a low radiation dose, thereby reducing the radiation damage done to the biological sample. The K3's ability to collect at a high frame rate along with the use of a bright electron gun, which reduces the exposure time per frame, allows for more micrographs to be collected on the Krios within a given duration. The Krios is engineered for high mechanical stability and is housed in a controlled room, contributing to the collection of higher resolution images.

The benefits of the Krios were combined with an extended collection to capture more particles, particularly particles frozen in a rare orientation. Three grids (with 1.3 mg/ml

CD163-Hp(1-1)Hb, blotted for 2.5 – 4 s at a blot force of 7) were subjected to data collection at a pixel size of 0.832 Å and a dose of 41.68 $e^-/Å^2$ for six days. 39,445 micrographs were pre-processed in SIMPLE and picked using a template from an Arctica collection (Figure 23). The particles identified were subjected to 2D classification as well as 3D reconstruction and refinement to generate an initial volume, which was used as a template to re-pick. The micrographs were re-picked because the template used at first might lack features that a higher-resolution volume from a Krios dataset might exhibit.

After re-picking, 15.7 million particles were found and subjected to three rounds of 2D classification (Figure 23). From these, 3.5 million particles were selected to generate seven initial 3D volumes. Of these, three failed to refine to high resolutions. The remaining four could be grouped into pairs, with two representing two CD163 molecules bound to one HpHb and two corresponding to a trimeric assembly of CD163 bound to one HpHb. Within each pair of the dimer and trimer complex, one volume had more features than the other. The maps with greater detail underwent further 3D-classification. Volumes with nearly identical features were combined and subjected to non-uniform and CTF refinement as well as per-particle defocus optimisation. Finally, high-resolution maps of dimeric and trimeric CD163 bound to Hp(1-1)Hb were obtained and sharpened using DeepEMhancer (Sanchez-Garcia et al., 2021). The dimer resolved to 2.8 Å whereas the trimer resolved to 3.1 Å (Figure 24A and B). Neither map showed substantial preferred orientation, which facilitated refinement to high resolution (Figure 24C and D).

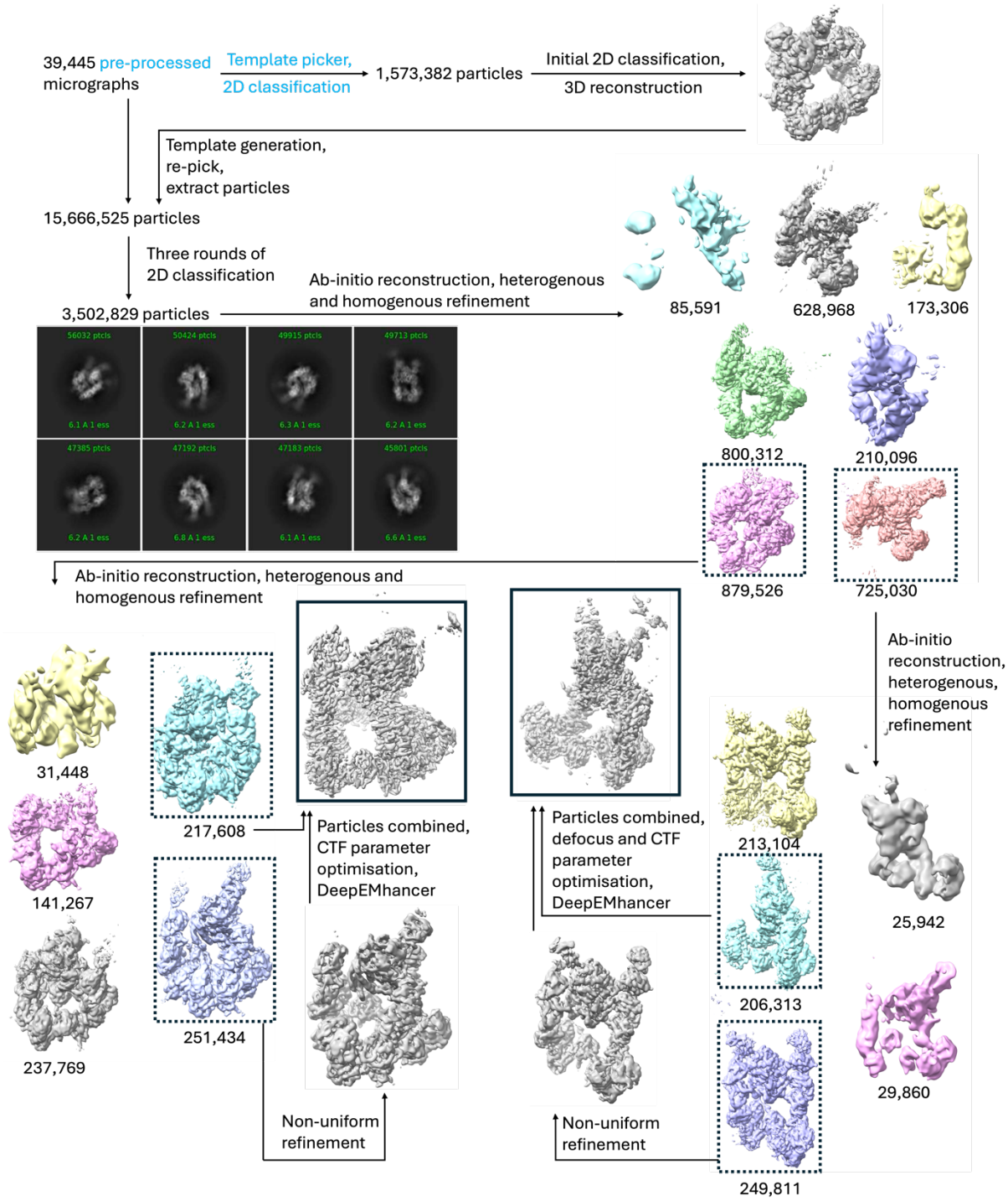


Figure 23: Data processing pipeline for CD163-Hp(1-1)Hb imaged on Titan Krios. Processing steps conducted in SIMPLE 3.0 are written in blue whereas steps performed in CryoSPARC v4.2-4.4 are written in black.

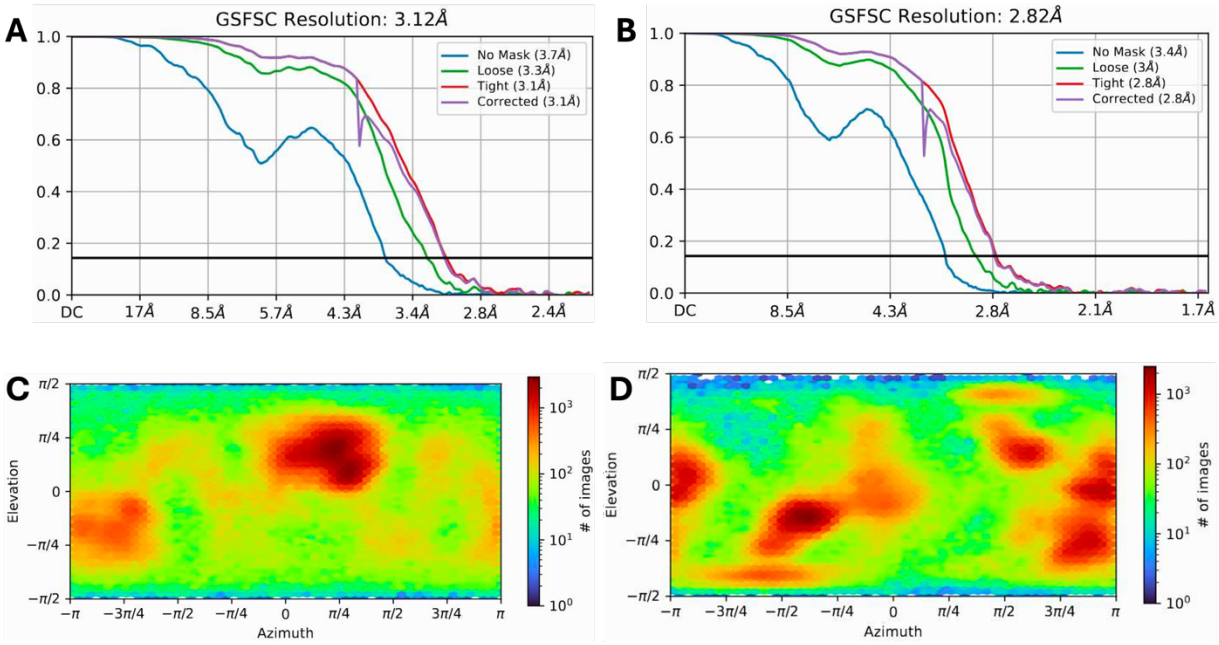


Figure 24: Statistics of the trimeric and dimeric CD163-Hp(1-1)Hb maps. A) and B) depict the gold-standard FSC curves of the trimer and dimer, respectively. C) and D) display the angular particle distribution during the final refinement of the trimer and dimer complexes, respectively.

After obtaining the high-resolution volumes of the trimer and dimer complexes, the next objective was to build a molecular model into each map. The trimer resolved the trimeric 'base' of CD163 well whereas the dimer exhibited a high resolution for the ligand and the contact sites within the 'arms' of CD163. To construct the models, AlphaFold2 predicted SRCR domains (Figure 8) were docked into the dimer for SRCR domains 2-4 and into the trimer for SRCR domains 5-9 and manually adjusted as needed. A crystal structure of human HpSPHb (Lane-Serff et al., 2014) fit well into the ligand density. As described in detail in Chapter 2.4.3, the models were iteratively refined and adjusted until the geometric constraints and the map-to-model fit reached satisfactory scores.

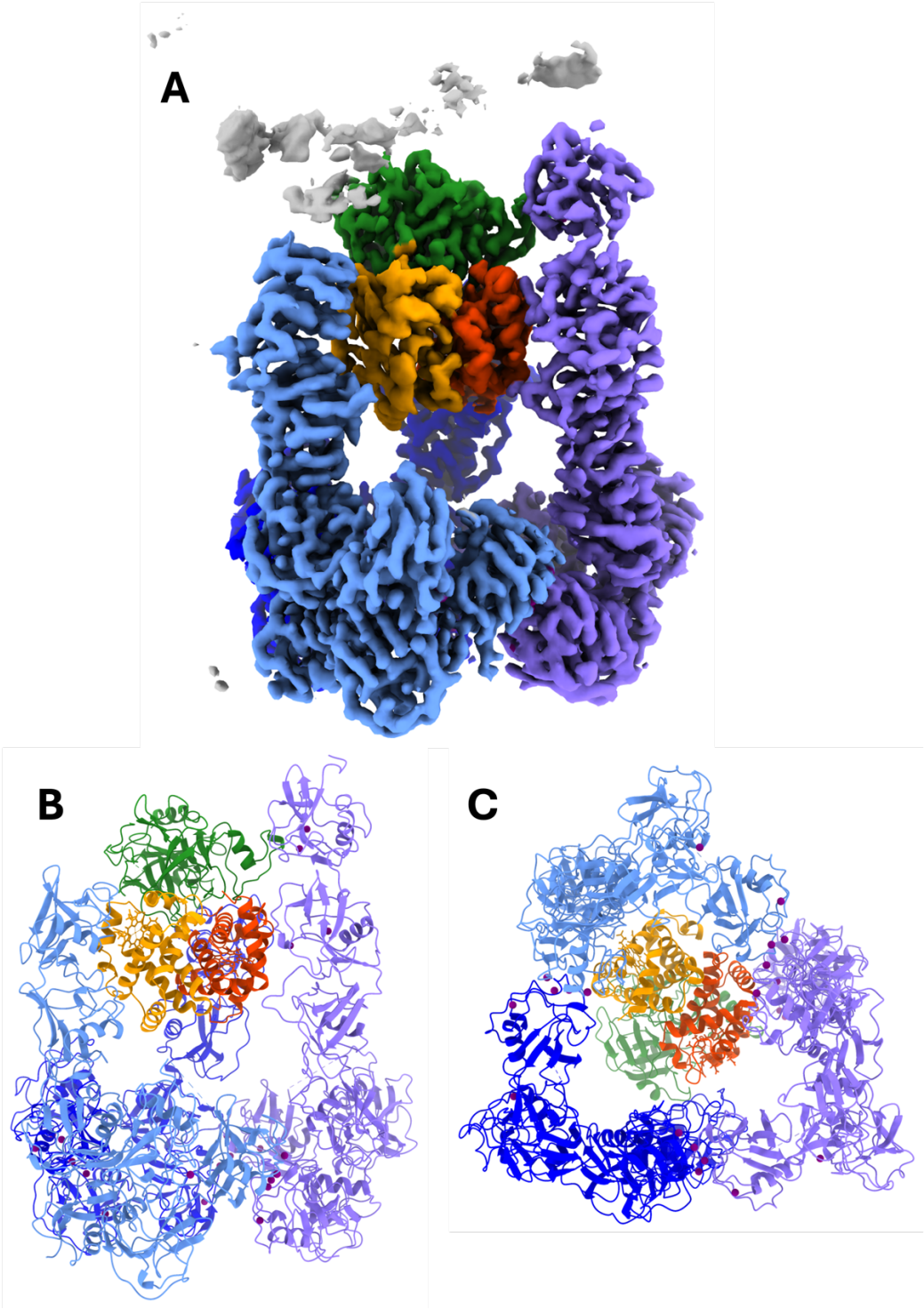


Figure 25: Structure of trimeric CD163 bound to Hp(1-1)Hb. A) 3.1 Å map displayed with chains coloured. The CD163 protomers are depicted in different shades of blue, Hb is shown in orange and red, respectively, and Hp is displayed in green. The violet spheres likely represent calcium ions. B) and C) present the corresponding model from the side and bottom of the complex, respectively.

The structure of trimeric CD163 bound to Hp(1-1)Hb resolves eight out of nine SRCR domains of CD163 in one of the subunits and seven SRCR domains in the other two subunits, as well as Hb and the SP domain of Hp (Figure 25). Within modelled parts of the map, the complex is 145 Å long and 130 Å wide. The map corroborates earlier interpretations presented in Chapter 3.4.1. However, this structure reveals more unexpected features. Two of the three CD163 'arms' interact with both Hp and Hb while the third one only binds to Hb. CD163 binding to Hp and Hb at the same time likely increases its specificity for HpHb over the individual components. Overall, contacts to Hb are overall more extensive than contacts to Hp. Surprisingly, CD163 engages with the asymmetric 'head' of Hp(1-1)Hb from all three sides using the same surface of the three subunits of CD163. These interactions are facilitated by a highly charged surface that both Hp(1-1)Hb and CD163 exhibit. The exact molecular mechanisms underlying these interactions will be discussed in Chapter 4.

Another feature revealed by the model is the presence of spherical densities observed both at the CD163 inter-protomeric interface and at the interface between ligand and receptor (Figure 25B and C). These were thought to likely correspond to calcium ions, as previous studies have shown an effect of calcium of ligand binding (Madsen et al., 2004). This was present in the buffer during grid freezing and regulate this receptor (see Chapter 4).

In addition to the trimer, a dimer of CD163 bound to HpHb (Figure 26) was also identified in the dataset. Subsequent experiments, shown in Chapter 4.2, confirm that the dimer is not an artefact of the trimer disassembling during grid freezing but is genuinely present in solution. Interestingly, while one of the 'arms' adopts the same position found in the corresponding 'arm' in the trimer, the second 'arm' adopts an orientation not found in the trimer (Figure 26B). The variability in the binding site is also enabled by interactions between the highly charged surfaces of ligand and receptor.

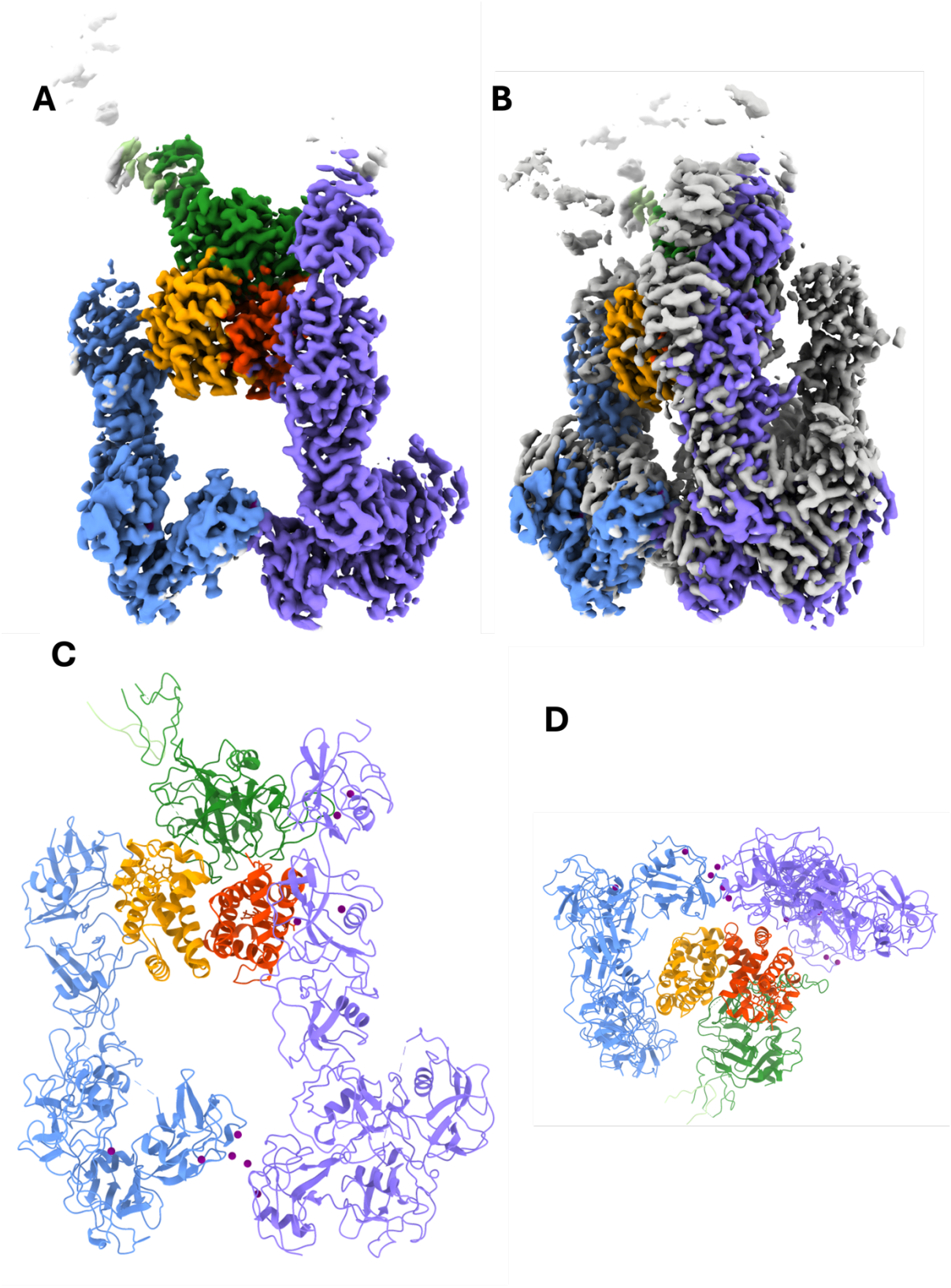


Figure 26: Structure of the CD163 dimer bound to Hp(1-1)Hb. A) 2.8 Å map of the complex. B) Overlay of the dimeric structure (coloured) onto the trimeric map (grey). C) and D) provide different views of the model built into the volume.

Table 3: Cryo-EM data collection, refinement and validation statistics for dimeric and trimeric CD163-Hp(1-1)Hb.

| | Dimeric CD163-Hp(1-1)Hb | Trimeric CD163-Hp(1-1)Hb |
|---|---|---|
| **Data collection and processing** | | |
| Microscope | Titan Krios | |
| Detector | Gatan K3 with BioQuantum Imaging Filter | |
| Magnification | 58,149 | |
| Voltage (kV) | 300 | |
| Electron exposure (e-/Å$^2$) | 41.68 | |
| Defocus range (μm) | -0.4 to -2.0 | |
| Pixel size (Å) | 0.832 | |
| Symmetry imposed | C1 | |
| Initial particle images (no.) | 15,666,525 | |
| Final particle images (no.) | 456,124 | 469,042 |
| Map resolution (Å) | 2.82 | 3.12 |
| FSC threshold 0.143 | | |
| Map resolution range (Å) | 2.25 - 35.8 | 2.54 - 40.9 |
| FSC threshold 0.5 | | |
| **Refinement** | | |
| Initial model used | AlphaFold2, 4X0L, 4WJG | |
| Model resolution (Å) | 3.41 | 3.63 |
| FSC threshold 0.5 | | |
| Model composition | | |
| Non-hydrogen atoms | 15,182 | 22,095 |
| Protein residues | 1,962 | 2,856 |
| Ligands | 23 | 45 |
| B factors (Å$^2$) | | |
| Protein | 80.71 | 83.18 |
| Ligands | 56.07 | 101.47 |
| R.m.s deviations | | |
| Bond lengths (Å) | 0.006 | 0.003 |
| Bond angles (°) | 0.988 | 0.567 |
| Validation | | |
| MolProbity score | 1.98 | 1.59 |
| Clashscore | 8.66 | 5.88 |
| Poor rotamers (%) | 1.37 | 0.30 |
| Ramachandran plot | | |
| Favoured (%) | 93.82 | 96.02 |
| Allowed (%) | 6.08 | 3.95 |
| Disallowed (%) | 0.10 | 0.04 |
| Model vs. data fit | | |
| CC (mask) | 0.68 | 0.70 |
| CC (box) | 0.70 | 0.72 |

## 3.5 Discussion

The structural insights provided in this chapter are novel and surprising. One of the novel discoveries is the multimeric state of CD163, which raises questions about its function. One possible explanation for multimerisation could be related to the regulation of ligand scavenging and release. It is plausible that only multimeric receptor may only take up HpHb. This hypothesis is supported by the absence of a monomeric receptor bound to the ligand. Additionally, the structures reveal that receptor multimerisation is facilitated by calcium ions, whose concentration decreases as the receptor is internalised in endosomes. This reduction in calcium concentration has previously been shown to lead to ligand release, and it is possible that it triggers receptor disassembly within the endosome aiding in HpHb release. Calcium ions are not only present at inter-protomeric interfaces of CD163 but are too observed between receptor and ligand. These ions also likely play a crucial role at facilitating ligand binding in the extracellular space and ligand release in the endosome.

While CD163 bound to Hp(1-1)Hb was shown to form multimers, it is tempting to speculate that unliganded CD163 forms multimers as well. The calcium ions seen at the 'base' of CD163 could mediate multimerisation without the ligand although it is plausible that the ligand further stabilises the multimers by reducing flexibility in the 'arms'.

A consequence of multimerisation is the presence of asymmetric binding. The receptor could have evolved to engage with as many HpHb binding sites as possible to increase its affinity to the ligand and scavenge HpHb even at very low ligand concentrations. Given the toxicity of Hb, this likely provides protective benefits to the host organism. Experimentally, however, it is difficult to validate any hypothesis regarding asymmetric binding. Since CD163 uses a common interface to bind HpHb from all three sides, mutating residues in one 'arm' would affect the binding of other 'arms'. Furthermore, Hb is obtained from its native source, and Hp is purchased from a commercial supplier that purified the protein from plasma, making mutations of Hp or Hb not feasible.

The structures presented here demonstrate that CD163 binds to a single 'head' of HpSPHb with contacts to both Hb and Hp, contrary to predictions made by Andersen et al. (Figure 9). Although initially surprising, this observation provides the ideal explanation for how CD163 prevents uptake of Hp in serum and how CD163 recognises different Hp phenotypes conjugated to Hb which have different multimeric states (i.e. Hp(1-1)Hb vs Hp(2-2)Hb). The structures show very extensive interactions between the receptor and Hb with limited contacts to only the SP domain of Hp. The presumably weak interaction between CD163 and Hp prevents the uptake of the latter from serum before it is conjugated to Hb. Since the binding is exclusive to HpSP, every Hp phenotype can be recognised because they all contain the SP domain. If CD163 predominately bound to Hp, as suggested by Andersen et al., CD163 would not be able to distinguish between different Hp phenotypes. In a 2006 study, D. J. Schaer et al. used an uptake assay to show that Hb can be uptaken by CD163 and postulated that Hb uses the same binding site as HpHb. While a CD163-Hb complex structure is not directly available, Hb likely uses the same binding site as HpHb because CD163 primarily contacts Hb in the structures elucidated. This suggests the possibility of a direct Hb uptake facilitated by CD163, which might be useful when Hp is depleted during extended intravascular haemolysis.

The insights generated in this chapter, including the binding of CD163 to a single 'head' of HpHb, the calcium-mediated multimerisation, and the calcium-mediated mode of ligand binding, will be further explored in Chapter 4.

# 4. Molecular mechanisms of haptoglobin-haemoglobin scavenging by CD163

## 4.1 Summary

The cryo-EM structures of CD163-Hp(1-1)Hb revealed surprising features which are likely to influence the molecular mechanism of HpHb scavenging by CD163. These are characterised and validated through biophysical and cell-based uptake experiments in this chapter.

The first question addressed is how ligand selectivity operates, as CD163 specifically selects for HpHb by binding to a single 'head' of this ligand, making more extensive contacts to Hb than to Hp. Binding and uptake experiments were established and used to compare uptake of HpSPHb, Hp(1-1)Hb, Hp(2-2)Hb, Hb and Hp(1-1) to determine ligand selectivity. For the wild-type receptor, binding affinities and uptake efficiencies across all HpHb constructs were independent of the ligand type and only reliant on concentrations of HpHb 'heads'. In comparison, Hb showed lower affinity and uptake, and Hp exhibited negligible binding and uptake.

Secondly, cryogenic electron microscopy revealed spherical densities at the CD163 inter-protomeric interface and at the interface between receptor and ligand. While these densities could not be directly confirmed as calcium ions through cryo-electron microscopy methods, binding experiments and population-based methods demonstrated that CD163 receptor multimerisation and ligand binding are both separately regulated by calcium. Using a CD163 mutant that cannot multimerise, I was able to show that multimerisation enhances the uptake of Hp(1-1)Hb and Hb but not that of Hp(2-2)Hb. Ligand binding itself is directly controlled by the calcium ions, with neither wild-type receptor nor 'monomer mutant' able to bind HpHb without calcium.

## 4.2 The binding of CD163 to a single ‘head’ of HpHb

### 4.2.1 Formation of a Hp(2-2)Hb complex

The structures showed that a single ‘head’ of the HpHb ‘dumbbell’ binds to CD163, with contacts primarily to Hb (Figure 25 and Figure 26). To validate this observation, the binding affinity and uptake efficiency of Hp(1-1)Hb were compared to those of HpSPHb, Hp(2-2)Hb, Hb and Hp(1-1). For this purpose, all these ligands were purified. While the production of Hb, Hp(1-1)Hb and HpSPHb were described in Chapter 3, the purification of Hp(2-2)Hb is described in the following.

Like Hp(1-1), Hp(2-2) was also acquired from a commercial source. Due to its ability to form higher order oligomers (Tamara et al., 2020), its complex with Hb was separated on the Superose 6 10/300, a column designated for the purification of large protein assemblies. This complex eluted as two distinct peaks with the first containing Hp(2-2)Hb and the second containing excess Hb (Figure 27A). To visualise the large sizes of the Hp(2-2) molecules, the sample was analysed using non-reducing SDS-PAGE (Figure 27B). Performing reducing SDS-PAGE on the same sample confirmed that the complexes were assembled from individual Hp protomers (Figure 27C).

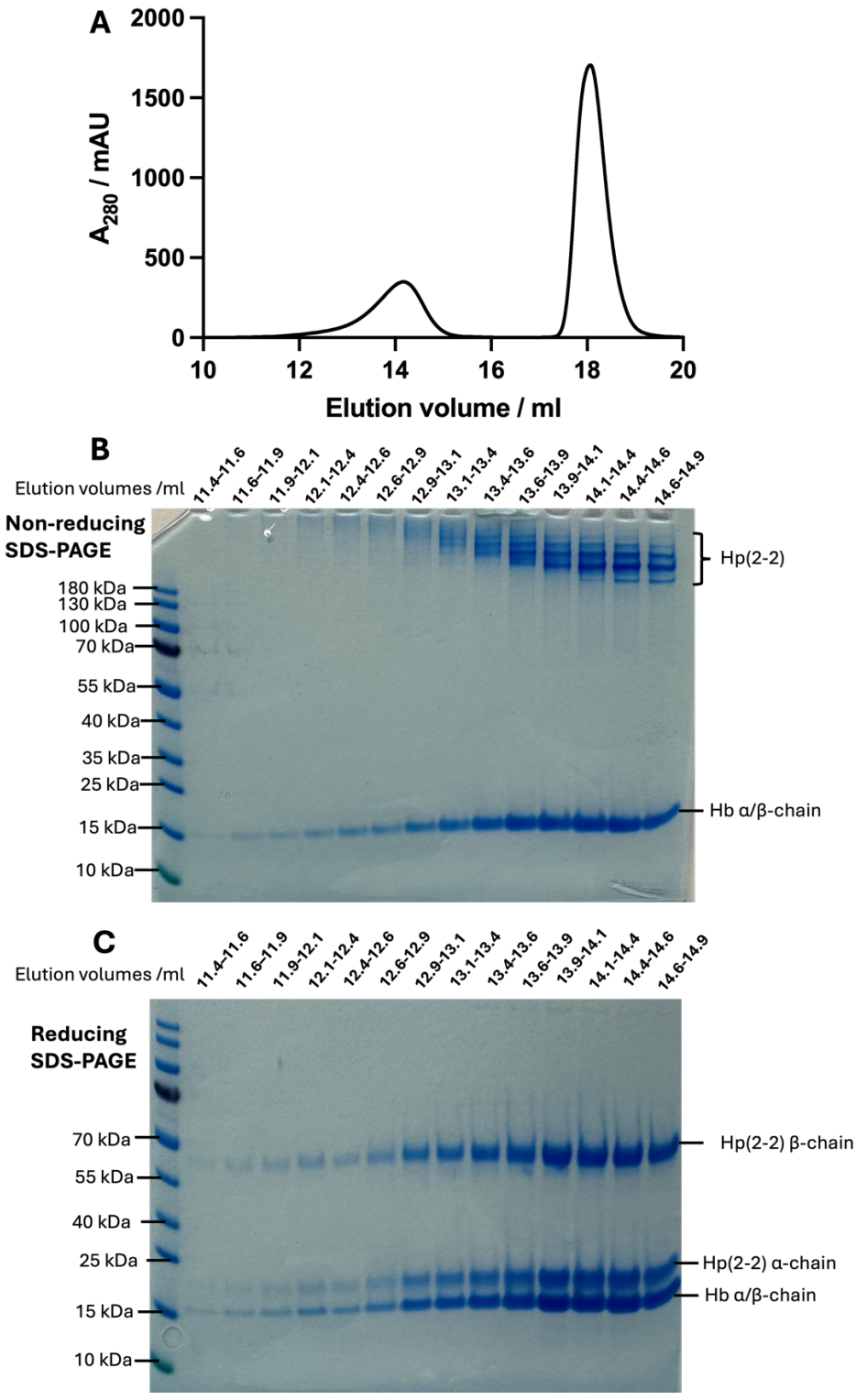


Figure 27: Formation of Hp(2-2)Hb. A) SEC trace of Hp(2-2)Hb with excess Hb. B) and C) depict non-reducing and reducing SDS-PAGE gels of Hp(2-2)Hb. At 17.8 and 27.3 kDa, the α- and β-chain of Hp(2-2) have larger molecular weights than their Hp(1-1) counterparts. The provided mass for Hp(2-2) β-subunit does not account for four covalently attached N-linked glycans.

### 4.2.2 Characterisation of ligand specificity using surface plasmon resonance spectroscopy

To imitate the orientation of a membrane receptor presented on the membrane while capturing a ligand from serum, SPR was set up with CD163, which was immobilised on the SPR sensor chip surface using a biotin-streptavidin interaction. To accomplish that, CD163 was expressed with an Avi-tag at the C-terminus (Fairhead & Howarth, 2015), which was biotinylated during expression (Figure 28A). The biotinylation of CD163 was directly validated in SPR experiments, as CD163 was captured on the chip surface when it was flowed onto immobilised streptavidin (Figure 28B).

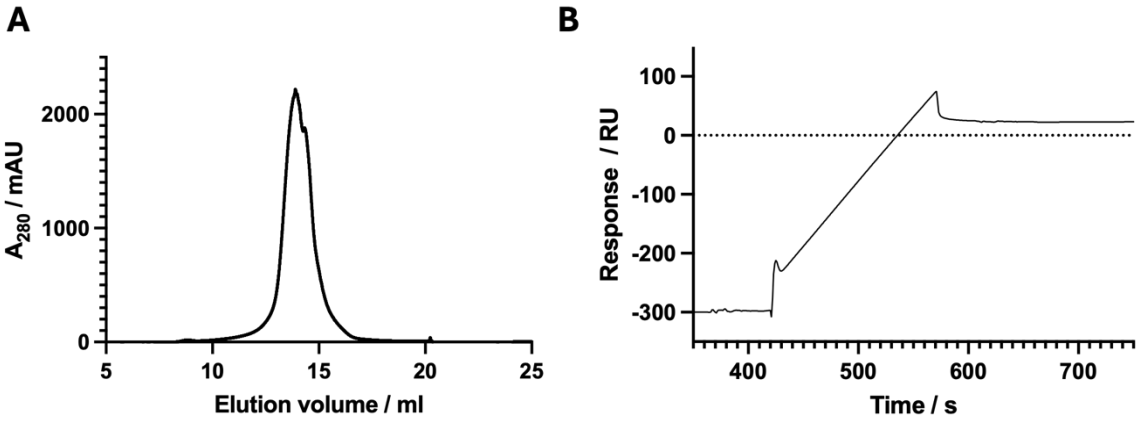


Figure 28: Purification of Avi-tagged CD163. A) SEC chromatogram of Avi-tagged CD163. B) SPR sensorgram for the interaction between biotinylated CD163 and immobilised streptavidin.

Immobilised CD163 enabled the assessment of binding kinetics for the receptor and various ligands (Figure 29 and Table 4). The SPR curves for Hp(1-1)Hb and HpSPHb (Figure 29A and B) both fit a 1:1 binding model, yielding dissociation constants ($K_D$) of 276 ± 35.1 pM and 1.29 ± 0.130 nM, respectively, based on triplicate analysis. These values indicate a high-affinity interaction between receptor and the two ligands, with differences potentially caused by interactions between ligand and SRCR domains unseen in the structure.

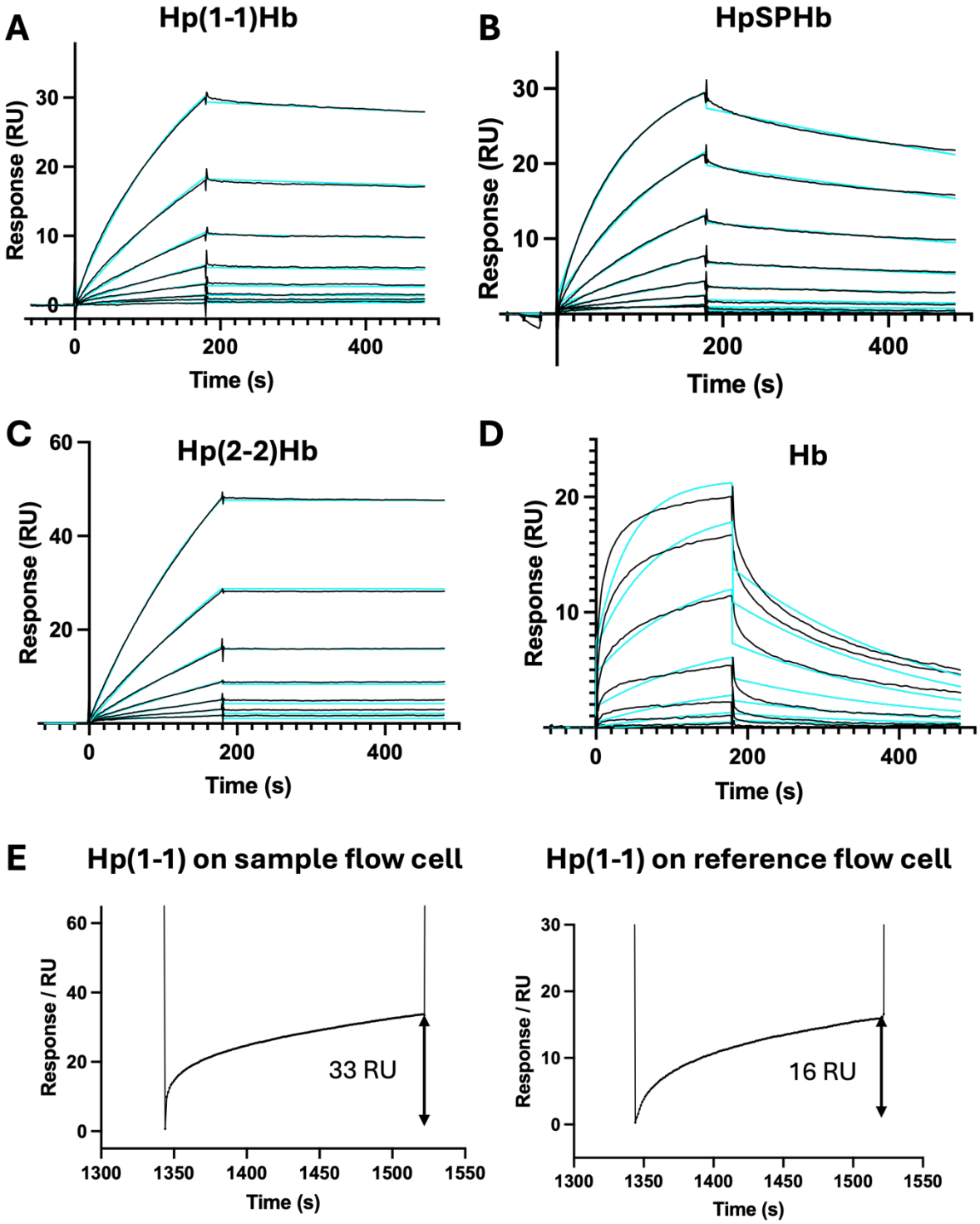


Figure 29: SPR analysis of interactions between wild-type CD163 and various ligands. A) Injection of Hp(1-1)Hb in a two-fold dilution series from 10 – 0.078 nM. B) HpSPHb from 20 – 0.16 nM. C) Hp(2-2)Hb from 10 – 0.16 nM. D) Hb from 2,000 – 31.25 nM. E) Comparison between Hp(1-1) injections on sample and reference flow cell. For A) to D), only one representative measurement was shown although triplicate data was collected for each. In A) to C), the SPR buffer contained HBS with 2.5 mM $CaCl_2$. For D) and E), that buffer was supplemented with 8 mg/ml carboxymethyl dextran.

Table 4: SPR-derived dissociation constants ($K_D$) for the interactions between wild-type CD163 and Hp(1-1)Hb or HpSPHb. Each SPR measurement was performed in triplicate.

| Ligand | $K_D$ ± standard deviation |
|---|---|
| Hp(1-1)Hb | 276 ± 35.1 pM |
| HpSPHb | 1.29 ± 0.130 nM |

When analysing the CD163-Hp(2-2)Hb interaction, it became apparent that the ligand did not dissociate from CD163 even after 5 min (Figure 29C). Since Hp(2-2)Hb forms higher-order oligomers (Figure 7), multiple 'heads' are likely able to bind different CD163 multimers immobilised on the sensor chip surface at the same time, resulting in slower dissociation. This increase in apparent affinity, known as avidity, does not reflect the intrinsic affinity between one 'head' of Hp(2-2)Hb and CD163.

The SPR curves for the interaction between Hb or Hp to CD163 did not produce useful results. While the binding of Hb to CD163 did not fit to a 1:1 binding model (Figure 29D), the SPR curve for Hp closely resembled that of the reference cell, suggesting that CD163 does not bind to Hp (Figure 29E). Since the sensor chip surface contains a streptavidin-oligonucleotide conjugate, addition of DNA (e.g. salmon sperm DNA) to the buffer might reduce non-specific binding to the reference cell and produce a different shape in the SPR curve. Unfortunately, calcium ions are crucial for the CD163 interaction (Chapter 4.4) and caused DNA to precipitate in the buffer, such that this experiment was not successful. Since carboxymethyl dextran is used as a matrix on the sensor chip surface, its addition to the buffer was tested as well. The dextran did not significantly change the shapes of the SPR curves, which are the ones depicted in Figure 29D and E. Therefore, I did not use SPR to quantify the interactions with Hb and Hp.

### 4.2.3 Assessment of the binding of Hb and Hp to CD163 by microscale thermophoresis

Microscale thermophoresis (MST) was used to quantify the interaction between CD163 and Hb or Hp. As described in Chapter 2.3.2, MST measures the thermophoretic movement of molecules, which differs depending on whether proteins are in an unbound state or form a complex. By following the thermophoretic behaviour of a sample containing a fluorescently labelled ligand (Hb or Hp) and a serially diluted, unlabelled ligand (CD163), binding parameters, including the $K_D$, can be quantified.

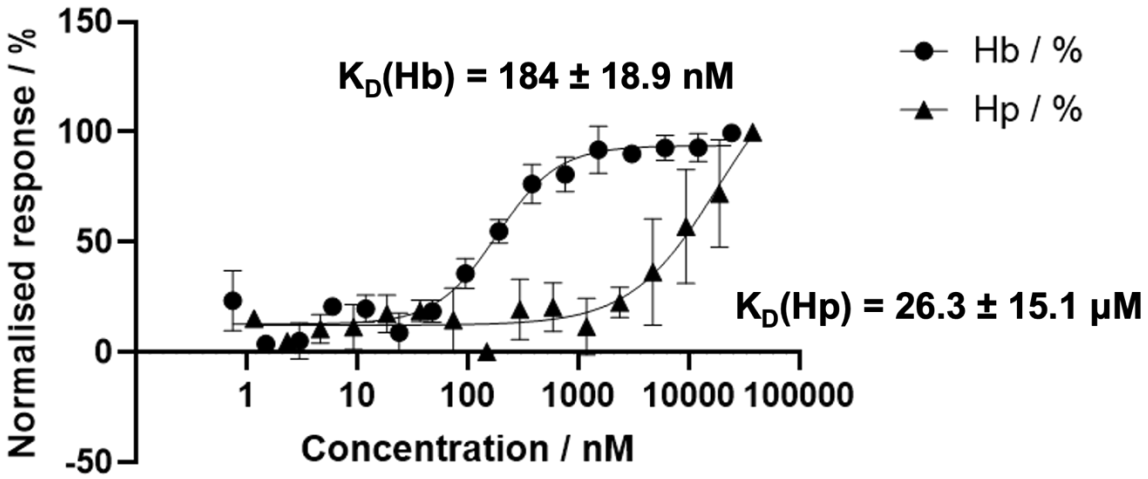


Figure 30: MST responses showing the binding of CD163 to Hb (●) and Hp (▲). Each measurement was performed in triplicate. The dissociation constants are quantified as mean ± standard deviation.

The MST-derived $K_D$ of the CD163-Hb interaction is approximately 184 nM, whereas affinity of CD163 for Hp is 140-fold weaker (Figure 30). These values are significantly larger than the SPR affinities for HpHb and align with structural insights, which suggest that CD163 binds to a single HpHb 'head' and predominately interacts with Hb.

### 4.2.4 Analysis of CD163-Hp(1-1)Hb and CD163-HpSPHb complexes using mass photometry

To further characterise the binding of CD163 to one HpHb 'head', an orthogonal method, mass photometry (MP), was used. In MP, the adsorption of the sample protein onto the glass surface is recorded over time and compared to the movie captured for a mass standard (Sonn-Segev et al., 2020). This comparison is used to determine the molar mass distribution of the proteins present within the sample. Unfortunately, MP has an upper limit of measurable concentration at 100 nM, with concentrations above the threshold causing overcrowding in the movie and peak broadening in the mass distribution. As the affinities of CD163 to Hb and Hp were above the limit, an accurate characterisation of the resulting complexes via MP was impeded. However, MP is still useful to visualise the existence and distribution of multimeric states, particularly for unliganded CD163 as well as the CD163-Hp(1-1)Hb and CD163-HpSPHb complexes, even at low concentrations.

Before analysing CD163-HpHb complexes, CD163, Hp(1-1)Hb and HpSPHb were each characterised independently to obtain their individual molar masses according to MP. At a low concentration of 18 nM, CD163 was predominately monomeric, with some dimers and trimers present (Figure 31A). This finding demonstrates that CD163 on its own is already capable of forming multimers even without the ligand. This was anticipated, as the contacts mediating multimerisation are in the CD163 'base'. As expected, the MP probability densities indicate that Hp(1-1)Hb and HpSPHb form dimeric Hp(1-1)Hb and monomeric HpSPHb, respectively (Figure 31B and C).

I next analysed the complexes of CD163 with its ligands. Upon addition of CD163 to Hp(1-1)Hb and HpSPHb, peaks corresponding to the liganded dimer and trimer appeared (Figure 31D and E). These findings demonstrate that a single 'head' of HpHb binds to CD163 because the 'single-headed' HpSPHb can also induce the formation of liganded complexes.

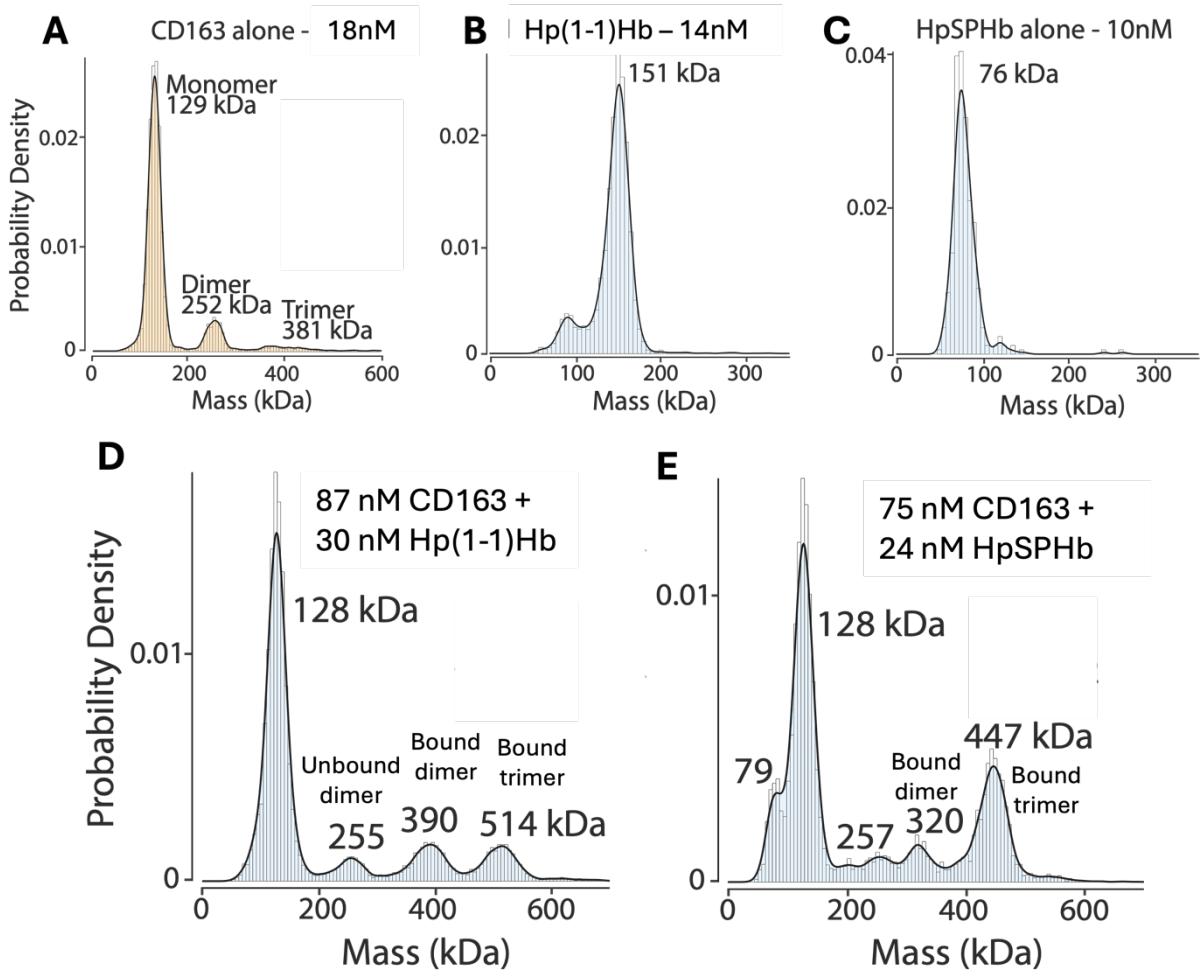


Figure 31: MP spectra for unliganded CD163 (A), Hp(1-1)Hb (B), HpSPHb (C), CD163-Hp(1-1)Hb (D) and CD163-HpSPHb (E). The concentrations provided in the spectra refer to monomeric forms of the proteins (i.e. monomeric CD163, one 'head' of Hp(1-1)Hb). Every sample was recorded in triplicate, with the most representative spectrum being shown.

Unbound, monomeric CD163 was still dominant. This observation seemingly contradicts the findings from cryo-EM, which only showed multimers (Figure 23). However, the grids frozen for cryo-EM contained complexes at a concentration of 12 μM, which is at least 400-times higher than the concentrations used for MP. This significantly higher concentration might push the equilibrium towards multimers. It should further be noted that CD163 monomers might be too small to be resolved by cryo-EM.

The unliganded dimer was also observed in the MP spectra. The mass of the unliganded dimer, however, roughly corresponded to that of a liganded monomer, the existence of which is referenced in Chapter 4.3.

When comparing the MP spectra of unbound CD163 and liganded CD163, an increase in the density of the trimer peak is observed (Figure 31A, D and E). This suggests that the ligands promote the formation of a CD163 trimer, potentially by providing all three 'arms' an additional interaction interface, causing the overall stabilisation of the CD163 'base'.

### 4.2.5 Comparison of uptake efficiencies for various HpHb ligands

The cryo-EM structures and binding experiments demonstrated that CD163 binds to a single 'head' of HpHb, with more CD163-mediated contacts with Hb than with Hp. To further validate the function of this scavenger receptor, a cell-based uptake experiment was established. A stable cell line that constitutively expresses CD163 has proven to be effective in producing reliable uptake results (Kristiansen et al., 2001; C. A. Schaer et al., 2006; D. J. Schaer et al., 2006). Stable cell lines offer two key advantages. Firstly, the transgene is passed onto the daughter cells, eliminating the need for repeated transfections. Secondly, this system offers a negative control and the opportunity to introduce specific mutations into the receptor. While generating stable cells expressing a transgene, a parental cell line is transfected, which itself can serve as a negative control for the uptake experiments.

As described in Chapter 2.5, the stable cell lines used for this dissertation were generated using the Flip-In-293 System, which integrates the transgene consistently into a defined genomic locus that is transcriptionally active. Since the CD163-GFP fusion is encoded on a plasmid containing a hygromycin resistance gene, the cells were selected in hygromycin post-transfection to remove parental cells lacking CD163 expression. To ensure all untransfected cells or cells with low CD163 expression were eliminated, cells were additionally subjected to FACS sorting (Figure 32). Although the FACS plots demonstrated that most cells that survived selection expressed high levels of CD163, the cells were still sorted to remove the few CD163- cells. Cells with high expression levels of CD163 in the untransfected population were likely contaminants carried over during measurement of selected cells.

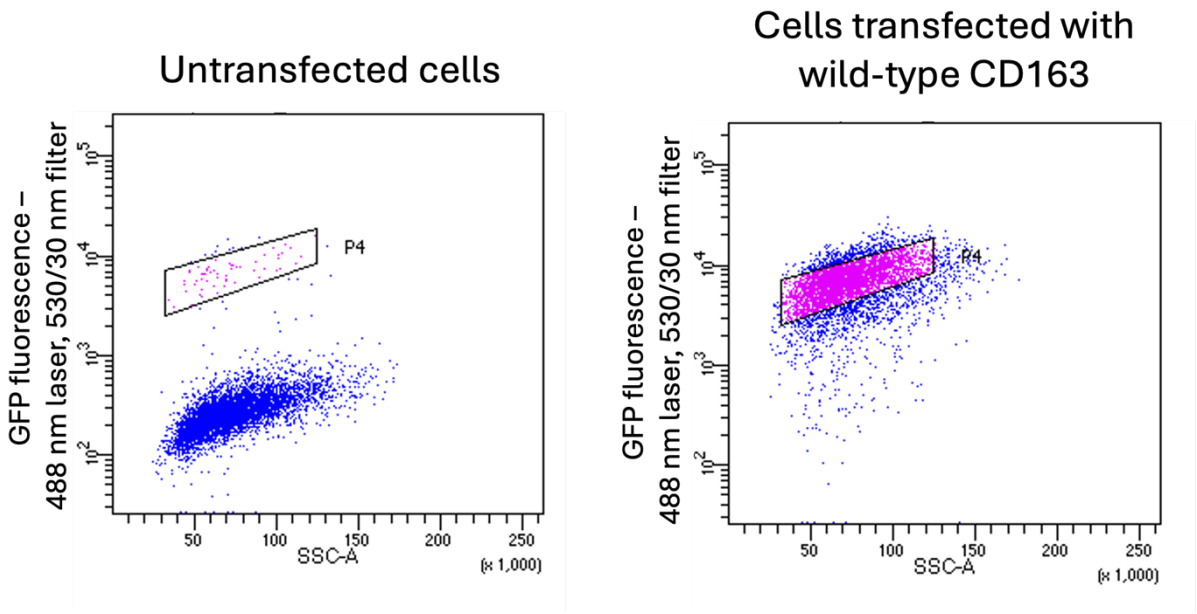


Figure 32: FACS sorting of cells transfected with CD163-GFP and selected in hygromycin. The gate in the plot for the transfected cells depicts the gate used for sorting. The area of the side scatter (SSC-A) quantifies the internal complexity of a detected cell.

Having generated the CD163-expressing stable cell line, an uptake experiment was established. Hp(1-1)Hb was the ligand used for structural characterisation of the CD163 complexes and was also tested initially in this assay. Over the course of an hour, Hp(1-1)Hb was, however, also taken up by untransfected cells as efficiently as by CD163+ cells (Figure 33A), indicating that the uptake was non-specific and likely enabled by pinocytosis. Unlike Hp(1-1)Hb, Hp(2-2)Hb forms high-order oligomers (Figure 7), potentially reducing non-specific uptake. Indeed, Hp(2-2)Hb was taken up by CD163+ cells significantly more efficiently than by untransfected cells (Figure 33B). It should be noted that this assay was established just before thesis submission. Therefore, the presented measurements were only performed once.

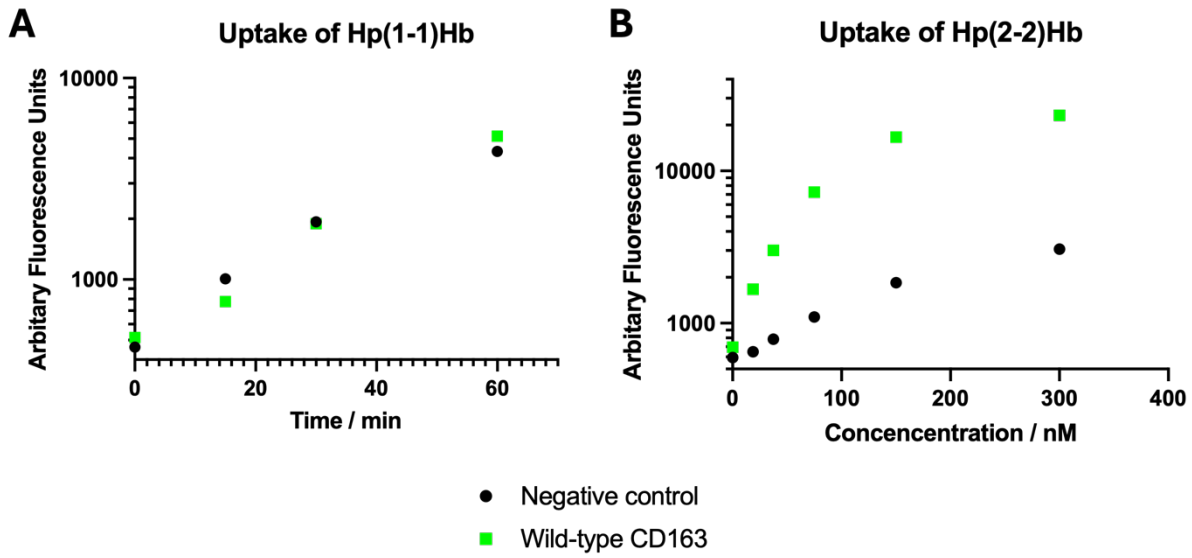


Figure 33: Uptake of Hp(1-1)Hb and Hp(2-2)Hb by CD163+ cells and untransfected cells (negative control). A) Direct uptake of Hp(1-1)Hb over the course of 60 min. Ca. 150,000 adherent HEK293 cells were incubated with 500 nM Alexa Fluor 594-labelled Hp(1-1)Hb for the indicated duration at 37 °C, washed in a calcium-free buffer and measured on FACS. B) Uptake of Hp(2-2)Hb in a concentration titration assay. 150,000 adherent HEK293 cells were incubated for 30 min at 37 °C in the indicated concentration of labelled Hp(2-2)Hb, washed and detected on FACS.

This initial experiment led me to conduct all future uptake studies with Hp(2-2)Hb being directly internalised. To compare uptake efficiencies between different ligands, a competition experiment was established. This measures the competition between various, unlabelled ligands and fluorescently labelled Hp(2-2)Hb, which is specifically internalised at a low concentration (e.g. 50 nM). While the concentration of labelled Hp(2-2)Hb remained unchanged, the unlabelled ligands were titrated to generate a competition uptake curve.

All HpHb variants were internalised with similar efficiency (Figure 34). The uptake of the HpHb ligands was only dependent on the concentrations of 'heads' and was independent of their specific phenotypes or their multimerisation. This finding agrees with structural insights, which revealed that CD163 binds to a 'head' of HpHb, without interacting with the CCP domains of Hp. Compared to all HpHb ligands, however, Hb is a weaker competitor of Hp(2-2)Hb uptake. This observation is also consistent with the structures and binding experiments that showed CD163 contacts both Hb and Hp and that its

affinity for Hp(1-1)Hb and HpSPHb is stronger than its affinity for Hb alone. Furthermore, the competition uptake experiments revealed that Hp(1-1) and BSA are taken up with equivalent efficiency, which agrees with previous data that show binding to Hp is 140-times weaker than to Hb.

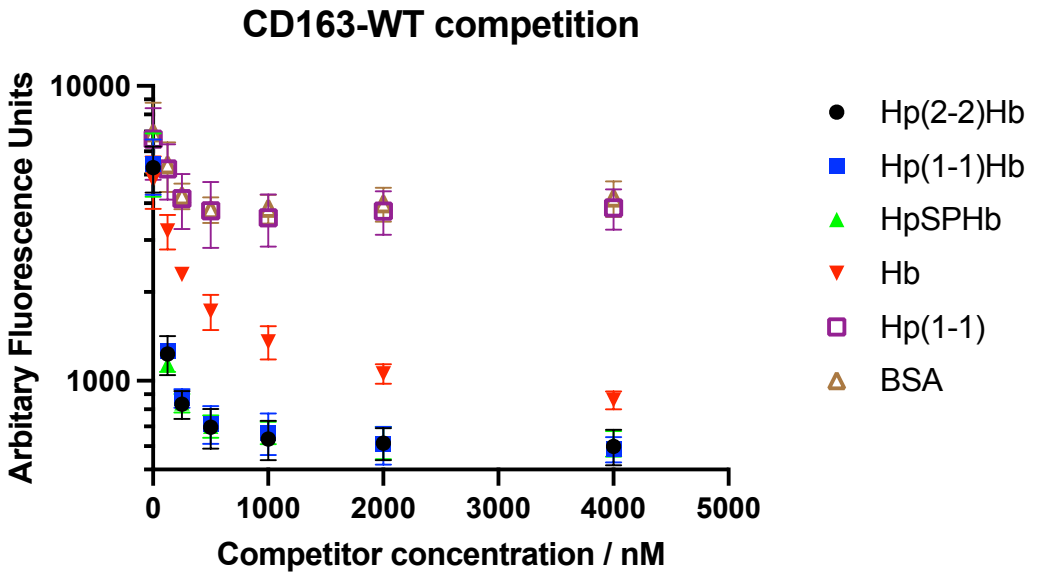


Figure 34: Uptake of fluorescently labelled Hp(2-2)Hb in the presence of various competitors. ~150,000 adherent HEK293 cells expressing CD163-WT were incubated with 50 nM Alexa Fluor 594-labelled Hp(2-2)Hb together with a competitor at the given concentration for 30 min at 37 °C, washed in PBS and measured on FACS. Each data point was measured in triplicate. Mean ± standard deviation is shown.

## 4.3 Calcium-mediated multimerisation

### 4.3.1 Calcium ions at the inter-protomeric interface

Another interesting finding from the cryo-EM structures is the potential for calcium-mediated multimerisation of CD163. The cryo-EM structures showed three spherical densities at each inter-protomeric interface that are coordinated by negatively charged residues (Figure 35). A lysine residue from the opposing CD163 chain neutralises the negatively charged cluster.

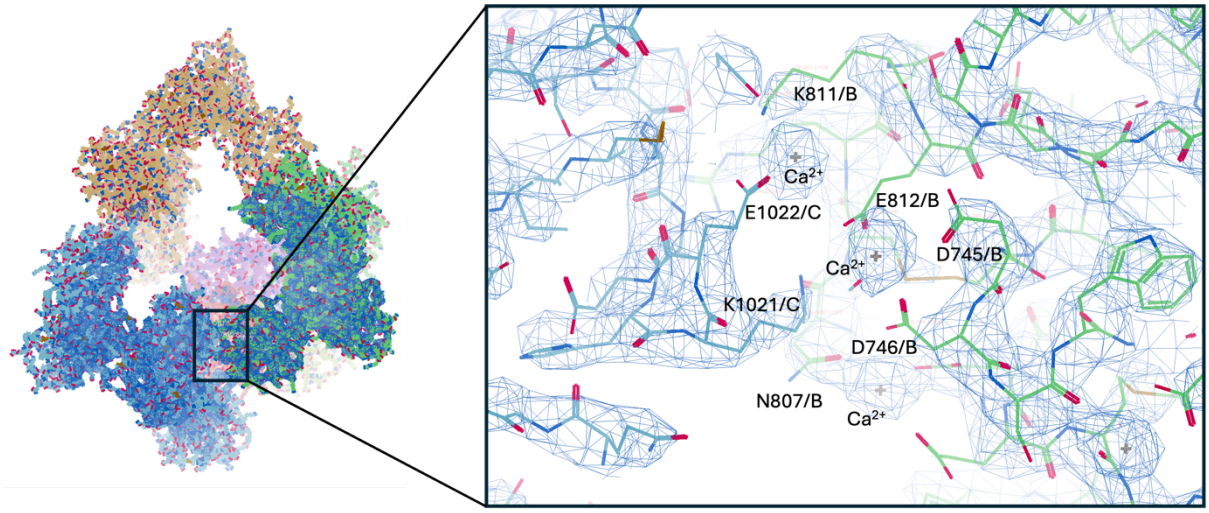


Figure 35: Close-up view of the inter-protomeric 'base' between chains B and C of trimeric CD163-Hp(1-1)Hb. The displayed model and map were visualised using Coot 0.9.8.8.

Previous studies have shown that CD163 is regulated by calcium, which is why samples for cryo-EM included 2.5 mM $CaCl_2$. While the presence of calcium ions could not be directly confirmed using cryo-EM analysis, the spherical densities likely correspond to calcium. I therefore used biophysical methods to investigate whether calcium affects multimerisation of CD163.

### 4.3.2 The effect of calcium on the multimerisation of CD163

MP directly evaluates the effect of calcium ions on different populations of CD163. When EDTA is added to chelate calcium ions, CD163, either in the presence or absence of Hp(1-1)Hb, did not form multimers (Figure 36). Notably, monomeric CD163 has a similar molar mass to Hp(1-1)Hb (Figure 31B), causing these two populations to merge into a single peak in the MP spectrum.

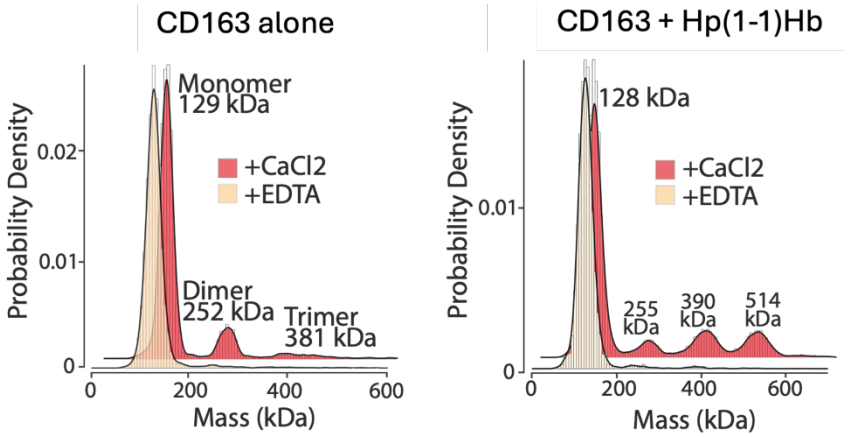


Figure 36: MP spectra for CD163 alone and CD163 with Hp(1-1)Hb in the presence of either 2.5 mM $CaCl_2$ or 5 mM EDTA. For CD163 alone, 18 nM of monomeric CD163 was analysed. For the receptor-ligand complexes, 87 nM CD163 and 30 nM Hp(1-1)Hb 'heads' were examined with $CaCl_2$. In the presence of EDTA, 30 nM CD163 and 10 nM Hp(1-1)Hb 'heads' were tested. Every measurement was conducted in triplicate, with the most representative replicate being displayed.

To validate the findings from MP, another molecular weight detection technique, SEC-MALLS, was employed. Unlike MP, SEC-MALLS does not detect each molecule individually but collects light scattering measurements from the bulk sample as it elutes from SEC. Initially, 0.4 mg/ml CD163 was assessed in the presence and absence of $CaCl_2$. In the absence of calcium ions, CD163 was at a mass of 123 kDa suggesting that it is monomeric (Figure 37, Table 5). The addition of calcium ions resulted in a single broad peak with a predicted average mass size between that of a monomer and a dimer, suggesting that the peak contains a mixture of monomers and multimers. As cryo-EM analysis yielded predominantly higher molecular weight components, I next assessed whether multimerisation of CD163 is concentration-dependent. To test this hypothesis, increasing concentrations of CD163 were analysed using SEC-MALLS. Indeed, I found that the position of the peak corresponding to CD163 shifted to a higher molecular weight as the concentation increased, reaching a mass in between a dimer and trimer at 2.7 mg/ml. Therefore, CD163 shows concentration-dependent multimerisation which also requires calcium ions.

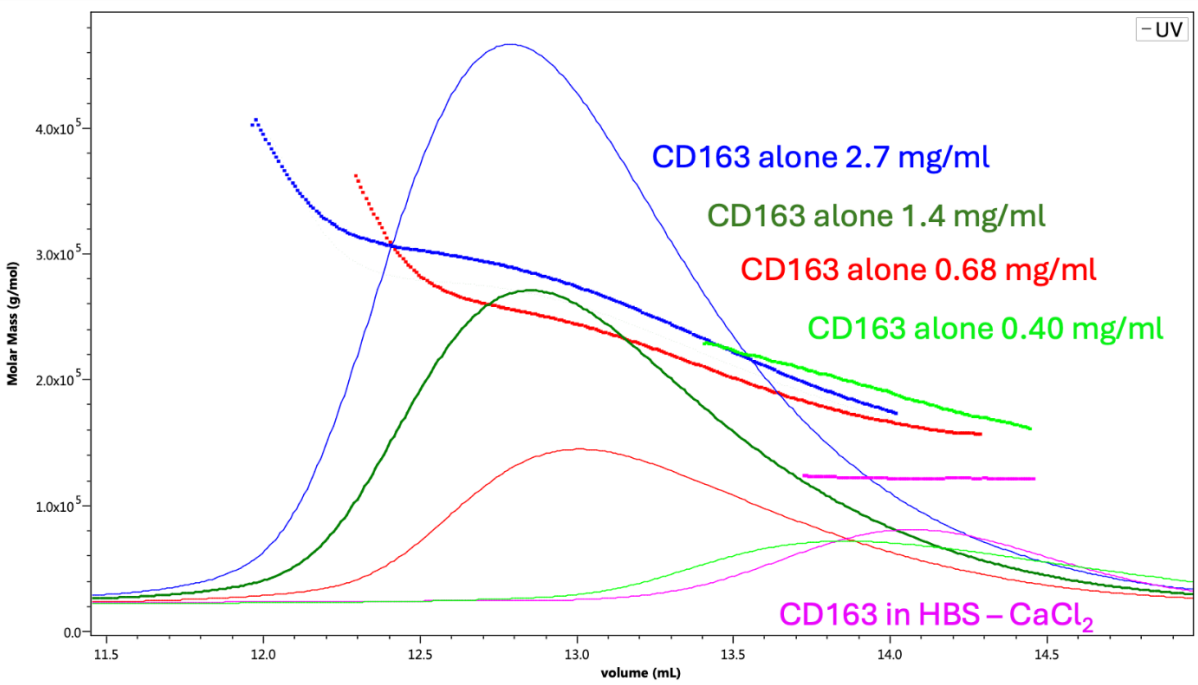


Figure 37: SEC-MALLS traces for unliganded CD163. To simplify the plot, a representative replicate was shown for each sample. The exact molar masses are shown in Table 5.

Table 5: Summary of SEC-MALLS results for CD163 alone. The buffers used were either HBS (20 mM HEPES pH 7.5, 150 mM NaCl) with or without 2.5 mM $CaCl_2$.

| Sample | Buffer | Molar mass (kDa) | Replication |
|---|---|---|---|
| CD163 alone 0.40 mg/ml | HBS - $CaCl_2$ | 123.1 | Triplicate |
| CD163 alone 0.40 mg/ml | HBS + $CaCl_2$ | 192.0 | Triplicate |
| CD163 alone 0.68 mg/ml | HBS + $CaCl_2$ | 223.7 | Duplicate |
| CD163 alone 1.4 mg/ml | HBS + $CaCl_2$ | 250.6 | Duplicate |
| CD163 alone 2.7 mg/ml | HBS + $CaCl_2$ | 271.1 | Duplicate |

The calcium- and concentration-dependence of CD163 multimersation is also observed in the presence of Hp(1-1)Hb (Figure 38, Table 6). Replacing $CaCl_2$ with $MgCl_2$ results in a monomeric species, suggesting that multimerisation is specifically regulated by calcium. Additionally, reducing the pH from 7.5 to 6 causes CD163 to mostly form monomers even in the presence of $CaCl_2$. The aspartates and glutamates coordinating the calcium ions (Figure 35) likely become protonated, which disrupts their ability to bind

calcium ions. The reduction of both calcium concentration and pH is associated with internalisation in the endosome, suggesting that these mechanisms work together to facilitate ligand release after uptake.

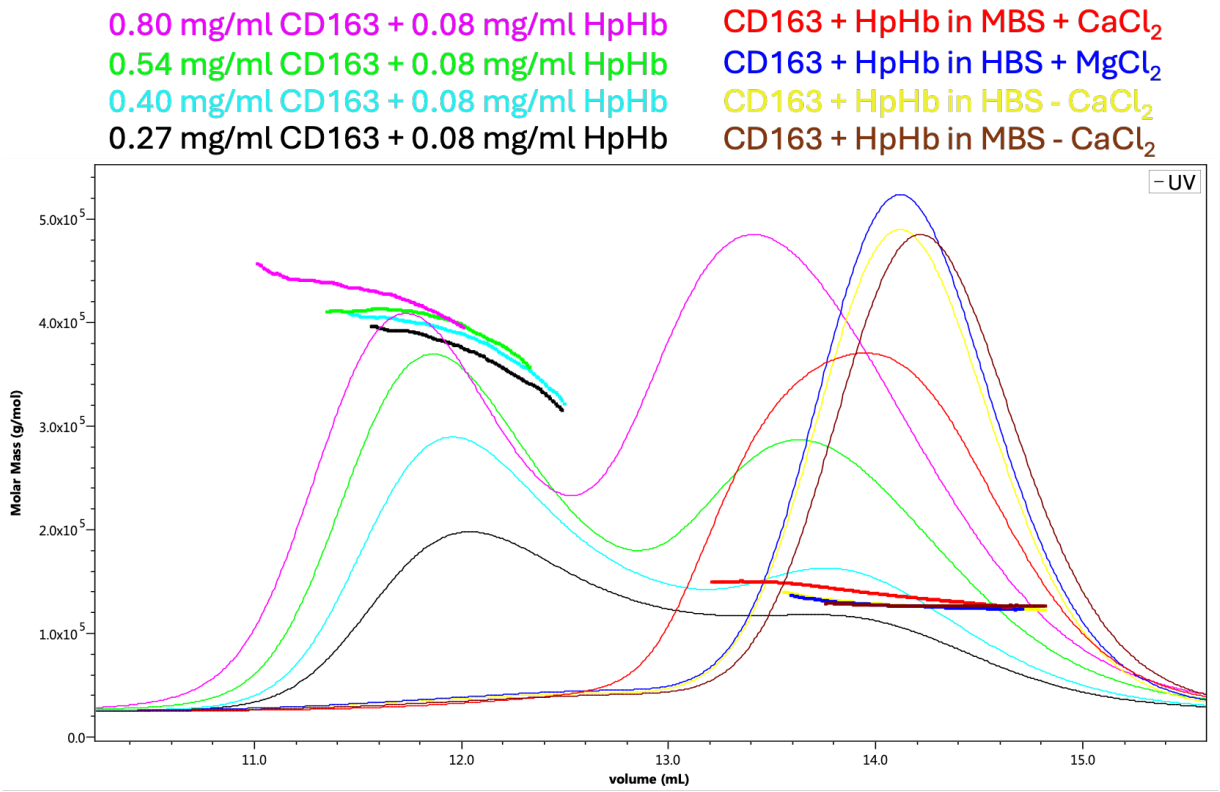


Figure 38: SEC-MALLS analysis of CD163 in the presence of Hp(1-1)Hb. Only a representative replicate was shown for each sample. For samples containing $CaCl_2$ at pH 7.5, only the masses for the first peak (corresponding to CD163-Hp(1-1)Hb complexes) were determined. The exact molecular weights are displayed in Table 6.

Table 6: Summary of SEC-MALLS data for CD163 with Hp(1-1)Hb. The buffers used were either HBS or MBS (MES pH 6.0, 150 mM NaCl) with or without 2.5 mM $CaCl_2$ or 2.5 mM $MgCl_2$.

| Sample | Buffer | Molar mass (kDa) | Replication |
|---|---|---|---|
| 0.40 mg/ml CD163 + 0.08 mg/ml HpHb | HBS - $CaCl_2$ | 128.2 | Triplicate |
| 0.27 mg/ml CD163 + 0.08 mg/ml HpHb | HBS + $CaCl_2$ | 361.8 | Duplicate |
| 0.40 mg/ml CD163 + 0.08 mg/ml HpHb | HBS + $CaCl_2$ | 385.6 | Duplicate |
| 0.54 mg/ml CD163 + 0.08 mg/ml HpHb | HBS + $CaCl_2$ | 403.8 | Duplicate |
| 0.80 mg/ml CD163 + 0.08 mg/ml HpHb | HBS + $CaCl_2$ | 427.2 | Duplicate |
| 0.40 mg/ml CD163 + 0.08 mg/ml HpHb | HBS + $MgCl_2$ | 128.3 | Triplicate |
| 0.40 mg/ml CD163 + 0.08 mg/ml HpHb | MBS + $CaCl_2$ | 146.3 | Triplicate |
| 0.40 mg/ml CD163 + 0.08 mg/ml HpHb | MBS - $CaCl_2$ | 127.2 | Triplicate |

### 4.3.3 Design of a CD163 'monomer mutant' and its binding and uptake of HpHb

As calcium ions enable multimerisation, I next investigated the role of this multimerisation in HpHb uptake. Cryo-EM structures revealed that all two or three subunits of multimeric CD163 simultaneously bind Hp(1-1)Hb. This raises the possibility that multimerisation of CD163 may be required for uptake of HpHb. To test this hypothesis, an R809T mutant of CD163 was produced, introducing an N-linked glycan that is predicted to disrupt the inter-protomeric interface (Figure 39A), hindering multimerisation.

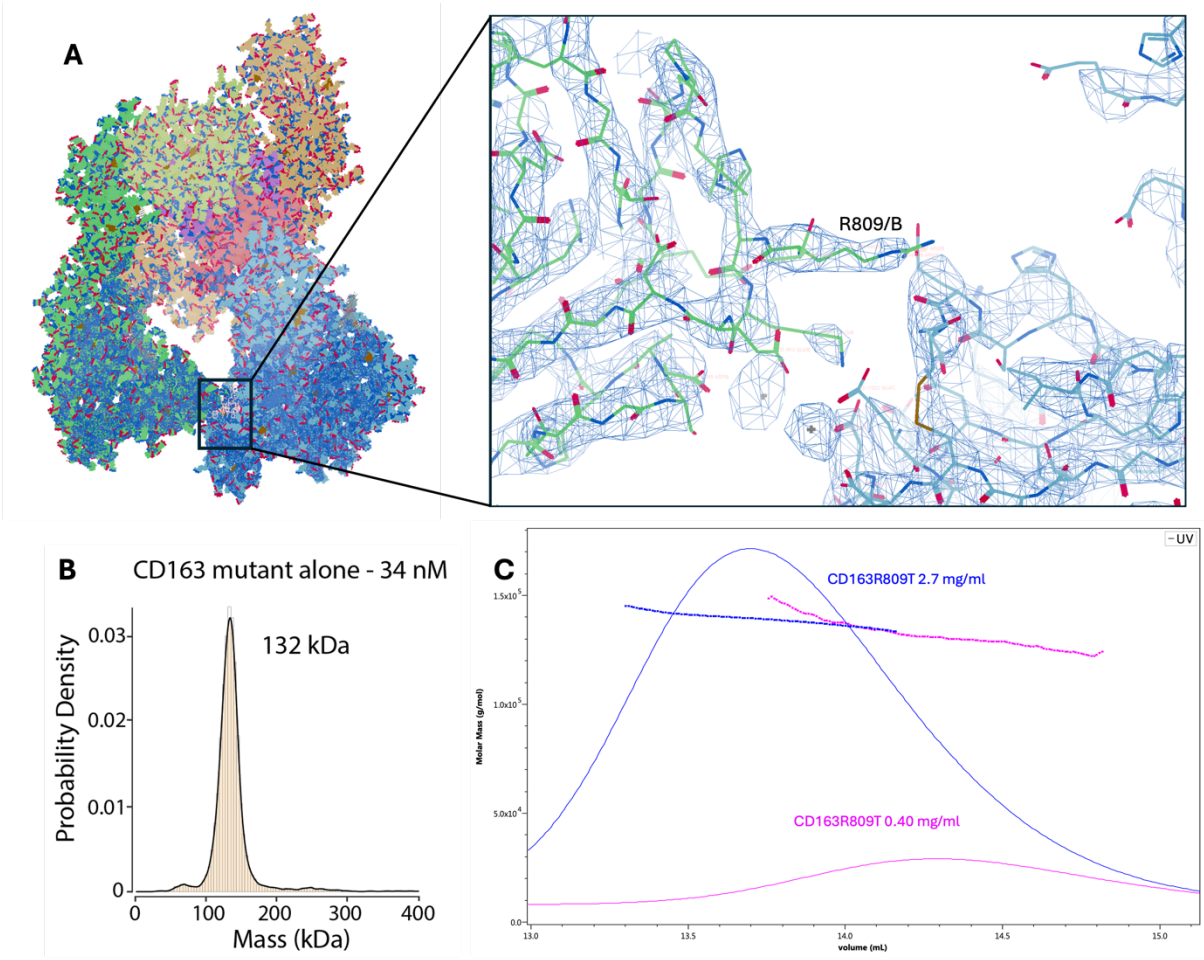


**D**

| Sample for SEC-MALLS | Buffer | Molar mass (kDa) |
|---|---|---|
| CD163R809T alone 0.40 mg/ml | HBS + $CaCl_2$ | 130.3 |
| CD163R809T alone 2.7 mg/ml | HBS + $CaCl_2$ | 138.7 |

Figure 39: Generation of CD163 'monomer mutant'. A) Close-up view of residue R809 in CD163. The residue is positioned at the inter-protomeric interface. The backbone of chain B of CD163 is depicted in green whereas the one of chain A is shown in blue. B) MP spectrum of CD163-R809T in HBS with 2.5 mM $CaCl_2$. C) and D) SEC-MALLS analysis of CD163-R809T at 0.40 and 2.7 mg/ml in HBS with 2.5 mM $CaCl_2$. The measurements were performed in duplicate. Only a representative replicate is shown in C).

MP was employed to confirm that CD163-R809T is unable to multimerise. While this mutant did not form multimers in MP (Figure 39B), the concentrations used were only 34 nM, which might be insufficient to observe multimers. Therefore, SEC-MALLS was also used to validate the mutant's inability to multimerise. In SEC-MALLS, CD163-R809T remained monomeric, even at concentrations as high as 2.7 mg/ml (Figure 39C and D), a

level at which the wild-type receptor exhibited a mass between dimeric and trimeric CD163 (Table 5).

After confirming that R809T disrupts the ability of CD163 to multimerise, the next objective is to evaluate whether the 'monomer mutant' can still bind HpHb. Surprisingly, CD163-R809T was able to bind Hp(1-1)Hb in SPR with a similar affinity to CD163-WT (Figure 40A), although the binding kinetics differed from those observed between the wild-type receptor and ligand (Figure 29A). However, the immobilised protein is naturally concentrated on the SPR sensor chip surface. As a result, monomeric CD163 might behave like a multimer when surface coupled in this way. To exclude this effect as a cause of binding, the interaction between CD163-R809T and Hp(1-1)Hb was assessed using MST, a solution-based technique. Interestingly, MST also revealed a nanomolar interaction between the 'monomer mutant' and the ligand (Figure 40B), indicating that monomeric CD163 is indeed capable of binding HpHb. This conclusion was validated in an uptake experiment, which demonstrated that the uptake efficiencies of CD163-WT and CD163-R809T for Hp(2-2)Hb are similar (Figure 40C).

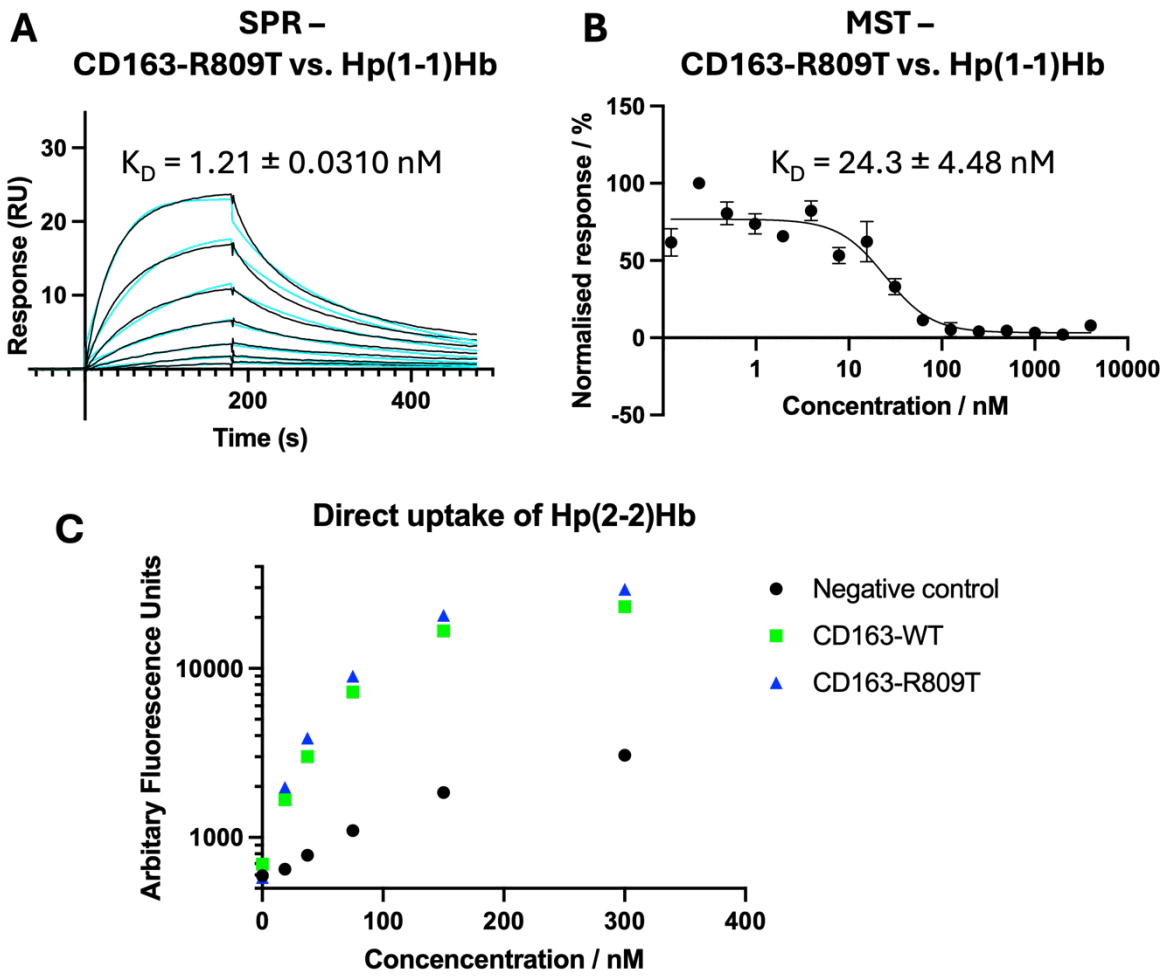


Figure 40: Binding and uptake results for CD163-R809T. A) SPR sensorgrams for CD163-R809T (immobilised) and Hp(1-1)Hb (analyte). Hp(1-1)Hb was injected in a two-fold dilution series from 5 – 0.08 nM. B) MST curves for the interaction between CD163-R809T and fluorescently labelled Hp(1-1)Hb. Both SPR and MST were performed in triplicate. The $K_D$-values are provided as the mean ± standard deviation. C) Uptake of fluorescent Hp(2-2)Hb by stable cells expressing CD163-WT, CD163-R809T or by untransfected cells (negative control). The uptake experiment was performed in singlicate. The uptake data for CD163-WT and the negative control were previously shown in Figure 33C and are only depicted for comparison.

### 4.3.4 The importance of multimerisation for the uptake of Hb and Hp(1-1)Hb

As multimerisation is not required for Hp(2-2)Hb uptake, I next investigated whether it affects the uptake of other ligands. The cryo-EM structures showed that all three 'arms' of CD163 contact Hb (Figure 25 and Figure 26). Despite that, the binding affinity and uptake efficiency of CD163-WT for Hb are significantly lower than the ones for HpHb (Figure 30 and Figure 34). Based on these observations, I hypothesised that, while multimerisation is not required for the uptake of high affinity ligands, such as HpHb, it may enable the scavenging of a lower-affinity ligand, such as Hb. I therefore used MST to measure the affinity of the monomeric mutant, CD163-R809T, to Hb. This revealed that the monomer mutant bound to Hb with an affinity around 10-fold lower than WT CD163 (Figure 41).

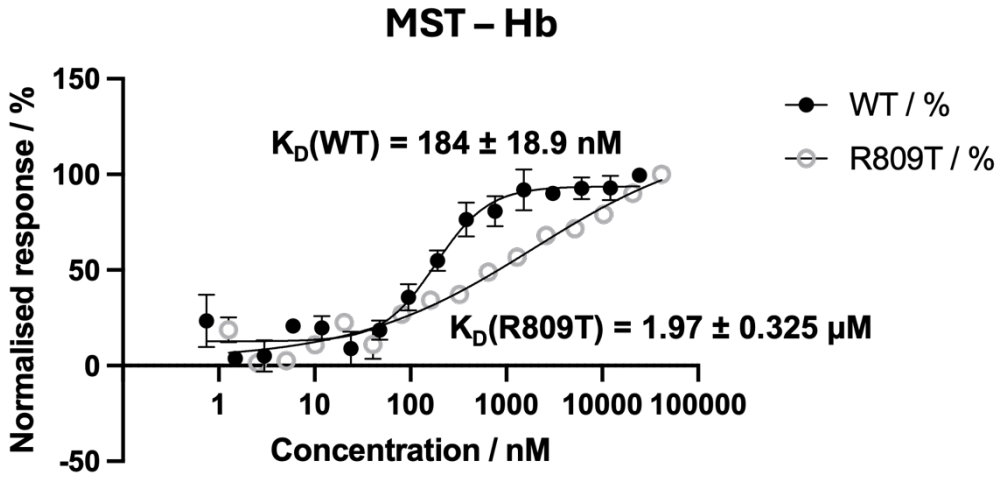


Figure 41: MST curves for the interactions between CD163-WT or CD163-R809T and Hb. The data for the Hb-CD163-WT interaction were depicted in Figure 30 and are only displayed for comparison. The measurements were conducted in triplicate. The dissociation constants are shown as mean ± standard deviation.

This finding was validated in an uptake experiment that showed cells expressing CD163-R809T cannot take up Hb (Figure 42). Interestingly, the uptake efficiency of Hp(1-1)Hb is also reduced compared to that of Hp(2-2)Hb, which was not the case for CD163-WT (Figure 34). The wild-type receptor forms multimers and likely uses multiple 'arms' to increase binding strength through avidity. This avidity is seemingly crucial to scavenging

Hp(1-1)Hb, which has two HpHb ‘heads’, of which only one can engage with the membrane receptors at a time due the orientation (Figure 6). Unlike Hp(1-1)Hb, Hp(2-2)Hb exhibits at least three ‘heads’ (Figure 7) allowing this multimeric ligand to bind multiple monomeric receptors at once. This is likely how Hp(2-2)Hb is still scavenged by CD163-R809T. These results highlight the important role of receptor multimerisation in the uptake of Hb and Hp(1-1)Hb, supporting the conclusion that multimerisation of CD163 is not required for efficient uptake of high-affinity ligands, but becomes important for uptake of lower affinity ligands, such as Hb.

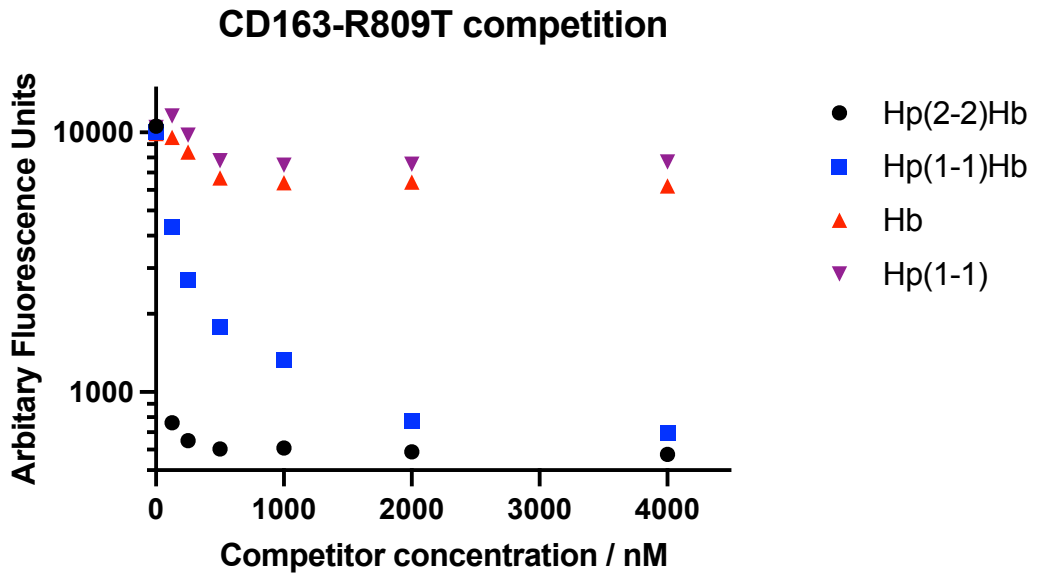


Figure 42: Uptake of fluorescent Hp(2-2)Hb in the presence of competitors by cell expressing CD163-R809T. Due to time constraints, the measurements could only be performed in singlicate.

## 4.4 Calcium-mediated ligand binding

In addition to revealing calcium ions at the inter-protomeric interfaces, the cryo-EM volumes also revealed putative calcium ions at the interfaces between the CD163 ‘arms’ and Hp(1-1)Hb (Figure 43). The structure of dimeric CD163-Hp(1-1)Hb resolved densities for putative calcium ions between the SRCR domain 2 and Hp, as well as SRCR domain 3 and the α-subunit of Hb. Similar to the interactions observed at the ‘base’, these calcium ions were coordinated by a cluster of negatively charged residues, which were neutralised by a lysine, provided here by either Hp or Hb.

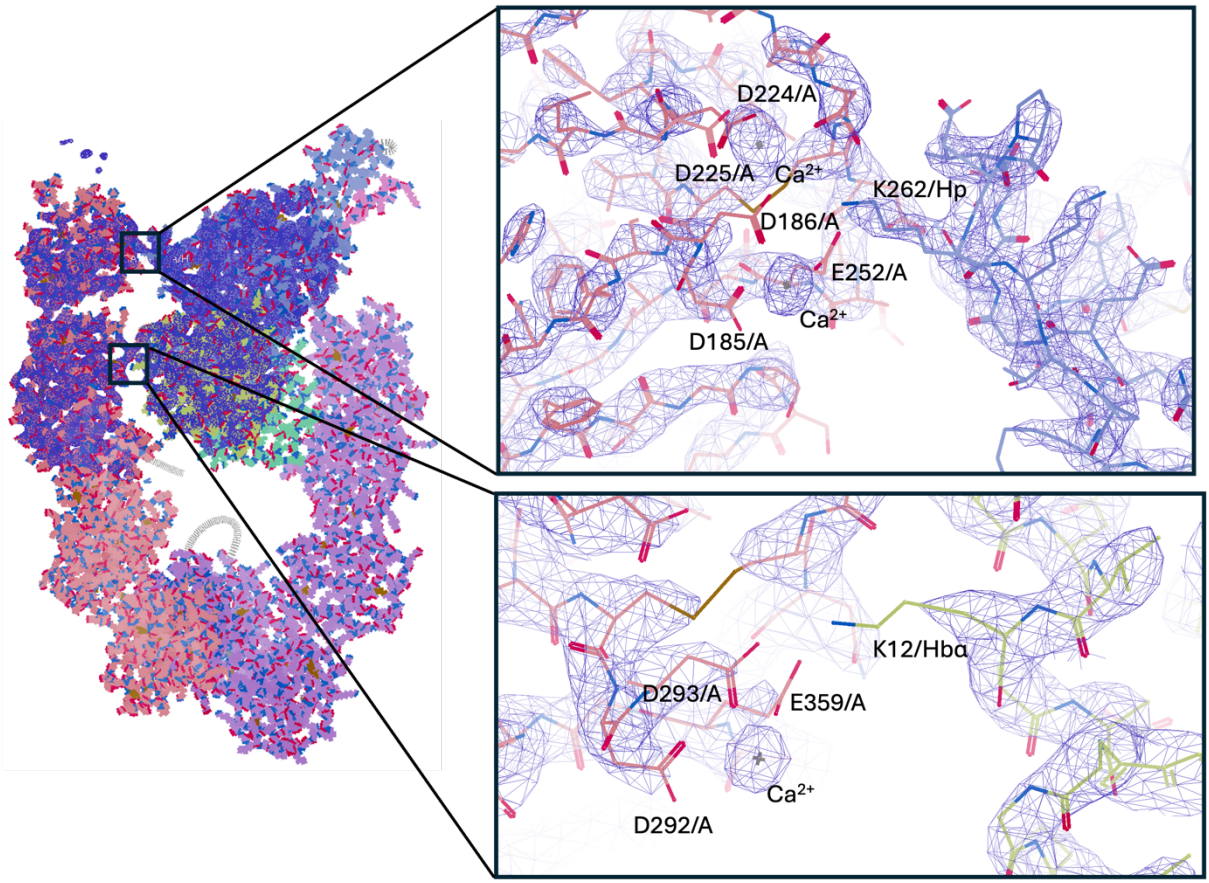


Figure 43: Close-up view of the interface between Hp(1-1)Hb and the A-chain of CD163, as observed in the structure of dimeric CD163-Hp(1-1)Hb. Map and model were illustrated using Coot 0.9.8.8.

In the absence of the calcium ions, the electrostatic potential of the CD163 surface would likely change, making it unlikely for the lysine residues to interact with their respective binding sites in CD163. Therefore, it is probable that the calcium ions directly mediate ligand binding.

To test this hypothesis, the Hp(1-1)Hb binding ability of CD163-WT and CD163-R809T was assessed in a calcium-free and low pH buffer on SPR. Neither wild-type receptor nor 'monomer mutant' were able to bind Hp(1-1)Hb without calcium or at pH 6 (Figure 44), indicating that the binding of CD163 to HpHb is calcium-mediated. Therefore, calcium mediates both the direct interaction of CD163 with its ligand, as well as CD163 multimerisation.

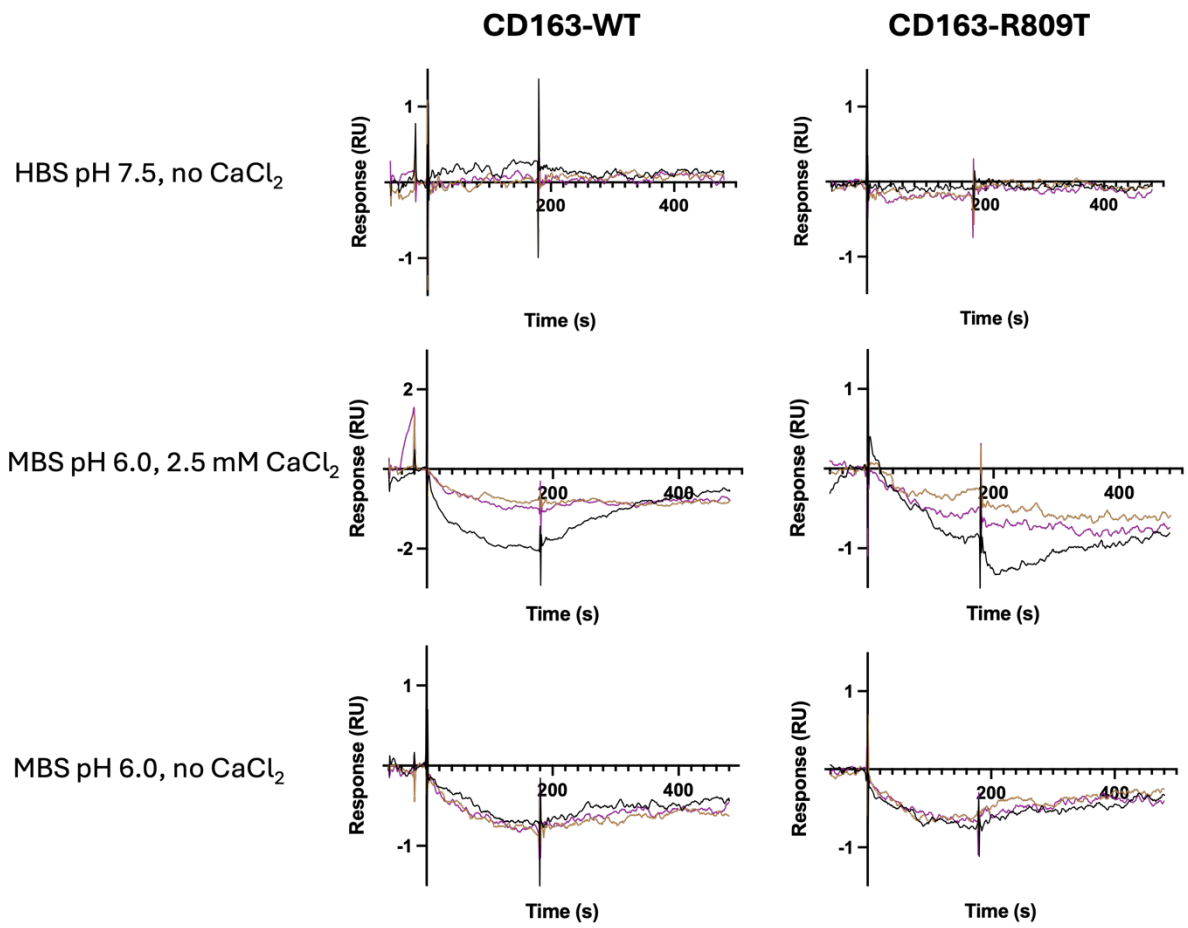


Figure 44: SPR sensorgrams to assess interactions between Hp(1-1)Hb and CD163-WT or CD163-R809T in calcium-free or low pH buffers. Hp(1-1)Hb was injected at 10 nM in triplicate. This concentration corresponds to the highest concentration used to detect binding between CD163-WT and Hp(1-1)Hb in calcium-containing buffers (Figure 29A). Moreover, 10 nM exceeded the highest concentration used for the interaction between CD163-R809T and Hp(1-1)Hb (Figure 40A).

Due to the timing of thesis submission, this observation could not be validated in a cell-based experiment. To perform the experiment, I would have used stable cells expressing either CD163-WT or CD163-R809T and washed them thoroughly in a buffer containing EGTA before performing uptake of labelled Hp(2-2)Hb in EGTA-containing buffer. Since EGTA may impair the cells' ability to take up ligands via clathrin-mediated endocytosis, I would have conducted a control experiment using labelled transferrin. This protein should still be taken up via the transferrin receptor that is expressed by almost all human cells (Ponka & Lok, 1999).

## 4.5 Discussion

The structural insights presented in Chapter 3 were validated in this chapter. Binding and uptake experiments confirmed that CD163 indeed selects for HpHb by binding to its 'head', contacting both Hb and Hp at the same time. For the wild-type receptor, differences in uptake efficiencies between HpHb phenotypes are negligible. Surprisingly, however, the 'monomer mutant' can only scavenge Hp(2-2)Hb efficiently (Figure 45). This finding implies that scavenging of HpHb requires avidity provided by either the ligand or the receptor. It is further tempting to speculate that the *Hp2* evolved from *Hp1* to compensate for multimerisation deficiencies in CD163. Comparing the frequencies of mutations within the CD163 'base' between individuals with at least a copy of *Hp2* and *Hp1* homozygotes would be interesting.

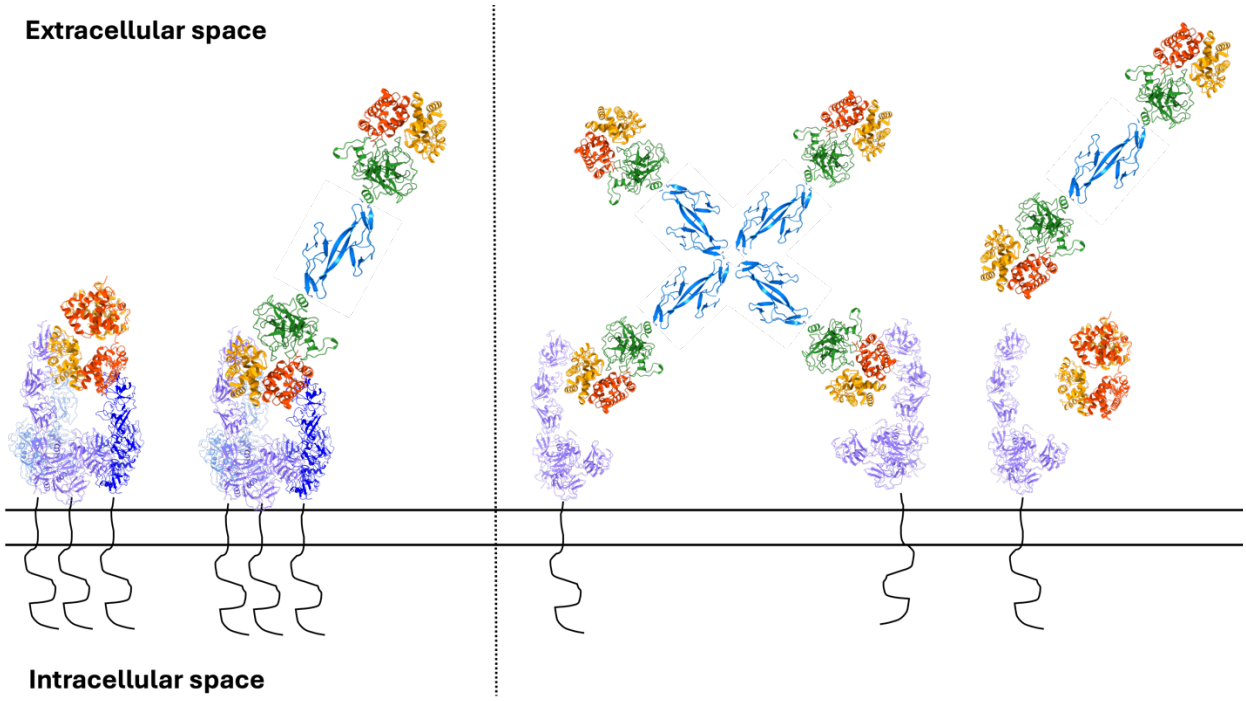


Figure 45: Schematic illustration depicting differences between the scavenging capabilities of CD163-WT and CD163-R809T. While the multimeric receptor enables efficient uptake of Hp(2-2)Hb and Hp(1-1)Hb, and Hb to a lesser degree, the monomeric receptor efficiently scavenges only Hp(2-2)Hb, has reduced uptake rates for Hp(1-1)Hb and does not lead to the internalisation of Hb.

While HpHb is most effectively bound and uptaken, CD163 has affinity for Hb and can lead to its uptake, even in the absence of Hp (Figure 45). This mechanism is also dependent on receptor multimerisation and could be particularly useful during severe or systemic haemolysis, when Hp is depleted, and could complement the haemopexin-CD91 pathway of Hb detoxification.

The calcium-dependency of the receptor for ligand binding was demonstrated in this chapter. Calcium ions at the interface between ligand and receptor directly mediate HpHb binding. CD163 engages with HpHb in the calcium-rich, neutral-pH setting of the plasma and subsequently releases the ligand in the calcium-free, acidic milieu of the endosome, enabling the regulation of ligand binding and Hb detoxification based on the environment conditions.

In summary, the results presented in this chapter revealed that multiple molecular mechanisms govern the function of CD163. An additional mechanism, which has evaded the structures and data discussed so far, is introduced in Chapter 5.

# 5. Discovery and characterisation of an ‘arm-to-arm’ contact in unliganded CD163

## 5.1 Summary

The aim of this chapter was to elucidate the cryo-EM structures of unliganded, dimeric and trimeric CD163, which were initially observed using mass photometry (Figure 31A). Unliganded protein samples were prepared using the same grid types, concentrations and buffer conditions as for CD163-HpHb samples. Populations of dimeric and trimeric CD163 were resolved to 3.1 and 3.6 Å, respectively. While trimeric CD163 showed parts of the unliganded ‘arms’ at low resolution, dimeric CD163 exhibited a conformation characterised by the ‘arms’ binding to each other. Comparisons of the ligand binding interfaces with the inter-protomeric interface of the CD163 dimer revealed significant overlaps. This suggests that HpHb likely competes with the inter-protomeric interaction in the ‘arms’ before it can bind CD163, a process referred to as autoinhibition.

I aimed to determine whether autoinhibition occurs by generating CD163 mutants that can bind HpHb but cannot form the ‘arm-to-arm’ contact. Due to the significant overlap between the ligand binding and presumed autoinhibition interfaces, only two sites could be identified for mutational analysis. While one of the mutants likely misfolded, the other mutant did not bind to Hb and exhibited reduced uptake rates for HpHb, potentially disputing the autoinhibition hypothesis. An alternative explanation for these findings is that the ‘arm-to-arm’ contact in dimeric CD163 serves a different, unknown function.

## 5.2 Cryo-EM structures of unliganded CD163

Since the contacts mediating the formation of CD163 multimers are in the ‘base’, it is plausible that CD163 can multimerise, even in the absence of HpHb. Although this theory was demonstrated by mass photometry (Figure 31A), structural characterisation of unliganded CD163 is still beneficial, particularly to visualise the conformation of the

‘arms’. Indeed, the hypothesis was that the arms would be flexible, but become ordered when binding to ligands, allowing the scavenger receptor to ‘mould’ itself around ligands of different shapes and structures. In cryo-EM, features become visible and well-resolved when they align across multiple particles during processing. In contrast, features that exhibit continuous flexibility are averaged out because flexibility prevents alignment. Due to unliganded CD163 lacking HpHb entirely, the expectation was that the ‘arms’ are likely to be mostly flexible and, therefore, invisible in the cryo-EM structures.

The unliganded CD163 sample was prepared similarly to the CD163-HpHb sample for cryo-EM analysis. A single grid, containing CD163 at 1.3 mg/ml, was blotted for 2.5 s at a force of 7 and subjected to data collection using the Titan Krios. The data were acquired at a pixel size of 0.832 Å and a dose of 42.82 $e^-/Å^2$ over a period of two days. A total of 19,412 micrographs were obtained, pre-processed in SIMPLE, picked using a template from a pilot data collection and 2D-classified, yielding 0.8 million particles that were exported to CryoSPARC (Figure 46).

There, the particles were 2D- and 3D-classified to produce a high-resolution volume, which was used to re-pick all micrographs. 13.8 million particles were identified and subjected to two rounds of 2D-classification. The selected 3.3 million particles were used for *ab initio* reconstruction, which generated seven volumes. Of the seven volumes, one clearly corresponded to a CD163 dimer, and one was assigned to a CD163 trimer. The trimer was further 3D-classified to remove contaminating dimer particles. The final 96,576 particle stack was subjected to non-uniform refinement, yielding the final volume.

The dimer class underwent two rounds of 3D-classification to remove contaminant ‘particles’. 723,620 particles corresponding to the CD163 dimer were combined (Figure 46) and subjected to homogenous and non-uniform refinement. The volumes displayed in the following were sharpened using DeepEMhancer (Sanchez-Garcia et al., 2021).

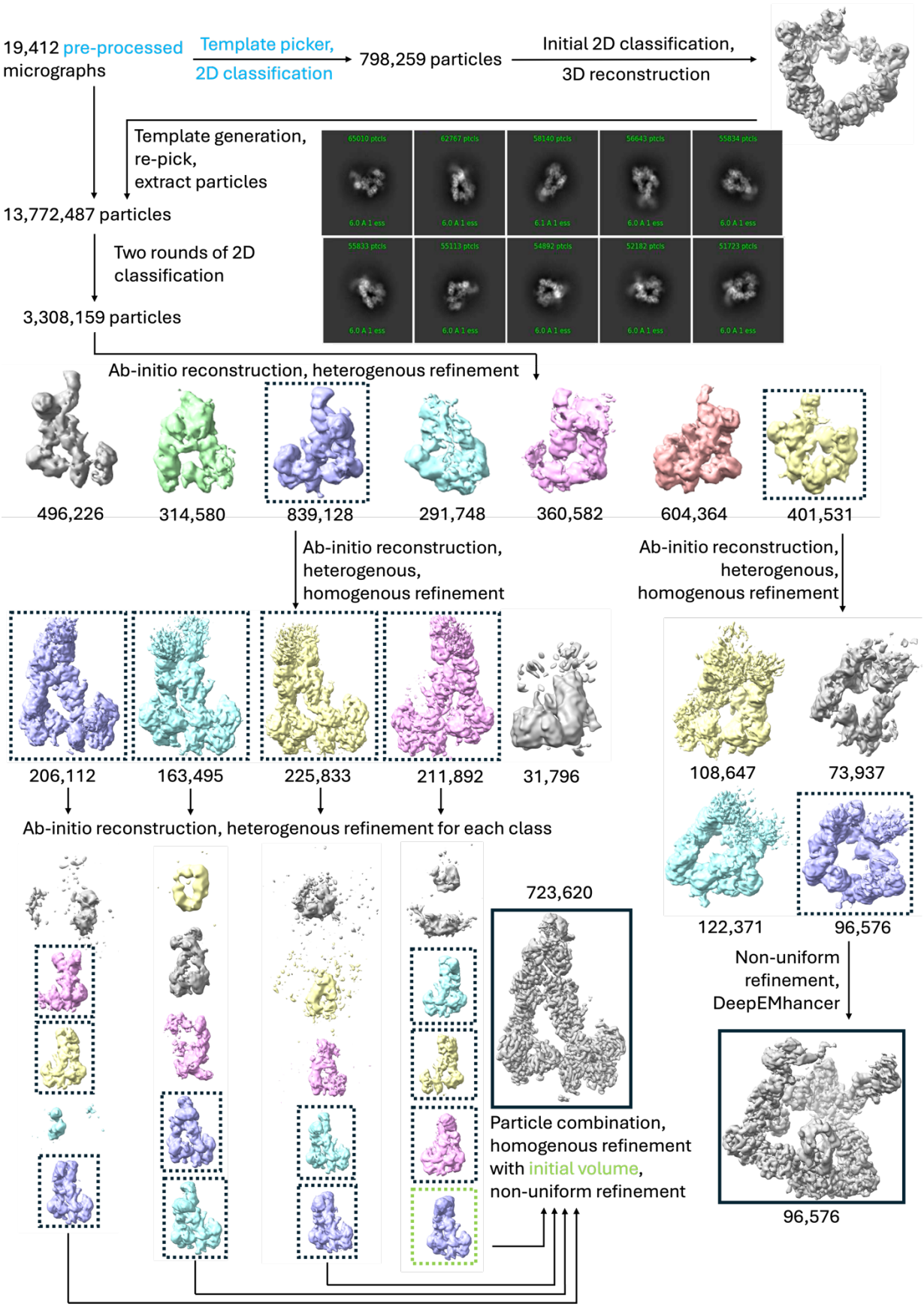


Figure 46: Data processing workflow for unliganded CD163. Steps conducted in SIMPLE 3.0 are written in blue while jobs performed in CryoSPARC v4.2-4.4 are written in black.

The lack of particles and preferred orientation prevented reconstruction of the unliganded CD163 trimer at a resolution below 3.5 Å (Figure 47A and B). However, key features of the unliganded trimer were visible. As expected, CD163 can form the trimer, characterised by a triangular 'base', even in the absence of the ligand (Figure 47C and D). This is because the contacts mediating the trimer are already present in the 'base'. This shows that trimers form without ligand, resulting in trimers on the cell surface which are poised to bind to ligands, including those of lower affinity.

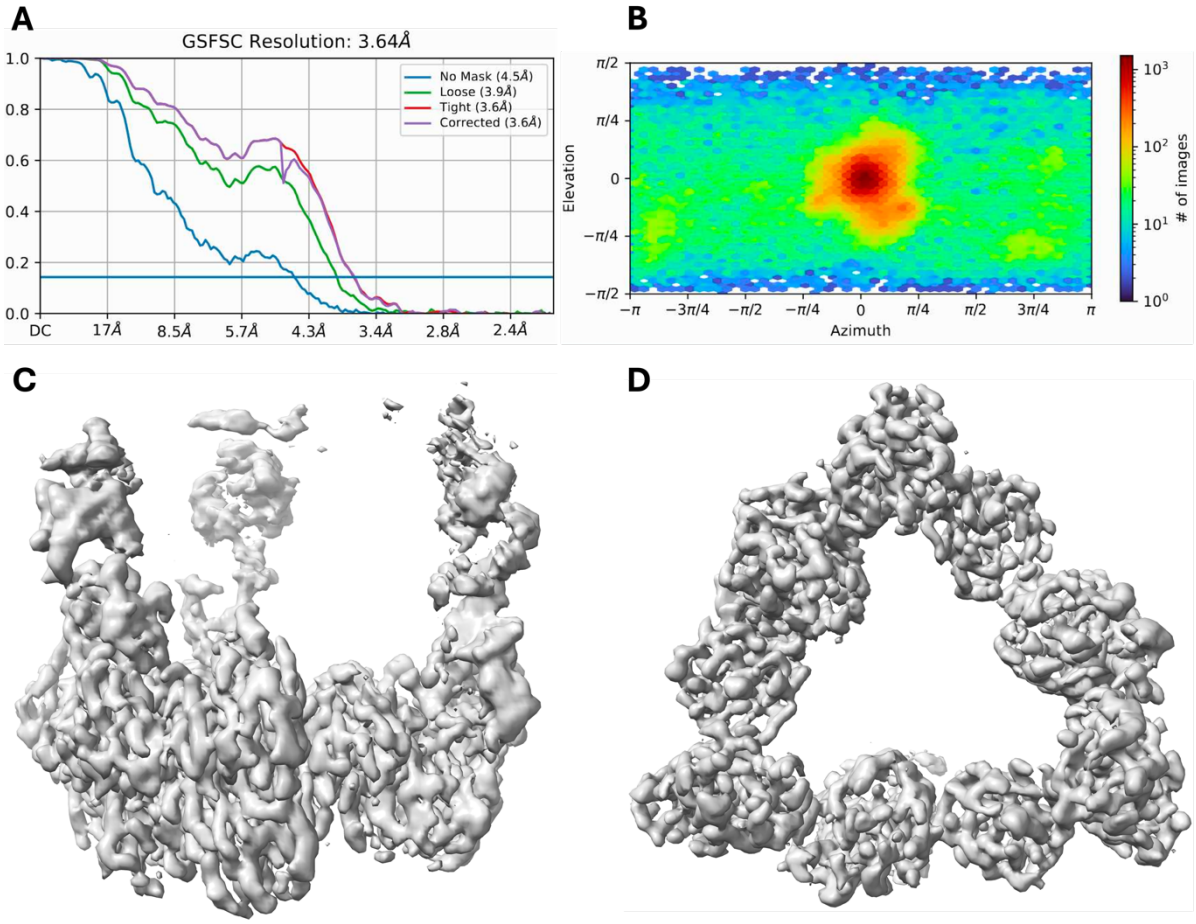


Figure 47: Statistics and map of the unliganded CD163 trimer. A) Gold-standard FSC curves for the final volume of the trimer. All curves are characterised by an intial decrease followed by an increase in correlation. This could suggest a flexible feature at ca. 6 Å, which is not aligning to a high resolution. B) Angular particle distribution during non-uniform refinement of trimer. C) and D) represent side and bottom-up views of the protein.

Furthermore, only parts of the 'arms' that are closest to the 'base' are visible in the volume. This is indicative of continuous flexibility in the 'arms' when the ligand is absent.

For unliganded CD163, 96,576 trimer and 723,620 dimer particles were identified (Figure 46). This trimer-to-dimer ratio shows fewer trimers compared to the dataset for CD163-HpHb, where 469,042 trimer and 456,124 dimer particles were detected (Figure 23). This observation agrees with the findings from MP (Figure 31) that also show a lower trimer-to-dimer ratio for CD163 alone, improving upon ligand addition. These results suggest that the ligand promotes trimer formation, likely by providing all three 'arms' with an additional interaction interface, reducing the flexibility within the molecule and stabilising the trimer. Additionally, at higher local concentrations on the cell surface, the prevalence of trimers would further increase, as the proximity of CD163 molecules enhances trimer formation.

The dimer class was resolved to 3.1 Å, owing to the larger number of dimer particles identified and the availability of more diverse views (Figure 48A and B). Similar to the liganded dimer, the 'base' is also stabilised by calcium ions, which are coordinated by acidic residues from one chain and neutralised by basic residues from the other (Figure 48C, D and E).

However, the most striking feature of the unliganded dimer is that the 'arms' bind to each other (Figure 48C, D and E), with SRCR domains 2 and 3 of one 'arm' interacting with domains 3 and 4 of the other. Unlike interactions between the 'arms' and HpHb, the 'arm-to-arm' contacts are not mediated by calcium ions but rather mainly rely on hydrogen bonds (Figure 49A), salt bridges (Figure 49B) and hydrophobic interactions (Figure 49C). Compared to dimeric CD163-HpHb, particularly the 'arm' of chain A, depicted in purple (Figure 48F), undergoes significant translation to enable interactions with the 'arm' of chain C. Overall, this interaction raises questions about its function, which will be explored in detail in this chapter.

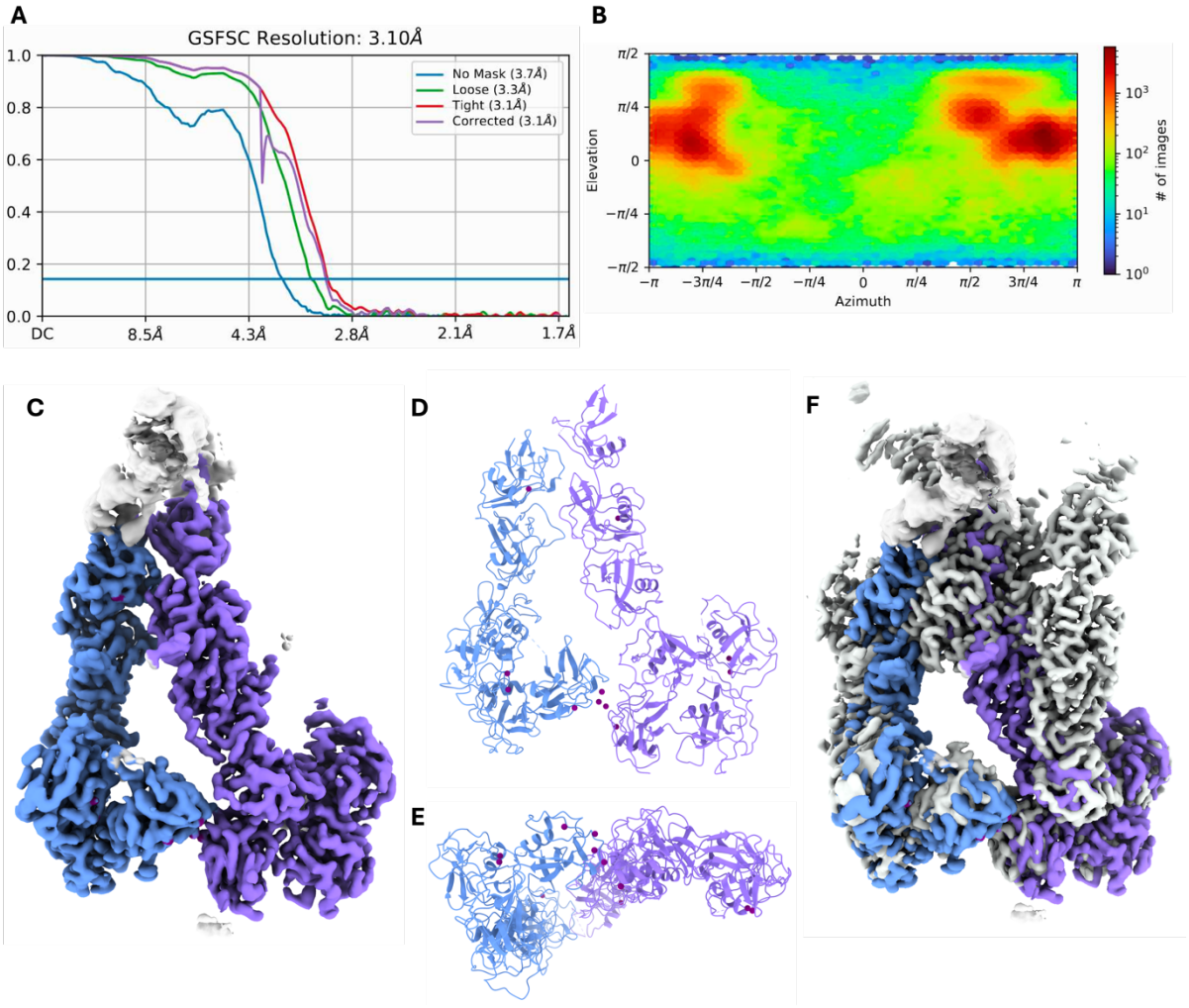


Figure 48: Statistics, volume and model of the unliganded CD163 dimer. A) and B) present the gold-standard FSC curves and particle angular distribution, respectively, obtained after the final non-uniform refinement of the volume. C) Map of the unliganded CD163 dimer. D) and E) provide side and bottom-up views of the model, with the two CD163 protomers shown in different shades of blue, and the calcium ion densities in dark purple. F) Overlay of unliganded dimeric CD163 onto the map of liganded dimeric CD163 (grey).

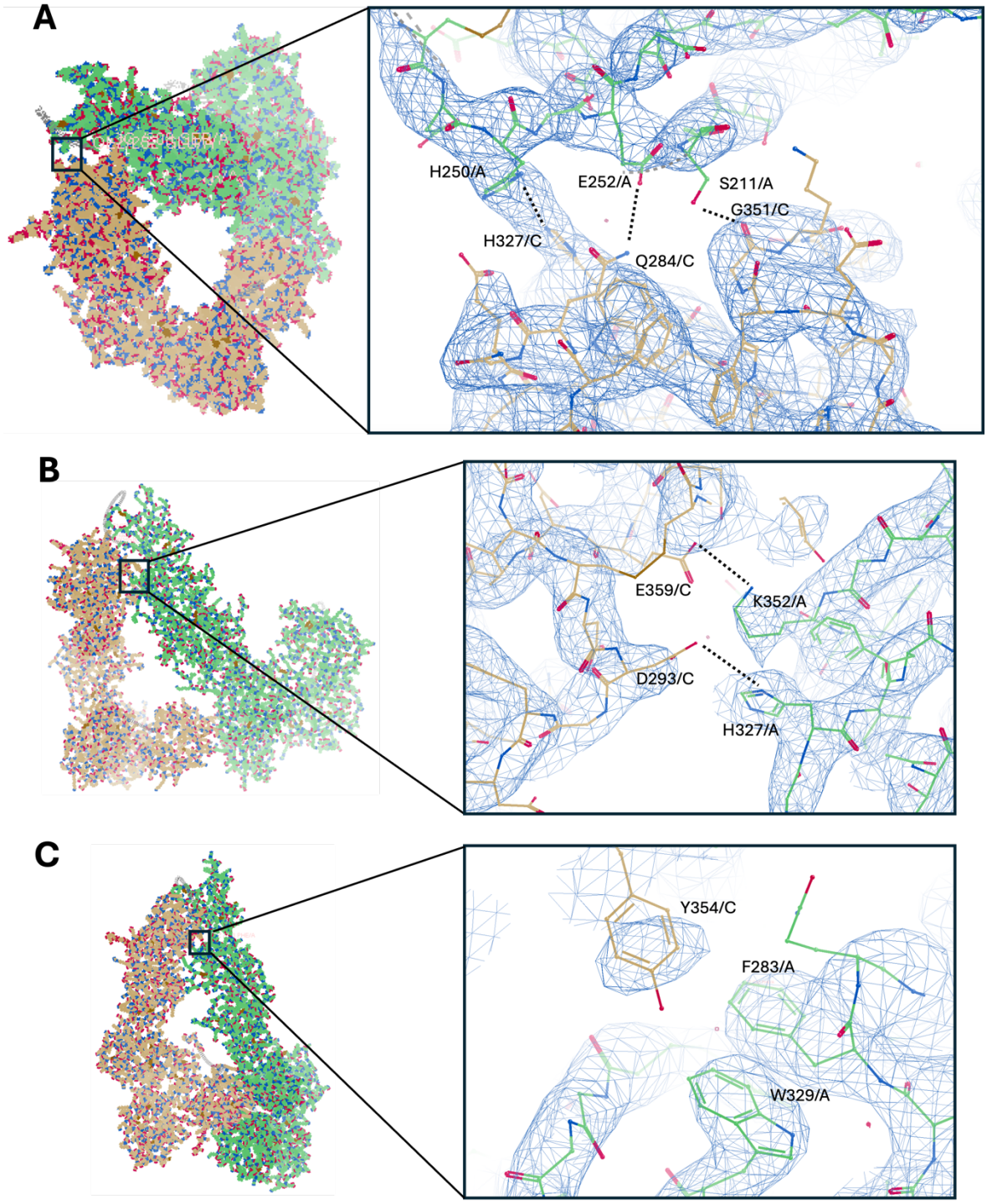


Figure 49: Close-up view of the N-terminal SRCR domains within the 'arms' showing selected hydrogen bonds (A), salt bridges (B) and hydrophobic interactions (C) mediating the inter-protomeric interaction. Dashed lines indicate predicted hydrogen bonds and salt bridges. Coot 0.9.8.8 was used display the protein.

Table 7: Cryo-EM data collection, refinement and validation statistics for unliganded dimeric CD163 as well as data collection statistics for unliganded trimeric CD163. While a model was successfully built for the dimer, model building for the trimer was challenging due to the low resolution of the volume. However, key features were already visible in the trimer map. Therefore, a model was not constructed for the unliganded CD163 trimer.

| | Unliganded dimeric CD163 | Unliganded trimeric CD163 |
|---|---|---|
| **Data collection and processing** | | |
| Microscope | Titan Krios | |
| Detector | Gatan K3 with BioQuantum Imaging Filter | |
| Magnification | 58,149 | |
| Voltage (kV) | 300 | |
| Electron exposure (e-/Å$^2$) | 42.82 | |
| Defocus range (μm) | -0.6 to -1.8 | |
| Pixel size (Å) | 0.832 | |
| Symmetry imposed | C1 | |
| Initial particle images (no.) | 13,772,487 | |
| Final particle images (no.) | 723,620 | 96,576 |
| Map resolution (Å) | 3.10 | 3.64 |
| FSC threshold 0.143 | | |
| Map resolution range (Å) | 2.57 – 40.5 | 3.05 – 58.0 |
| FSC threshold 0.5 | | |
| **Refinement** | | |
| Initial model used | AlphaFold2, dimeric and trimeric CD163-Hp(1-1)Hb | |
| Model resolution (Å) | 3.80 | |
| FSC threshold 0.5 | | |
| Model composition | | |
| Non-hydrogen atoms | 10,305 | |
| Protein residues | 1,341 | |
| Ligands | 22 | |
| B factors (Å$^2$) | | |
| Protein | 98.13 | |
| Ligands | 30.00 | |
| R.m.s deviations | | |
| Bond lengths (Å) | 0.017 | |
| Bond angles (°) | 1.509 | |
| Validation | | |
| MolProbity score | 1.90 | |
| Clashscore | 8.93 | |
| Poor rotamers (%) | 0.37 | |
| Ramachandran plot | | |
| Favoured (%) | 93.59 | |
| Allowed (%) | 6.10 | |
| Disallowed (%) | 0.30 | |
| Model vs. data fit | | |
| CC (mask) | 0.70 | |
| CC (box) | 0.71 | |

## 5.3 Comparison of the ligand binding and inter-protomeric interfaces in the 'arms' of CD163

To provide a hypothesis about the function of the 'arm-to-arm' interactions in the unliganded CD163 dimer, these underlying interfaces were compared to the ligand binding interfaces within the 'arms'.

PDBe's Protein Interfaces, Surfaces and Assemblies (PISA) software was used to identify residues involved in each interface. PISA quantifies differences in solvation energy between associated and dissociated surfaces, stabilisation by hydrogen bonds, salt bridges, disulphide bonds and hydrophobic interactions to determine interacting residues (Krissinel & Henrick, 2007). Table 8 contains a list of all residues identified by PISA as interface residues in the 'arms' of the structures of the unliganded CD163 dimer, as well as in the liganded CD163 dimer and trimer. The surfaces involved in either ligand binding or the 'arm-to-arm' interactions are visualised in Figure 50.

Table 8: Summary of all interface residues in the 'arms' of unliganded CD163 dimer, liganded CD163 dimer and trimer, as determined by PDBePISA.

| Structure | Chain A residues | Chain B residues | Chain C residues |
|---|---|---|---|
| **Unliganded CD163 dimer** | R163 | N/A | Q284 |
| | S207 | | E286 |
| | F208 | | D293 |
| | S209 | | H327 |
| | G210 | | W329 |
| | S211 | | S332 |
| | H250 | | W350 |
| | E252 | | G351 |
| | F283 | | K352 |
| | Q284 | | H353 |
| | E286 | | Y354 |
| | H327 | | C355 |
| | W329 | | N356 |
| | W350 | | N358 |
| | G351 | | E359 |
| | K352 | | R400 |
| | Y354 | | L460 |
| | N356 | | D463 |
| | H357 | | H464 |
| | | | Y465 |

| Structure | Chain A residues | Chain B residues | Chain C residues |
|---|---|---|---|
| **Liganded CD163 dimer** | D186 | N/A | D293 |
| | E216 | | G294 |
| | N247 | | S332 |
| | C248 | | S334 |
| | D249 | | H348 |
| | H250 | | Y354 |
| | A251 | | E359 |
| | E252 | | D399 |
| | D293 | | R400 |
| | H353 | | G401 |
| | Y354 | | S440 |
| | C355 | | S441 |
| | N356 | | D463 |
| | E359 | | H464 |
| | D463 | | Y465 |
| | H464 | | |
| | Y465 | | |
| **Liganded CD163 trimer** | D186 | D293 | D293 |
| | E216 | D331 | G351 |
| | N247 | K346 | K352 |
| | C248 | H347 | H353 |
| | D249 | H348 | Y354 |
| | H250 | E349 | C355 |
| | A251 | W350 | N356 |
| | E252 | Y354 | N358 |
| | D293 | C355 | D463 |
| | H353 | E359 | H464 |
| | Y354 | R400 | Y465 |
| | C355 | T461 | |
| | N356 | D463 | |
| | E359 | H464 | |
| | R400 | Y465 | |
| | T461 | | |
| | D463 | | |
| | H464 | | |
| | Y465 | | |

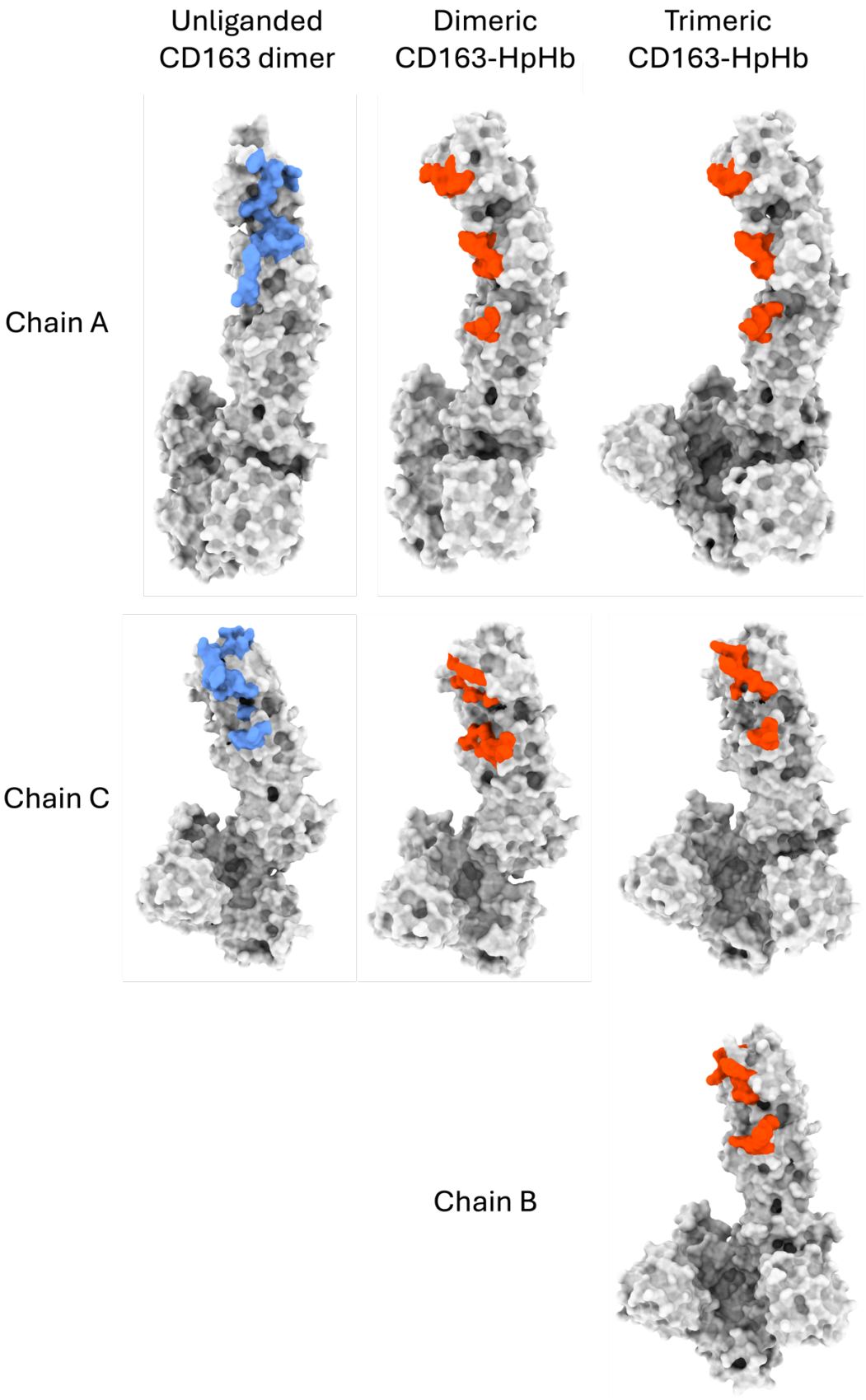


Figure 50: Surface diagram of CD163 in the unliganded CD163 dimer, as well as liganded CD163 dimer and trimer. Surfaces involved in the 'arm-to-arm' interface are coloured in blue whereas surfaces participating in ligand binding are displayed in red.

In chain C, there is significant overlap between the surfaces mediating ligand binding and the 'arm-to-arm' interactions. Although these surfaces also overlap in chain A, the extent is less pronounced in chain C. This overlap suggests a possible function for the 'arm-to-arm' contact. In this model, the surfaces involved in ligand binding are buried in unliganded CD163 due to inter-protomeric interactions. However, during intravascular haemolysis, HpHb is formed. This ligand binds to CD163 with high affinity (Figure 29A) and is, therefore, capable of competing with the relatively weak 'arm-to-arm' interactions. Such a mechanism is referred to as autoinhibition and is often observed in enzymes to prevent unintended catalytic activity (Adams, 2002; Hubbard, 2002). In this case, the autoinhibition could, for instance, prevent the uptake of lower affinity ligands, which are not able to compete with the autoinhibition interactions, such as Hp before it is conjugated to Hb.

## 5.4 Mutations in the 'arms' of CD163 and their effects on ligand binding and uptake

To assess the function of the 'arm-to-arm' contact and to test the model of autoinhibition, mutations which aim to disrupt the 'arm-to-arm' contact but not the ligand binding interface, were designed. Due to the significant overlap between these two types of interfaces, only two plausible mutations were identified. QGE284-286NGT and G351W introduce an N-linked glycan and a large aromatic residue, respectively, which would both conceptually prevent the interactions between the 'arms'.

Due to the size of a glycan, the positions of residue 284 in every 'arm' of unliganded dimeric CD163 and liganded trimeric CD163 were thoroughly examined to ensure that the glycan would not interfere with the ligand binding site. While a glycan is expected to disrupt the 'arm-to-arm' contact (Figure 51A), it should not prevent 'arms' B or C from binding HpHb (Figure 51B). There is a possibility that the mutation could displace SRCR domain 2 but the glycan could also cause N284 to reposition, avoiding clashes with SRCR domain 2.

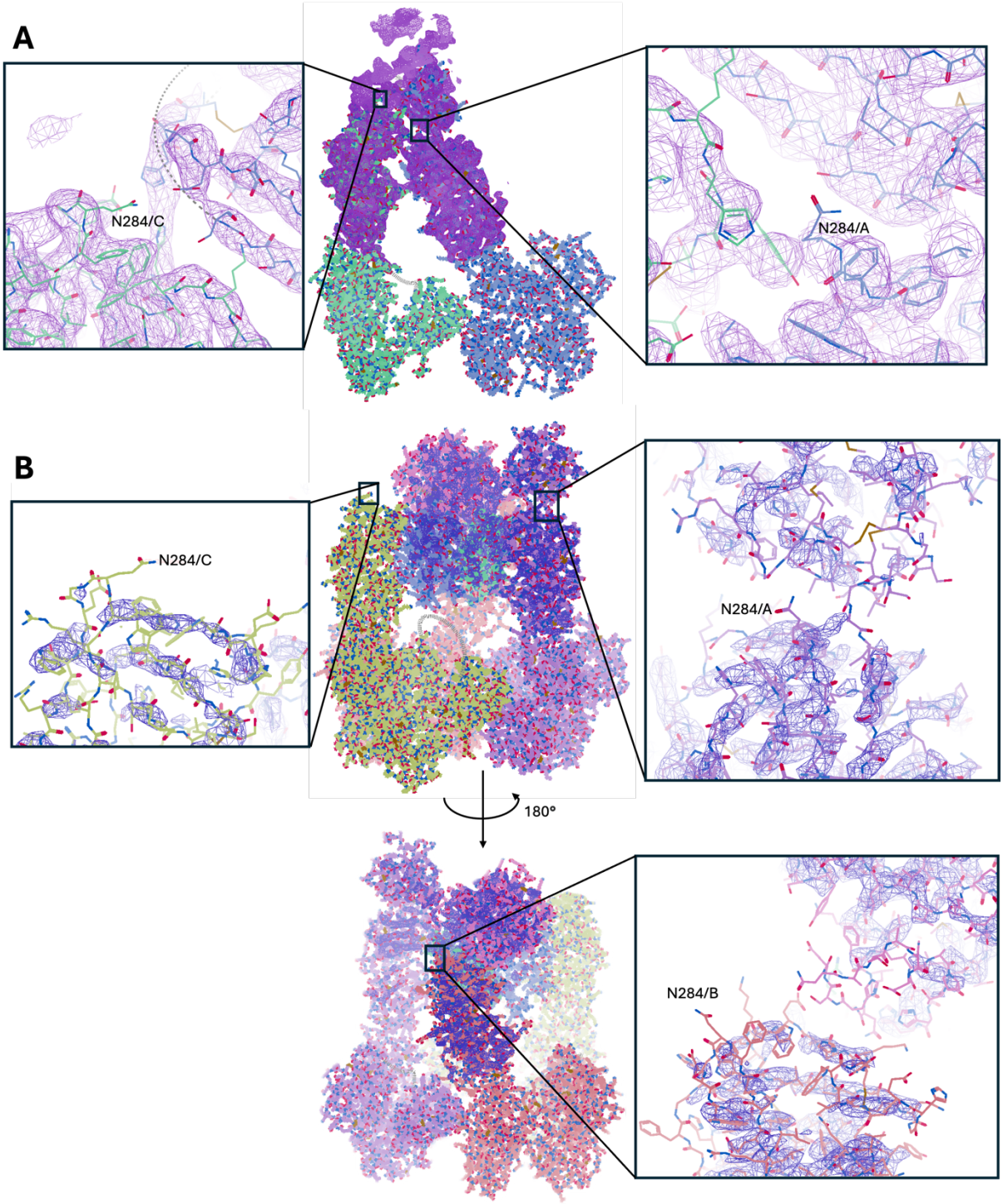


Figure 51: Close-up view of N284 in the unliganded CD163 dimer (A) and the liganded CD163 trimer (B).

These mutants of CD163 were expressed as Avi-tagged constructs (Figure 52), after which their ability to bind Hp(1-1)Hb was assessed on SPR. CD163-QGE284-286NGT showed binding to Hp(1-1)Hb at 696 pM (Figure 52B), an affinity comparable to CD163-WT (276 pM, Figure 29A). In contrast, CD163-G351W did not bind Hp(1-1)Hb even at

200 nM (Figure 52A), indicating that G351W is directly disrupting the ligand binding interface or that the mutant is misfolded. Circular dichroism (CD) spectroscopy can be employed to analyse the secondary structure of this mutant and compare it to CD163-WT. Since the mutation is not expected to affect the secondary structure, CD163-WT and -G351W should exhibit nearly identical CD spectra, assuming this mutation does not interfere with protein folding. However, due to time constraints, only the QGE284-286NGT mutant was further analysed in downstream experiments.

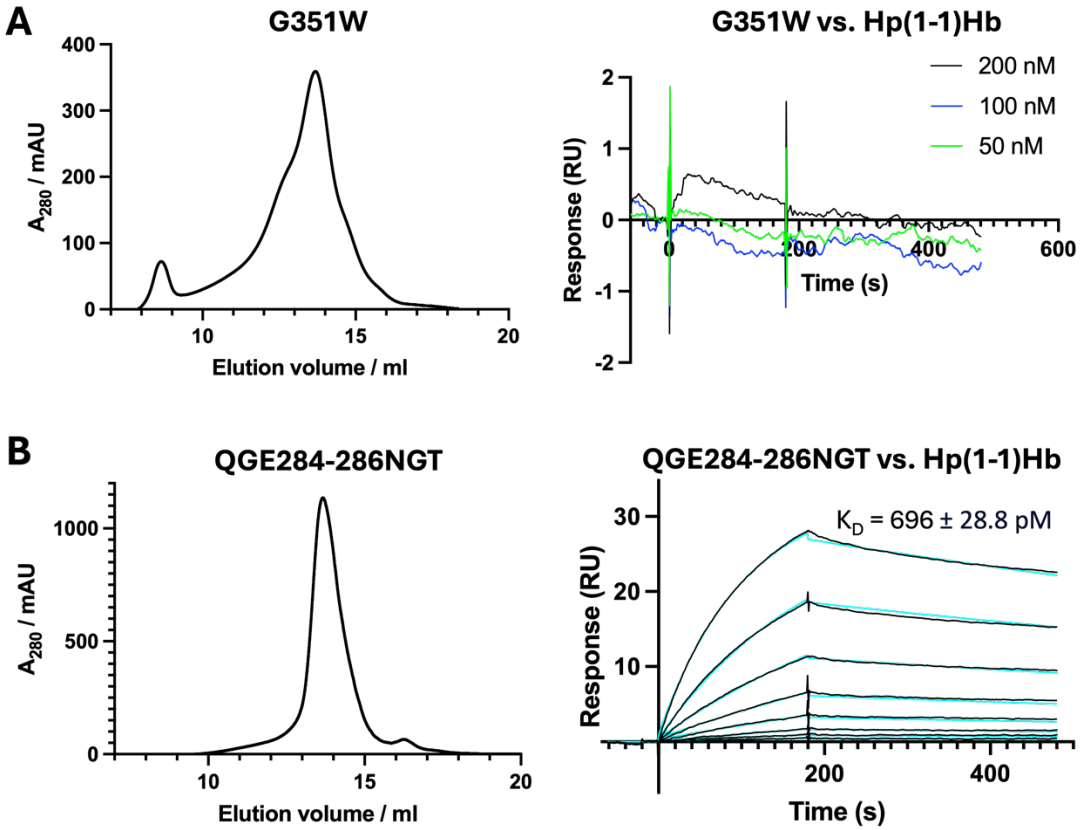


Figure 52: Purification and SPR analyses of CD163-G351W (A) and -QGE284-286NGT (B). For SPR measurements of QGE284-286NGT, Hp(1-1)Hb was injected in a two-fold dilution series from 10 – 0.078 nM. Although this measurement was performed in triplicate, only a representative replicate is shown.

Since QGE284-286NGT conceptually neither affects the ligand binding site nor disrupts any residues in the 'base' crucial to multimerisation, it was expected that this mutant should still be able to bind Hb, which is the component of HpHb the wild-type receptor primarily interacts with. The interaction between this mutant and Hb was characterised using MST. Interestingly, this mutant exhibited a 9-fold reduced Hb binding affinity (Figure 53), despite the SPR data demonstrating that CD163-QGE284-286NGT still binds to Hp(1-

1)Hb (Figure 52B). Therefore, these findings might suggest that CD163 uses a different binding site for Hb than for HpHb.

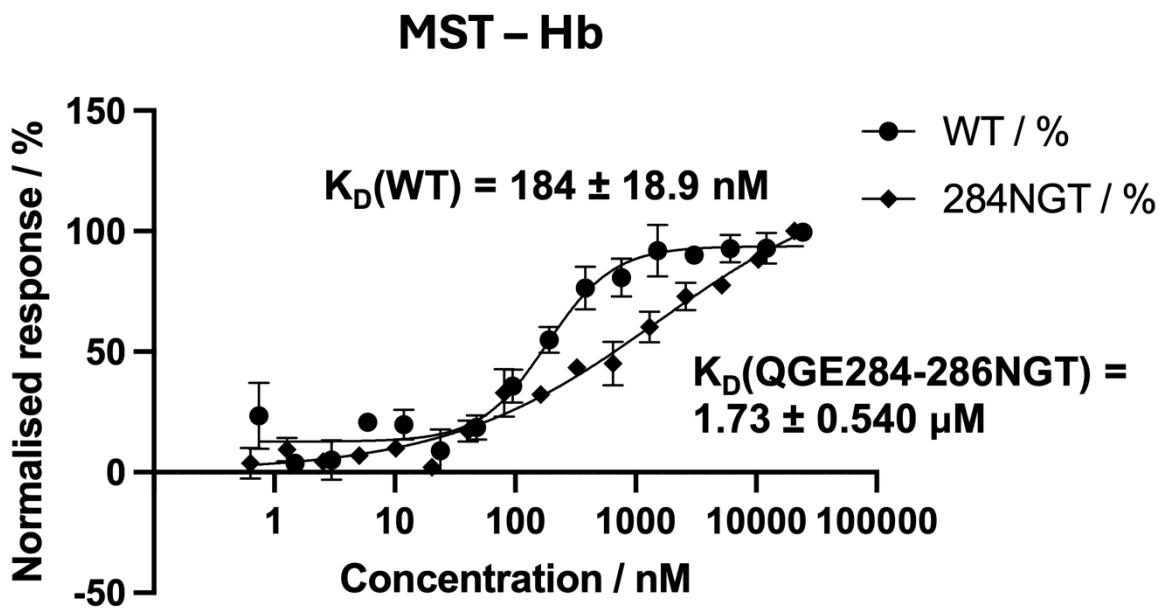


Figure 53: Evaluation of the Hb binding affinity of CD163-QGE284-286NGT using MST. The assay was conducted in triplicate, with the mean $K_D$ ± standard deviation shown.

To further assess the effects of CD163-QGE284-286NGT on the surface of a cell, uptake experiments were performed. If CD163-WT was autoinhibited, relieving the autoinhibition would enhance the uptake efficiency of ligands, as ligand binding would no longer compete against the 'arm-to-arm' contact. Here, stable cells expressing CD163-WT and CD163-QGE284-286NGT were generated, and their uptake of Hp(2-2)Hb was evaluated against that of untransfected HEK293 cells. While QGE284-286NGT led to marginally improved uptake compared to the negative control, CD163-WT resulted in significantly larger uptake of Hp(2-2)Hb (Figure 54). This observation would not appear to support the theory of autoinhibition. Overall, introducing an N-linked glycan at residue 284 might affect the stability of the CD163 dimer. This and other hypotheses will be extensively addressed in the next section.

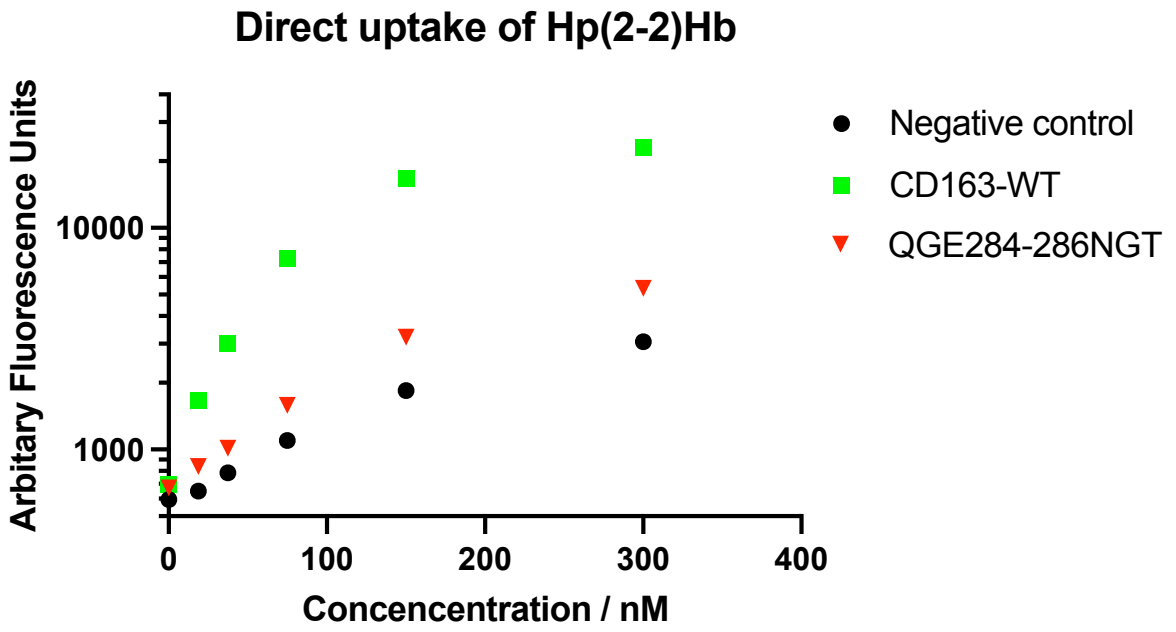


Figure 54: Uptake of fluorescent Hp(2-2)Hb by stable HEK293 cells expressing CD163-WT and -QGE284-286NGT as well as untransfected cells. This experiment was performed in singlicate. Results for CD163-WT and untransfected HEK293 cells were presented in Figure 33C and are only included for comparison purposes.

## 5.5 Discussion

The conformations of unliganded dimeric and trimeric CD163 were presented in this Chapter. In the absence of a bound ligand, the trimer is less stable, with a larger fraction of dimeric rather than monomeric receptor. In the presence of HpHb, an additional interaction interface is present, which reduces the flexibility across CD163 and stabilises the molecule. However, it should be mentioned that these conclusions were derived from experiments where the ectodomain of CD163 was free to diffuse before or throughout the measurement. In contrast, on the surface of a cell membrane, CD163 will be locally concentrated, further favouring trimerisation.

Interestingly, the dimer adopts an ‘arm-to-arm’ contact, which buries the ligand binding surfaces of CD163. Due to time constraints, the function of this conformation could not be conclusively determined and is still subject to further research. A hypothesis for the function of the ‘arm-to-arm’ contact is autoinhibition. The QGE284-286NGT mutant was specifically designed to block the ‘arm-to-arm’ interaction, without affecting the HpHb

binding site. In biophysical experiments, this mutant still binds to Hp(1-1)Hb using a high-affinity interaction but has a significantly reduced affinity towards Hb. In a preliminary singlicate experiment, this mutation exhibits impaired uptake of Hp(2-2)Hb. However, this requires more characterisation, including confirmation of surface receptor expression. Since relieving CD163 of autoinhibition would increase affinity and uptake efficiencies for ligands of CD163, these results do not appear to support autoinhibition. I currently do not have a strong hypothesis, which supports all the observations. Alternative theories for the function of the 'arm-to-arm' interaction are discussed in the following.

One possible role of the 'arm-to-arm' contact is to stabilise the unliganded dimer by reducing the flexibility of the 'arms' and preventing its dissociation into monomers. However, the induced stabilisation of the dimer is unlikely to be crucial for scavenging high-affinity ligands, as the 'monomer mutant' can take up Hp(2-2)Hb as efficiently as CD163-WT (Figure 40C).

The 'arm-to-arm' contact might stabilise the dimer to facilitate trafficking from the endoplasmic reticulum or the endosome to the cell membrane. Proteins involved in sorting could recognise the dimer and direct it to vesicles designated for the cell membrane. However, the monomeric mutant takes up Hp(2-2)Hb, indicating that monomeric CD163 is indeed trafficked to the cell membrane (Figure 40C), challenging this hypothesis.

Since CD163 is a scavenger receptor expressed on the surface of macrophages, it is exposed to various stress factors, including proteases. Therefore, the role of the 'arm-to-arm' contact might not be to induce multimerisation but to bury specific patches of CD163, as depicted in Figure 49. This conformation could protect the receptor from proteolytic conditions encountered by macrophages. To experimentally validate this hypothesis, recombinant CD163-WT and -QGE284-286NGT can be incubated with serum protease mixtures, and their cleavage can be analysed using SDS-PAGE. Significant differences in the formation of cleavage products would indicate that the 'arm-to-arm' contact provides shielding against proteolytic degradation.

In summary, this chapter shows that the unliganded form of CD163 retains its ability to form multimers, which is probably more pronounced at the higher local concentrations on the surface. As expected, a large fraction of these unliganded multimers exist with the ligand binding ‘arms’ flexible, ready to ‘mould’ around diverse ligands. However, the dimers adopt a conformation in which these ‘arms’ contact one another. The function of these contacts remains to be determined and will be the subject of continuing research.

# 6. Conclusions and future directions

## 6.1 Mechanisms of ligand selectivity

Since compartmentalisation is essential for life, regulating the uptake of wanted molecules is crucial for the survival of cells. The definition of 'wanted' particles is dependent on context. In the case of Hb detoxification, the uptake of Hb bound to any form of Hp is certainly desirable, as it facilitates the removal of harmful Hb from the plasma. Additionally, internalisation of free Hb is beneficial, as Hb is the component to be detoxified and becomes enriched in the serum during severe haemolysis, when Hp is depleted. Conversely, uptake and degradation of Hp is unfavourable because unconjugated Hp is valuable in the serum to scavenge free Hb.

This presents a unique set of challenges for CD163. The ligands it should recognise share a common Hb moiety but may include different Hp phenotypes with different structural arrangements. Moreover, CD163 should not bind to free Hp. How does CD163 selectively bind to the desired ligands (Hb and HpHb) while avoiding unwanted proteins like free Hp? In this case, nature has presented a unique solution to the problem.

CD163 scavenges HpHb by forming multimers, with each protomer collectively binding the complex in an asymmetric manner. One 'arm' recognises both Hp and Hb, a second 'arm' binds only to Hb and a third 'arm' forms contacts with a surface between Hp and Hb. Overall, there are more interactions with Hb, and contacts to Hp are primarily with HpSP. As HpSP is a domain all phenotypes of Hp have in common, this type of interaction ensures that CD163 can scavenge Hb bound to all Hp phenotypes. Additionally, this mode of binding enables CD163 to scavenge Hb but not Hp because CD163 predominantly binds to Hb within the HpHb complex.

Multimerisation plays a critical role in ligand selectivity. The avidity provided by multiple 'arms' binding simultaneously strengthens the hold of CD163 on the ligand, enabling scavenging of lower-affinity ligands, such as Hp(1-1)Hb and Hb. Conversely, free Hp

cannot by bound by all three ‘arms’ of the trimer or by both ‘arms’ of the dimer (Figure 25 and Figure 26), further preventing its uptake.

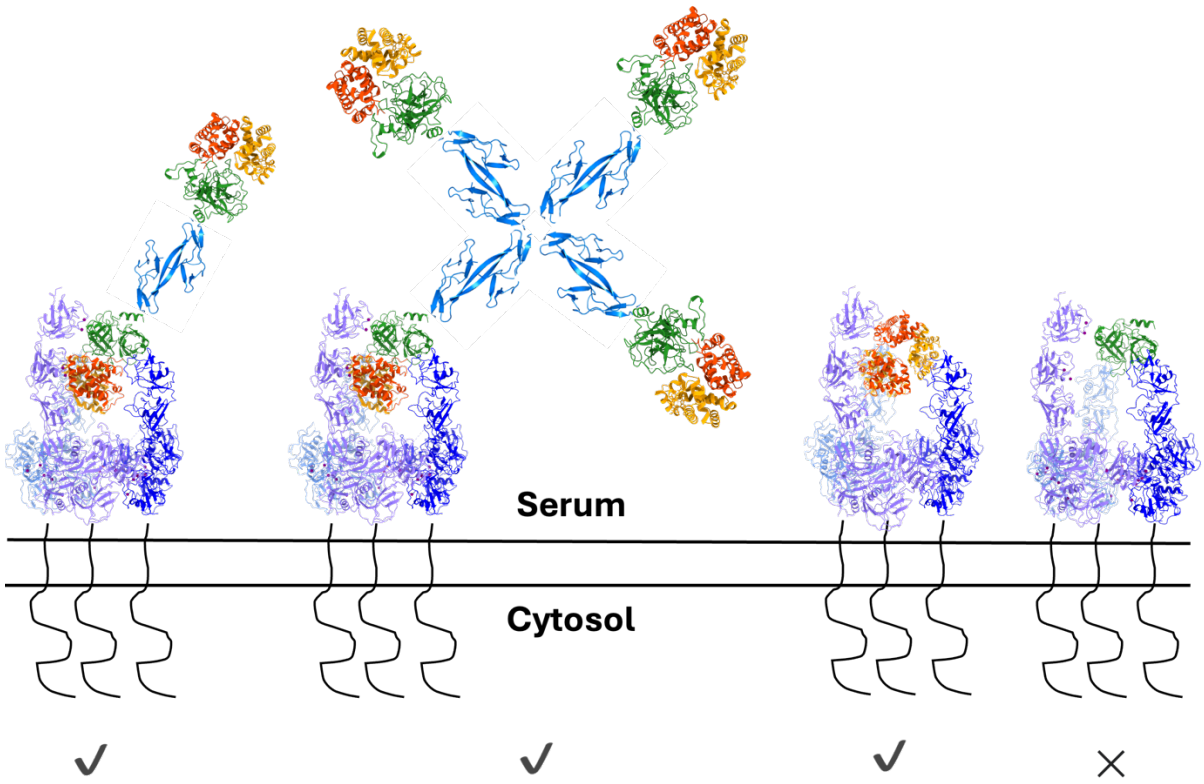


Figure 55: Schematic illustration conceptually depicting complexes between CD163 and various ligands, including Hp(1-1)Hb, Hp(2-2)Hb, Hb and unconjugated HpSP. In CD163-Hb, Hb is displayed as a tetramer, although it is not known whether CD163 takes up tetrameric or dimeric Hb. The symbols below each complex indicate whether ligand uptake occurs at physiological concentrations. It should be noted that CD163-Hp is shown for illustrative purposes only; such an interaction is unlikely to be stable and does not result in uptake.

## 6.2 Coordination of ligand binding and release with environment conditions

In addition to ligand selectivity, coordinating ligand binding and release with the receptor’s environment is essential for the function of scavenger receptors. Binding occurs in the serum, where free Hb accumulates during intravascular haemolysis. In contrast, ligand release takes place in the endosome of the macrophage, where Hb is degraded, allowing CD163 to recycle back to the cell membrane. Premature release of

Hb in the plasma could be detrimental to the host organism, as Hb would not be toxified. To address this challenge, CD163 has also evolved an elegant mechanism for regulating the conditions under which ligand is bound and released.

The concentration of calcium ions is approximately 1,000-times lower in the endosome than in the serum (Gerasimenko et al., 1998; Goldstein, 1990). CD163 uses this correlation between the calcium concentration and the environment to coordinate ligand binding and release. Calcium ions are seen at the interfaces between CD163 and Hp, CD163 and Hb, as well as in the inter-protomeric 'base' of the receptor (Figure 25 and Figure 26). They are coordinated by a cluster of acidic residues on one chain, which is further neutralised by a lysine side chain from the opposing molecule (Figure 35 and Figure 43). In the calcium-rich serum, this allows CD163 to multimerise and bind to its ligands. However, in the calcium-depleted conditions of the endosome, the absence of calcium ions prevents adequate neutralisation of the negatively charged cluster of residues, inhibiting receptor multimerisation and facilitating ligand release.

The use of calcium ions to regulate ligand binding and release is not exclusive to CD163. For instance, scavenging of low-density lipoproteins (LDL) is mediated by the LDL receptor (LDLR), which employs its complement-type repeat (CR) domains 3 and 4 to bind its ligands (Andersen & Moestrup, 2014). Similar to CD163, LDLR engages the receptor-associated protein (RAP) using a lysine residue and a cluster of negatively charged side chains coordinating a calcium ion (Fisher et al., 2006). Structural studies have revealed that ligand binding at low pH is further blocked by intramolecular interactions between the β-propeller domain of LDLR and CR domains 4 and 5 (Rudenko et al., 2002). These interactions also involve a calcium ion, which is still bound at low pH.

## 6.3 Future directions

The structure of the unliganded CD163 dimer, exhibiting an 'arm-to-arm' contact, was presented in this dissertation. The 'arm-to-arm' contact could regulate the function of CD163, making it important to explore its exact role, and this is subject to ongoing research. To design a mutant that specifically disrupts the 'arm-to-arm' contact but not the ligand binding interface, I will carefully re-examine all residues at both interfaces to ensure no potential mutation site was overlooked, aiming to selectively alter the 'arm-to-arm' interaction while not affecting ligand recognition.

When evaluating the 'arm-to-arm' contact, CD163-QGE284-286-NGT was assessed using biophysical assays. Compared to CD163-WT, this mutant displays similar affinity for Hp(1-1)Hb but significantly reduced affinity for Hb. These results could suggest that CD163 may use a different binding site for HpHb than for Hb. To obtain a clearer understanding for how CD163 scavenges Hb, the structure of the CD163-Hb complex should be investigated using cryo-EM. These studies could also provide insights into whether CD163 preferably recognises dimeric or tetrameric Hb.

While CD163 plays critical roles in physiology, it is also exploited in pathological conditions. Notably, CD163 serves as an intracellular receptor for the porcine reproductive and respiratory syndrome virus (PRRSV), which hijacks CD163 to enter macrophages (Calvert et al., 2007; Vanderheijden et al., 2003). SRCR domain 5 has been identified as the essential domain mediating viral entry (Van Gorp et al., 2010). However, the exact assembly of CD163 and the glycoproteins of PRRSV remains unknown. In the environment of the endosome, CD163 is likely a monomer. Reconstructing PRRSV during CD163 engagement using cryo-electron tomography would provide crucial insights into the molecular mechanisms of PRRSV entry.

While there is more to discover about CD163, this thesis offers the first structural and molecular characterisation of this receptor and reveals surprises. It demonstrates, for the first time, that CD163 forms multimers, which serve to enhance the uptake of lower affinity ligands. These studies also show how CD163 regulates binding and release of

ligands in different cellular locations. This work provides the first in-depth analysis of how this scavenger receptor functions, with findings that are likely applicable to related receptors.

# References


Abbe, E. (1873). Beiträge zur Theorie des Mikroskops und der mikroskopischen Wahrnehmung: I. Die Construction von Mikroskopen auf Grund der Theorie. *Archiv Für Mikroskopische Anatomie*, *9*(1), 413–418. https://doi.org/10.1007/BF02956173/METRICS

Adams, J. A. (2002). Activation Loop Phosphorylation and Catalysis in Protein Kinases: Is There Functional Evidence for the Autoinhibitor Model?†. *Biochemistry*, *42*(3), 601–607. https://doi.org/10.1021/BI020617O

Afonine, P. V., Poon, B. K., Read, R. J., Sobolev, O. V., Terwilliger, T. C., Urzhumtsev, A., & Adams, P. D. (2018). Real-space refinement in PHENIX for cryo-EM and crystallography. *Urn:Issn:2059-7983*, *74*(6), 531–544. https://doi.org/10.1107/S2059798318006551

Akahori, H., Karmali, V., Polavarapu, R., Lyle, A. N., Weiss, D., Shin, E., Husain, A., Naqvi, N., Van Dam, R., Habib, A., Choi, C. U., King, A. L., Pachura, K., Taylor, W. R., Lefer, D. J., & Finn, A. V. (2015). CD163 interacts with TWEAK to regulate tissue regeneration after ischaemic injury. *Nature Communications 2015 6:1*, *6*(1), 1–14. https://doi.org/10.1038/ncomms8792

Alquraini, A., & El Khoury, J. (2020). Scavenger receptors. *Current Biology*, *30*(14), R790–R795. https://doi.org/10.1016/j.cub.2020.05.051

Andersen, C. B. F., & Moestrup, S. K. (2014). How calcium makes endocytic receptors attractive. *Trends in Biochemical Sciences*, *39*(2), 82–90. https://doi.org/10.1016/J.TIBS.2013.12.003

Andersen, C. B. F., Stødkilde, K., Sæderup, K. L., Kuhlee, A., Raunser, S., Graversen, J. H., & Moestrup, S. K. (2017). Haptoglobin. *Https://Home.Liebertpub.Com/Ars*, *26*(14), 814–831. https://doi.org/10.1089/ARS.2016.6793

Andersen, C. B. F., Torvund-Jensen, M., Nielsen, M. J., De Oliveira, C. L. P., Hersleth, H. P., Andersen, N. H., Pedersen, J. S., Andersen, G. R., & Moestrup, S. K. (2012). Structure of the haptoglobin–haemoglobin complex. *Nature 2012 489:7416*, *489*(7416), 456–459. https://doi.org/10.1038/nature11369

Anderson, R. G. W., Brown, M. S., & Goldstein, J. L. (1977). Role of the coated endocytic vesicle in the uptake of receptor-bound low density lipoprotein in human fibroblasts. *Cell*, *10*(3), 351–364. https://doi.org/10.1016/0092-8674(77)90022-8

Aragón-Serrano, L., Carrillo-Serradell, L., Planells-Romeo, V., Isamat, M., Velasco-de Andrés, M., & Lozano, F. (2023). CD6 and Its Interacting Partners: Newcomers to the Block of Cancer Immunotherapies. *International Journal of Molecular Sciences 2023, Vol. 24, Page 17510*, *24*(24), 17510. https://doi.org/10.3390/IJMS242417510

Aricescu, A. R., Lu, W., & Jones, E. Y. (2006). A time- and cost-efficient system for high-level protein production in mammalian cells. *Acta Crystallographica Section D: Biological Crystallography*, *62*(10), 1243–1250. https://doi.org/10.1107/S0907444906029799

Berland, R., & Wortis, H. H. (2002). Origins and functions of B-1 cells with notes on the role of CD5. *Annual Review of Immunology*, *20*(Volume 20, 2002), 253–300. https://doi.org/10.1146/ANNUREV.IMMUNOL.20.100301.064833/CITE/REFWORKS

Bolton, W., & Perutz, M. F. (1970). Three Dimensional Fourier Synthesis of Horse Deoxyhaemoglobin at 2.8 Å Resolution. *Nature 1970 228:5271*, *228*(5271), 551–552. https://doi.org/10.1038/228551a0

Bottou, L. (2010). Large-Scale Machine Learning with Stochastic Gradient Descent. *Proceedings of COMPSTAT 2010 - 19th International Conference on Computational Statistics, Keynote, Invited and Contributed Papers*, 177–186. https://doi.org/10.1007/978-3-7908-2604-3_16

Bover, L. C., Cardó-Vila, M., Kuniyasu, A., Sun, J., Rangel, R., Takeya, M., Aggarwal, B. B., Arap, W., & Pasqualini, R. (2007). A Previously Unrecognized Protein-Protein Interaction between TWEAK and CD163: Potential Biological Implications. *The Journal of Immunology*, *178*(12), 8183–8194. https://doi.org/10.4049/JIMMUNOL.178.12.8183

Broglie, L. De. (1925). Recherches sur la théorie des Quanta. *Annales de Physique*, *10*(3), 22–128. https://doi.org/10.1051/ANPHYS/192510030022

Brown, M. S., Goldstein, J. L., Krieger, M., Ho, Y. K., & Anderson, R. G. (1979). Reversible accumulation of cholesteryl esters in macrophages incubated with acetylated lipoproteins. *Journal of Cell Biology*, *82*(3), 597–613. https://doi.org/10.1083/JCB.82.3.597

Caesar, J., Reboul, C. F., Machello, C., Kiesewetter, S., Tang, M. L., Deme, J. C., Johnson, S., Elmlund, D., Lea, S. M., & Elmlund, H. (2020). SIMPLE 3.0. Stream single-particle cryo-EM analysis in real time. *Journal of Structural Biology: X*, *4*, 100040. https://doi.org/10.1016/J.YJSBX.2020.100040

Caì, Y., Postnikova, E. N., Bernbaum, J. G., Yú, S., Mazur, S., Deiuliis, N. M., Radoshitzky, S. R., Lackemeyer, M. G., McCluskey, A., Robinson, P. J., Haucke, V., Wahl-Jensen, V., Bailey, A. L., Lauck, M., Friedrich, T. C., O'Connor, D. H., Goldberg, T. L., Jahrling, P. B., & Kuhn, J. H. (2015). Simian Hemorrhagic Fever Virus Cell Entry Is Dependent on CD163 and Uses a Clathrin-Mediated Endocytosis-Like Pathway. *Journal of Virology*, *89*(1), 844–856. https://doi.org/10.1128/JVI.02697-14/ASSET/D268292C-E663-44D9-AF43-6D872CACD3C6/ASSETS/GRAPHIC/ZJV9990999260009.JPEG

Calvert, J. G., Slade, D. E., Shields, S. L., Jolie, R., Mannan, R. M., Ankenbauer, R. G., & Welch, S.-K. W. (2007). CD163 Expression Confers Susceptibility to Porcine Reproductive and Respiratory Syndrome Viruses. *Journal of Virology*, *81*(14), 7371–7379. https://doi.org/10.1128/JVI.00513-07/ASSET/C40678A7-A13A-482B-9BFB-FA82D65EC44D/ASSETS/GRAPHIC/ZJV0140793870008.JPEG

Canton, J., Neculai, D., & Grinstein, S. (2013). Scavenger receptors in homeostasis and immunity. *Nature Reviews Immunology 2013 13:9*, *13*(9), 621–634. https://doi.org/10.1038/nri3515

Carlsen, C. U., Møller, J. K. S., & Skibsted, L. H. (2005). Heme-iron in lipid oxidation. *Coordination Chemistry Reviews*, *249*(3–4), 485–498. https://doi.org/10.1016/J.CCR.2004.08.028

Das, P. B., Dinh, P. X., Ansari, I. H., de Lima, M., Osorio, F. A., & Pattnaik, A. K. (2010). The minor envelope glycoproteins GP2a and GP4 of porcine reproductive and respiratory syndrome virus interact with the receptor CD163. *Journal of Virology*, *84*(4), 1731–1740. https://doi.org/10.1128/JVI.01774-09

De Genst, E. J., Guilliams, T., Wellens, J., Day, E. M., Waudby, C. A., Meehan, S., Dumoulin, M., Hsu, S. T. D., Cremades, N., Verschueren, K. H. G., Pardon, E., Wyns, L., Steyaert, J., Christodoulou, J., & Dobson, C. M. (2010). Structure and Properties of a Complex of α-Synuclein and a Single-Domain Camelid Antibody. *Journal of Molecular Biology*, *402*(2), 326–343. https://doi.org/10.1016/J.JMB.2010.07.001

Delputte, P. L., Costers, S., & Nauwynck, H. J. (2005). Analysis of porcine reproductive and respiratory syndrome virus attachment and internalization: distinctive roles for heparan sulphate and sialoadhesin. *The Journal of General Virology*, *86*(Pt 5), 1441–1445. https://doi.org/10.1099/VIR.0.80675-0

Doherty, G. J., & McMahon, H. T. (2009). Mechanisms of endocytosis. *Annual Review of Biochemistry*, *78*(Volume 78, 2009), 857–902. https://doi.org/10.1146/ANNUREV.BIOCHEM.78.081307.110540/1

Dokland, T. (2010). The structural biology of PRRSV. *Virus Research*, *154*(1–2), 86–97. https://doi.org/10.1016/J.VIRUSRES.2010.07.029

Emsley, P., & Cowtan, K. (2004). Coot: model-building tools for molecular graphics. *Urn:Issn:0907-4449*, *60*(12), 2126–2132. https://doi.org/10.1107/S0907444904019158

Epstein, A. L., Levy, R., Kim, H., Henle, W., Henle, G., & Kaplan, H. S. (1978). BIOLOGY OF THE HUMAN MALIGNANT LYMPHOMAS IV. Functional Characterization of Ten Dzffuse Histiocytic Lymphoma Cell Lines. *Cancer*, *42*, 2379–2391. https://doi.org/10.1002/1097-0142(197811)42:5

Etzerodt, A., Rasmussen, R., Svendsen, P., Chalaris, A., Schwarz, J., Galea, I., Møller, J., & Moestrup, S. K. (2013). Structural Basis for Inflammation-driven Shedding of CD163 Ectodomain and Tumor Necrosis Factor-Î± in Macrophages*. *Journal of Biological Chemistry*, *289*, 778–788. https://doi.org/10.1074/jbc.M113.520213

Fabriek, B. O., Bruggen, R. Van, Deng, D. M., Ligtenberg, A. J. M., Nazmi, K., Schornagel, K., Vloet, R. P. M., Dijkstra, C. D., & Van Den Berg, T. K. (2009). The macrophage scavenger receptor CD163 functions as an innate immune sensor for bacteria. *Blood*, *113*(4), 887–892. https://doi.org/10.1182/BLOOD-2008-07-167064

Fairhead, M., & Howarth, M. (2015). Site-specific biotinylation of purified proteins using BirA. *Methods in Molecular Biology*. https://doi.org/10.1007/978-1-4939-2272-7_12

Fisher, C., Beglova, N., & Blacklow, S. C. (2006). Structure of an LDLR-RAP Complex Reveals a General Mode for Ligand Recognition by Lipoprotein Receptors. *Molecular Cell*, *22*(2), 277–283. https://doi.org/10.1016/J.MOLCEL.2006.02.021

Frostell, Å., Vinterbäck, L., & Sjöbom, H. (2013). Protein-ligand interactions using SPR systems. *Methods in Molecular Biology*, *1008*, 139–165. https://doi.org/10.1007/978-1-62703-398-5_6/FIGURES/000611

Gerasimenko, J. V., Tepikin, A. V., Petersen, O. H., & Gerasimenko, O. V. (1998). Calcium uptake via endocytosis with rapid release from acidifying endosomes. *Current Biology*, *8*(24), 1335–1338. https://doi.org/10.1016/S0960-9822(07)00565-9

Goldstein, D. A. (1990). Serum Calcium. *THE JOURNAL OF INFECTIOUS DISEASES •*, *130*(5), 677–679. https://www.ncbi.nlm.nih.gov/books/NBK250/

Gordon, S. (2016). Phagocytosis: An Immunobiologic Process. *Immunity*, *44*(3), 463–475. https://doi.org/10.1016/J.IMMUNI.2016.02.026

Gourley, G. R. (1997). Bilirubin Metabolism and Kernicterus. *Advances in Pediatrics*, *44*(1), 173–229. https://doi.org/10.1016/S0065-3101(24)00052-5

Hallgren, J., Tsirigos, K. D., Damgaard Pedersen, M., Juan, J., Armenteros, A., Marcatili, P., Nielsen, H., Krogh, A., & Winther, O. (2022). DeepTMHMM predicts alpha and beta transmembrane proteins using deep neural networks. *BioRxiv*, 2022.04.08.487609. https://doi.org/10.1101/2022.04.08.487609

Helenius, A. (2018). Virus Entry: Looking Back and Moving Forward. *Journal of Molecular Biology*, *430*(13), 1853–1862. https://doi.org/10.1016/J.JMB.2018.03.034

Henne, W. M., Boucrot, E., Meinecke, M., Evergren, E., Vallis, Y., Mittal, R., & McMahon, H. T. (2010). FCHo proteins are nucleators of Clathrin-Mediated endocytosis. *Science*, *328*(5983), 1281–1284. https://doi.org/10.1126/SCIENCE.1188462/SUPPL_FILE/HENNE-SOM.REVISION.1.PDF

Hinshaw, J. E., & Schmid, S. L. (1995). Dynamin self-assembles into rings suggesting a mechanism for coated vesicle budding. *Nature 1995 374:6518*, *374*(6518), 190–192. https://doi.org/10.1038/374190a0

Hintz, K. A., Rassias, A. J., Wardwell, K., Moss, M. L., Morganelli, P. M., Pioli, P. A., Givan, A. L., Wallace, P. K., Yeager, M. P., & Guyre, P. M. (2002). Endotoxin induces rapid metalloproteinase-mediated shedding followed by up-regulation of the monocyte hemoglobin scavenger receptor CD163. *Journal of Leukocyte Biology*, *72*(4), 711–717. https://doi.org/10.1189/JLB.72.4.711

Hohenester, E., Sasaki, T., & Timpl, R. (1999). Crystal structure of a scavenger receptor cysteine-rich domain sheds light on an ancient superfamily. *Nature Structural Biology 1999 6:3*, *6*(3), 228–232. https://doi.org/10.1038/6669

Hsieh, F. L., Turner, L., Bolla, J. R., Robinson, C. V., Lavstsen, T., & Higgins, M. K. (2016). The structural basis for CD36 binding by the malaria parasite. *Nature Communications 2016 7:1*, *7*(1), 1–11. https://doi.org/10.1038/ncomms12837

Huang, F., Khvorova, A., Marshall, W., & Sorkin, A. (2004). Analysis of Clathrin-mediated Endocytosis of Epidermal Growth Factor Receptor by RNA Interference. *Journal of Biological Chemistry*, *279*(16), 16657–16661. https://doi.org/10.1074/jbc.C400046200

Hubbard, S. R. (2002). Protein tyrosine kinases: autoregulation and small-molecule inhibition. *Current Opinion in Structural Biology*, *12*(6), 735–741. https://doi.org/10.1016/S0959-440X(02)00383-4

Hvidberg, V., Maniecki, M. B., Jacobsen, C., Højrup, P., Møller, H. J., & Moestrup, S. K. (2005). Identification of the receptor scavenging hemopexin-heme complexes. *Blood*, *106*(7), 2572–2579. https://doi.org/10.1182/BLOOD-2005-03-1185

Jerabek-Willemsen, M., André, T., Wanner, R., Roth, H. M., Duhr, S., Baaske, P., & Breitsprecher, D. (2014). MicroScale Thermophoresis: Interaction analysis and beyond. *Journal of Molecular Structure*, *1077*, 101–113. https://doi.org/10.1016/J.MOLSTRUC.2014.03.009

Jumper, J., Evans, R., Pritzel, A., Green, T., Figurnov, M., Ronneberger, O., Tunyasuvunakool, K., Bates, R., Žídek, A., Potapenko, A., Bridgland, A., Meyer, C., Kohl, S. A. A., Ballard, A. J., Cowie, A., Romera-Paredes, B., Nikolov, S., Jain, R., Adler, J., … Hassabis, D. (2021). Highly accurate protein structure prediction with AlphaFold. *Nature*, *596*(7873), 583–589. https://doi.org/10.1038/s41586-021-03819-2

Kaksonen, M., & Roux, A. (2018). Mechanisms of clathrin-mediated endocytosis. *Nature Reviews Molecular Cell Biology 2018 19:5*, *19*(5), 313–326. https://doi.org/10.1038/nrm.2017.132

Kay, R. R. (2021). Macropinocytosis: Biology and mechanisms. *Cells & Development*, *168*, 203713. https://doi.org/10.1016/J.CDEV.2021.203713

Kelly, B. T., Graham, S. C., Liska, N., Dannhauser, P. N., Höning, S., Ungewickell, E. J., & Owen, D. J. (2014). AP2 controls clathrin polymerization with a membrane-activated switch. *Science*, *345*(6195), 459–463. https://doi.org/10.1126/SCIENCE.1254836/SUPPL_FILE/KELLY.SM.PDF

Kelly, B. T., McCoy, A. J., Späte, K., Miller, S. E., Evans, P. R., Höning, S., & Owen, D. J. (2008). A structural explanation for the binding of endocytic dileucine motifs by the AP2 complex. *Nature 2008 456:7224*, *456*(7224), 976–979. https://doi.org/10.1038/nature07422

Kerr, M. C., & Teasdale, R. D. (2009). Defining macropinocytosis. *Traffic*, *10*(4), 364–371. https://doi.org/10.1111/J.1600-0854.2009.00878.X

Kneidl, J., Löffler, B., Erat, M. C., Kalinka, J., Peters, G., Roth, J., & Barczyk, K. (2012). Soluble CD163 promotes recognition, phagocytosis and killing of Staphylococcus aureus via binding of specific fibronectin peptides. *Cellular Microbiology*, *14*(6), 914–936. https://doi.org/10.1111/J.1462-5822.2012.01766.X

Krissinel, E., & Henrick, K. (2007). Inference of Macromolecular Assemblies from Crystalline State. *Journal of Molecular Biology*, *372*(3), 774–797. https://doi.org/10.1016/J.JMB.2007.05.022

Kristiansen, M., Graversen, J. H., Jacobsen, C., Sonne, O., Hoffman, H. J., Law, S. K. A., & Moestrup, S. K. (2001). Identification of the haemoglobin scavenger receptor. *Nature 2001 409:6817*, *409*(6817), 198–201. https://doi.org/10.1038/35051594

Kumar, S., & Bandyopadhyay, U. (2005). Free heme toxicity and its detoxification systems in human. *Toxicology Letters*, *157*(3), 175–188. https://doi.org/10.1016/J.TOXLET.2005.03.004

Lane-Serff, H., MacGregor, P., Lowe, E. D., Carrington, M., & Higgins, M. K. (2014). Structural basis for ligand and innate immunity factor uptake by the trypanosome haptoglobin-haemoglobin receptor. *ELife*, *3*, e05553. https://doi.org/10.7554/ELIFE.05553

Law, S. K. A., Micklem, K. J., Shaw, J. M., Zhang, X. -P, Dong, Y., Willis, A. C., & Mason, D. Y. (1993). A new macrophage differentiation antigen which is a member of the scavenger receptor superfamily. *European Journal of Immunology*, *23*(9), 2320–2325. https://doi.org/10.1002/EJI.1830230940

Levy, A. P., Asleh, R., Blum, S., Levy, N. S., Miller-Lotan, R., Kalet-Litman, S., Anbinder, Y., Lache, O., Nakhoul, F. M., Asaf, R., Farbstein, D., Pollak, M., Soloveichik, Y. Z., Strauss, M., Alshiek, J., Livshits, A., Schwartz, A., Awad, H., Jad, K., & Goldenstein, H. (2009). Haptoglobin: Basic and Clinical Aspects.

*Https://Home.Liebertpub.Com/Ars*, *12*(2), 293–304. https://doi.org/10.1089/ARS.2009.2793

Lewis, W. H. (1937). Pinocytosis by Malignant Cells. *The American Journal of Cancer*, *29*(4), 666–679. https://doi.org/10.1158/AJC.1937.666

Li, R., Ma, H., Jiang, L., Qiao, S., Zhi, Y., Huang, M., Deng, R., & Zhang, G. (2018). The CD163 long-range scavenger receptor cysteine-rich repeat: expression, purification and X-ray crystallographic characterization. *Acta Crystallographica. Section F, Structural Biology Communications*, *74*(Pt 5), 322. https://doi.org/10.1107/S2053230X18005551

Li, X., Mooney, P., Zheng, S., Booth, C. R., Braunfeld, M. B., Gubbens, S., Agard, D. A., & Cheng, Y. (2013). Electron counting and beam-induced motion correction enable near-atomic-resolution single-particle cryo-EM. *Nature Methods 2013 10:6*, *10*(6), 584–590. https://doi.org/10.1038/nmeth.2472

Madsen, M., Møller, H. J., Nielsen, M. J., Jacobsen, C., Graversen, J. H., van den Berg, T., & Moestrup, S. K. (2004). Molecular Characterization of the Haptoglobin·Hemoglobin Receptor CD163. *Journal of Biological Chemistry*, *279*(49), 51561–51567. https://doi.org/10.1074/jbc.m409629200

McMahon, H. T., & Boucrot, E. (2011). Molecular mechanism and physiological functions of clathrin-mediated endocytosis. *Nature Reviews Molecular Cell Biology 2011 12:8*, *12*(8), 517–533. https://doi.org/10.1038/nrm3151

Meng, E. C., Goddard, T. D., Pettersen, E. F., Couch, G. S., Pearson, Z. J., Morris, J. H., & Ferrin, T. E. (2023). UCSF ChimeraX: Tools for structure building and analysis. *Protein Science*, *32*(11), e4792. https://doi.org/10.1002/PRO.4792

Moeller, J. B., Nielsen, M. J., Reichhardt, M. P., Schlosser, A., Sorensen, G. L., Nielsen, O., Tornøe, I., Grønlund, J., Nielsen, M. E., Jørgensen, J. S., Jensen, O. N., Mollenhauer, J., Moestrup, S. K., & Holmskov, U. (2012). CD163-L1 Is an Endocytic Macrophage Protein Strongly Regulated by Mediators in the Inflammatory Response. *The Journal of Immunology*, *188*(5), 2399–2409. https://doi.org/10.4049/JIMMUNOL.1103150

Møller, H. J., Holger, J. M., & Ller, H. J. M. Ø. (2012). Soluble CD163. *Scandinavian Journal of Clinical and Laboratory Investigation*, *72*(1), 1–13. https://doi.org/10.3109/00365513.2011.626868

Moreno, J. A., Muñoz-García, B., Martín-Ventura, J. L., Madrigal-Matute, J., Orbe, J., Páramo, J. A., Ortega, L., Egido, J., & Blanco-Colio, L. M. (2009). The CD163-expressing macrophages recognize and internalize TWEAK: Potential consequences in atherosclerosis. *Atherosclerosis*, *207*(1), 103–110. https://doi.org/10.1016/J.ATHEROSCLEROSIS.2009.04.033

Motley, A., Bright, N. A., Seaman, M. N. J., & Robinson, M. S. (2003). Clathrin-mediated endocytosis in AP-2–depleted cells. *The Journal of Cell Biology*, *162*(5), 909. https://doi.org/10.1083/JCB.200305145

Motsa, B. B., & Stahelin, R. V. (2023). A beginner's guide to surface plasmon resonance. *The Biochemist*, *45*(1), 18–22. https://doi.org/10.1042/BIO_2022_139

Nagata, S. (2018). Apoptosis and Clearance of Apoptotic Cells. *Annual Review of Immunology*, *36*(Volume 36, 2018), 489–517. https://doi.org/10.1146/ANNUREV-IMMUNOL-042617-053010/CITE/REFWORKS

Nathues, C., Zimmerli, U., Hauser, R., Nathues, H., Grosse Beilage, E., & Schüpbach-Regula, G. (2014). Risk Assessment of the Introduction of Porcine Reproductive and Respiratory Syndrome Virus via Boar Semen into Switzerland as an Example of a PRRSV-Free Country. *Transboundary and Emerging Diseases*, *61*(6), 546–554. https://doi.org/10.1111/TBED.12059

Neculai, D., Schwake, M., Ravichandran, M., Zunke, F., Collins, R. F., Peters, J., Neculai, M., Plumb, J., Loppnau, P., Pizarro, J. C., Seitova, A., Trimble, W. S., Saftig, P., Grinstein, S., & Dhe-Paganon, S. (2013). Structure of LIMP-2 provides functional insights with implications for SR-BI and CD36. *Nature 2013 504:7478*, *504*(7478), 172–176. https://doi.org/10.1038/nature12684

Neumann, E. J., Kliebenstein, J. B., Johnson, C. D., Mabry, J. W., Bush, E. J., Seitzinger, A. H., Green, A. L., & Zimmerman, J. J. (2005). Assessment of the economic impact of porcine reproductive and respiratory syndrome on swine production in the United States. *Journal of the American Veterinary Medical Association*, *227*(3), 385–392. https://doi.org/10.2460/JAVMA.2005.227.385

Nguyen, H. H., Park, J., Kang, S., & Kim, M. (2015). Surface Plasmon Resonance: A Versatile Technique for Biosensor Applications. *Sensors 2015, Vol. 15, Pages 10481-10510*, *15*(5), 10481–10510. https://doi.org/10.3390/S150510481

Nielsen, M. J., Vang Petersen, S., Jacobsen, C., Thirup, S., Enghild, J. J., Heilskov Graversen, J., & Moestrup, S. K. (2006). A Unique Loop Extension in the Serine Protease Domain of Haptoglobin Is Essential for CD163 Recognition of the Haptoglobin-Hemoglobin Complex *. *Journal of Biological Chemistry*, *282*, 1072–1079. https://doi.org/10.1074/jbc.M605684200

Ojala, J. R. M., Pikkarainen, T., Tuuttila, A., Sandalova, T., & Tryggvason, K. (2007). Crystal structure of the cysteine-rich domain of scavenger receptor MARCO reveals the presence of a basic and an acidic cluster that both contribute to ligand recognition. *Journal of Biological Chemistry*, *282*(22), 16654–16666. https://doi.org/10.1074/jbc.M701750200

Owen, D. J., & Evans, P. R. (1998). A Structural Explanation for the Recognition of Tyrosine-Based Endocytotic Signals. *Science*, *282*(5392), 1327–1332. https://doi.org/10.1126/SCIENCE.282.5392.1327

Paige, S. B., Frost, S. D. W., Gibson, M. A., Jones, J. H., Shankar, A., Switzer, W. M., Ting, N., & Goldberg, T. L. (2014). Beyond Bushmeat: Animal Contact, Injury, and Zoonotic Disease Risk in Western Uganda. *EcoHealth*, *11*(4), 534–543. https://doi.org/10.1007/S10393-014-0942-Y/TABLES/1

Paoli, M., Anderson, B. F., Baker, H. M., Morgan, W. T., Smith, A., & Baker, E. N. (1999). Crystal structure of hemopexin reveals a novel high-affinity heme site formed between two β-propeller domains. *Nature Structural Biology 1999 6:10*, *6*(10), 926–931. https://doi.org/10.1038/13294

Perutz, M. F. (1970). Stereochemistry of Cooperative Effects in Haemoglobin: Haem–Haem Interaction and the Problem of Allostery. *Nature 1970 228:5273*, *228*(5273), 726–734. https://doi.org/10.1038/228726a0

Perutz, M. F., Bolton, W., Diamond, R., Muirhead, H., & Watson, H. C. (1964). Structure of Hæmoglobin : An X-ray Examination of Reduced Horse Hæmoglobin. *Nature 1964 203:4946*, *203*(4946), 687–690. https://doi.org/10.1038/203687a0

Peter, B. J., Kent, H. M., Mills, I. G., Vallis, Y., Butler, P. J. G., Evans, P. R., & McMahon, H. T. (2004). BAR Domains as Sensors of Membrane Curvature: The Amphiphysin BAR Structure. *Science*, *303*(5657), 495–499. https://doi.org/10.1126/SCIENCE.1092586/SUPPL_FILE/PETER.SOM.PDF

Ponka, P., & Lok, C. N. (1999). The transferrin receptor: role in health and disease. *The*

*International Journal of Biochemistry & Cell Biology*, *31*(10), 1111–1137. https://doi.org/10.1016/S1357-2725(99)00070-9

Porta, J. C., Han, B., Gulsevin, A., Chung, J. M., Peskova, Y., Connolly, S., McHaourab, H. S., Meiler, J., Karakas, E., Kenworthy, A. K., & Ohi, M. D. (2022). Molecular architecture of the human caveolin-1 complex. *Science Advances*, *8*(19), 7232. https://doi.org/10.1126/SCIADV.ABN7232/SUPPL_FILE/SCIADV.ABN7232_MOVIE_S1.ZIP

PrabhuDas, M., Bowdish, D., Drickamer, K., Febbraio, M., Herz, J., Kobzik, L., Krieger, M., Loike, J., Means, T. K., Moestrup, S. K., Post, S., Sawamura, T., Silverstein, S., Wang, X.-Y., & El Khoury, J. (2014). Standardizing Scavenger Receptor Nomenclature. *The Journal of Immunology*, *192*(5), 1997–2006. https://doi.org/10.4049/JIMMUNOL.1490003

Punjani, A., Rubinstein, J. L., Fleet, D. J., & Brubaker, M. A. (2017). cryoSPARC: algorithms for rapid unsupervised cryo-EM structure determination. *Nature Methods 2017 14:3*, *14*(3), 290–296. https://doi.org/10.1038/nmeth.4169

Punjani, A., Zhang, H., & Fleet, D. J. (2020). Non-uniform refinement: adaptive regularization improves single-particle cryo-EM reconstruction. *Nature Methods 2020 17:12*, *17*(12), 1214–1221. https://doi.org/10.1038/s41592-020-00990-8

Rabinovitch, M. (1995). Professional and non-professional phagocytes: an introduction. *Trends in Cell Biology*, *5*(3), 85–87. https://doi.org/10.1016/S0962-8924(00)88955-2

Ramachandran, G. N., Ramakrishnan, C., & Sasisekharan, V. (1963). Stereochemistry of polypeptide chain configurations. *Journal of Molecular Biology*, *7*(1), 95–99. https://doi.org/10.1016/S0022-2836(63)80023-6

Ratajczak, W., Atkinson, S. D., & Kelly, C. (2022). The TWEAK/Fn14/CD163 axis—implications for metabolic disease. *Reviews in Endocrine and Metabolic Disorders*, *23*(3), 449–462. https://doi.org/10.1007/S11154-021-09688-4/FIGURES/3

Reichhardt, M. P., Loimaranta, V., Lea, S. M., & Johnson, S. (2020). *Structures of SALSA/DMBT1 SRCR domains reveal the conserved ligand binding mechanism of the ancient SRCR fold*. https://doi.org/10.26508/lsa.201900502

Ringstad, N., Gad, H., Löw, P., Di Paolo, G., Brodin, L., Shupliakov, O., & De Camilli, P. (1999). Endophilin/sh3p4 is required for the transition from early to late stages in

clathrin-mediated synaptic vesicle endocytosis. *Neuron*, *24*(1), 143–154. https://doi.org/10.1016/S0896-6273(00)80828-4

Rossow, K. D. (1998). Porcine reproductive and respiratory syndrome. *Veterinary Pathology*, *35*(1), 1–20. https://doi.org/10.1177/030098589803500101

Rother, R. P., Bell, L., Hillmen, P., & Gladwin, M. T. (2005). The Clinical Sequelae of Intravascular Hemolysis and Extracellular Plasma Hemoglobin: A Novel Mechanism of Human Disease. *JAMA*, *293*(13), 1653–1662. https://doi.org/10.1001/JAMA.293.13.1653

Rudenko, G., Henry, L., Henderson, K., Ichtchenko, K., Brown, M. S., Goldstein, J. L., & Deisenhofer, J. (2002). Structure of the LDL Receptor Extracellular Domain at Endosomal pH. *Science*, *298*(5602), 2353–2358. https://doi.org/10.1126/SCIENCE.1078124

Sanchez-Garcia, R., Gomez-Blanco, J., Cuervo, A., Carazo, J. M., Sorzano, C. O. S., & Vargas, J. (2021). DeepEMhancer: a deep learning solution for cryo-EM volume post-processing. *Communications Biology 2021 4:1*, *4*(1), 1–8. https://doi.org/10.1038/s42003-021-02399-1

Sarrias, M. R., Farnós, M., Mota, R., Sánchez-Barbero, F., Ibáñez, A., Gimferrer, I., Vera, J., Fenutría, R., Casals, C., Yélamos, J., & Lozano, F. (2007). CD6 binds to pathogen-associated molecular patterns and protects from LPS-induced septic shock. *Proceedings of the National Academy of Sciences*, *104*(28), 11724–11729. https://doi.org/10.1073/PNAS.0702815104

Schaer, C. A., Schoedon, G., Imhof, A., Kurrer, M. O., & Schaer, D. J. (2006). Constitutive endocytosis of CD163 mediates hemoglobin-heme uptake and determines the noninflammatory and protective transcriptional response of macrophages to hemoglobin. *Circulation Research*, *99*(9), 943–950. https://doi.org/10.1161/01.RES.0000247067.34173.1B/SUPPL_FILE/CIRCRES5831-SUPPL.PDF

Schaer, D. J., Schaer, C. A., Buehler, P. W., Boykins, R. A., Schoedon, G., Alayash, A. I., & Schaffner, A. (2006). CD163 is the macrophage scavenger receptor for native and chemically modified hemoglobins in the absence of haptoglobin. *Blood*, *107*(1), 373–380. https://doi.org/10.1182/BLOOD-2005-03-1014

Scheres, S. H. W., & Chen, S. (2012). Prevention of overfitting in cryo-EM structure determination. *Nature Methods 2012 9:9*, *9*(9), 853–854. https://doi.org/10.1038/nmeth.2115

Shaanan, B. (1983). Structure of human oxyhaemoglobin at 2·1resolution. *Journal of Molecular Biology*, *171*(1), 31–59. https://doi.org/10.1016/S0022-2836(83)80313-1

Shaw, T. M., Maloney, S. M., Nennig, K., Ramuta, M. D., Norton, A., Ibarra, R., Kuehnert, P., Brinton, M., Faaberg, K., Kuhn, J. H., O'Connor, D. H., Warren, C. J., & Bailey, A. L. (2023). Ectopic expression of murine CD163 enables cell-culture isolation of lactate dehydrogenase-elevating virus 63 years after its discovery. *Journal of Virology*, *97*(10). https://doi.org/10.1128/JVI.00930-23/SUPPL_FILE/JVI.00930-23-S0005.PDF

Sheikine, Y., & Sirsjö, A. (2008). CXCL16/SR-PSOX—A friend or a foe in atherosclerosis? *Atherosclerosis*, *197*(2), 487–495. https://doi.org/10.1016/J.ATHEROSCLEROSIS.2007.11.034

Shi, M., Lam, T. T. Y., Hon, C. C., Hui, R. K. H., Faaberg, K. S., Wennblom, T., Murtaugh, M. P., Stadejek, T., & Leung, F. C. C. (2010). Molecular epidemiology of PRRSV: A phylogenetic perspective. *Virus Research*, *154*(1–2), 7–17. https://doi.org/10.1016/J.VIRUSRES.2010.08.014

Sirotkin, V., Beltzner, C. C., Marchand, J. B., & Pollard, T. D. (2005). Interactions of WASp, myosin-I, and verprolin with Arp2/3 complex during actin patch assembly in fission yeast. *Journal of Cell Biology*, *170*(4), 637–648. https://doi.org/10.1083/JCB.200502053

Smith, A., & McCulloh, R. J. (2015). Hemopexin and haptoglobin: Allies against heme toxicity from hemoglobin not contenders. *Frontiers in Physiology*, *6*(JUN), 146258. https://doi.org/10.3389/FPHYS.2015.00187/BIBTEX

Smith, S. M., & Smith, C. J. (2022). Capturing the mechanics of clathrin-mediated endocytosis. *Current Opinion in Structural Biology*, *75*, 102427. https://doi.org/10.1016/J.SBI.2022.102427

Some, D., Amartely, H., Tsadok, A., & Lebendiker, M. (2019). Characterization of proteins by size-exclusion chromatography coupled to multi-angle light scattering (Sec-mals). *Journal of Visualized Experiments*. https://doi.org/10.3791/59615

Sonn-Segev, A., Belacic, K., Bodrug, T., Young, G., VanderLinden, R. T., Schulman, B. A., Schimpf, J., Friedrich, T., Dip, P. V., Schwartz, T. U., Bauer, B., Peters, J. M., Struwe, W. B., Benesch, J. L. P., Brown, N. G., Haselbach, D., & Kukura, P. (2020). Quantifying the heterogeneity of macromolecular machines by mass photometry. *Nature Communications 2020 11:1*, *11*(1), 1–10. https://doi.org/10.1038/s41467-020-15642-w

Sousa, R., Liao, H. S., Cuéllar, J., Jin, S., Valpuesta, J. M., Jin, A. J., & Lafer, E. M. (2016). Clathrin-coat disassembly illuminates the mechanisms of Hsp70 force generation. *Nature Structural & Molecular Biology 2016 23:9*, *23*(9), 821–829. https://doi.org/10.1038/nsmb.3272

Sun, Y., Martin, A. C., & Drubin, D. G. (2006). Endocytic Internalization in Budding Yeast Requires Coordinated Actin Nucleation and Myosin Motor Activity. *Developmental Cell*, *11*(1), 33–46. https://doi.org/10.1016/j.devcel.2006.05.008

Sweitzer, S. M., & Hinshaw, J. E. (1998). Dynamin undergoes a GTP-dependent conformational change causing vesiculation. *Cell*, *93*(6), 1021–1029. https://doi.org/10.1016/S0092-8674(00)81207-6

Takei, K., Slepnev, V. I., Haucke, V., & De Camilli, P. (1999). Functional partnership between amphiphysin and dynamin in clathrin-mediated endocytosis. *Nature Cell Biology 1999 1:1*, *1*(1), 33–39. https://doi.org/10.1038/9004

Tamara, S., Franc, V., & Heck, A. J. R. (2020). A wealth of genotype-specific proteoforms fine-tunes hemoglobin scavenging by haptoglobin. *Proceedings of the National Academy of Sciences of the United States of America*, *117*(27), 15554–15564. https://doi.org/10.1073/PNAS.2002483117/SUPPL_FILE/PNAS.2002483117.SAPP.PDF

Teitelbaum, S. L. (2000). Bone Resorption by Osteoclasts. *Science*, *289*(5484), 1504–1508. https://doi.org/10.1126/SCIENCE.289.5484.1504

Thomsen, J. H., Etzerodt, A., Svendsen, P., & Moestrup, S. K. (2013). The Haptoglobin-CD163-Heme Oxygenase-1 Pathway for Hemoglobin Scavenging. *Oxidative Medicine and Cellular Longevity*, *2013*(1), 523652. https://doi.org/10.1155/2013/523652

Thorne, R. E. (2020). Hypothesis for a mechanism of beam-induced motion in cryo-electron microscopy. *IUCrJ*, *7*(3), 416–421.

https://doi.org/10.1107/S2052252520002560/UA5002SUP1.PDF

Tolosano, E., & Altruda, F. (2002). Hemopexin: Structure, function, and regulation. *DNA and Cell Biology*, *21*(4), 297–306. https://doi.org/10.1089/104454902753759717

Traub, L. M. (2009). Tickets to ride: selecting cargo for clathrin-regulated internalization. *Nature Reviews Molecular Cell Biology 2009 10:9*, *10*(9), 583–596. https://doi.org/10.1038/nrm2751

Ungewickell, E., Ungewickell, H., Holstein, S. E. H., Lindner, R., Prasad, K., Barouch, W., Martini, B., Greene, L. E., & Eisenberg, E. (1995). Role of auxilin in uncoating clathrin-coated vesicles. *Nature 1995 378:6557*, *378*(6557), 632–635. https://doi.org/10.1038/378632a0

Van Gorp, H., Van Breedam, W., Van Doorsselaere, J., Delputte, P. L., & Nauwynck, H. J. (2010). Identification of the CD163 Protein Domains Involved in Infection of the Porcine Reproductive and Respiratory Syndrome Virus. *Journal of Virology*, *84*(6), 3101–3105. https://doi.org/10.1128/JVI.02093-09/SUPPL_FILE/REV_SUPPL_MAT.DOC

Vanderheijden, N., Delputte, P. L., Favoreel, H. W., Vandekerckhove, J., Van Damme, J., van Woensel, P. A., & Nauwynck, H. J. (2003). Involvement of sialoadhesin in entry of porcine reproductive and respiratory syndrome virus into porcine alveolar macrophages. *Journal of Virology*, *77*(15), 8207–8215. https://doi.org/10.1128/JVI.77.15.8207-8215.2003

Vera, J., Fenutria, R., Cañadas, O., Figueras, M., Mota, R., Sarrias, M. R., Williams, D. L., Casals, C., Yelamos, J., & Lozano, F. (2009). The CD5 ectodomain interacts with conserved fungal cell wall components and protects from zymosan-induced septic shock-like syndrome. *Proceedings of the National Academy of Sciences of the United States of America*, *106*(5), 1506–1511. https://doi.org/10.1073/PNAS.0805846106/SUPPL_FILE/0805846106SI.PDF

Vinothkumar, K. R., & Henderson, R. (2016). *Single particle electron cryomicroscopy: trends, issues and future perspective*. https://doi.org/10.1017/S0033583516000068

Wahl-Jensen, V., Johnson, J. C., Lauck, M., Weinfurter, J. T., Moncla, L. H., Weiler, A. M., Charlier, O., Rojas, O., Byrum, R., Ragland, D. R., Huzella, L., Zommer, E., Cohen, M., Bernbaum, J. G., Caì, Y., Sanford, H. B., Mazur, S., Johnson, R. F., Qin, J., …

Kuhn, J. H. (2016). Divergent simian arteriviruses cause simian hemorrhagic fever of differing severities in macaques. *MBio*, *7*(1). https://doi.org/10.1128/MBIO.02009-15/ASSET/40E4D707-63E3-4162-A087-8ECAA2D69CD1/ASSETS/GRAPHIC/MBO0011626910006.JPEG

Wang, H., Shen, L., Chen, J., Liu, X., Tan, T., Hu, Y., Bai, X., Li, Y., Tian, K., Li, N., & Hu, X. (2019). Deletion of CD163 Exon 7 Confers Resistance to Highly Pathogenic Porcine Reproductive and Respiratory Viruses on Pigs. *International Journal of Biological Sciences*, *15*(9), 1993. https://doi.org/10.7150/IJBS.34269

Warren, C. J., Yu, S., Peters, D. K., Barbachano-Guerrero, A., Yang, Q., Burris, B. L., Worwa, G., Huang, I. C., Wilkerson, G. K., Goldberg, T. L., Kuhn, J. H., & Sawyer, S. L. (2022). Primate hemorrhagic fever-causing arteriviruses are poised for spillover to humans. *Cell*, *185*(21), 3980-3991.e18. https://doi.org/10.1016/J.CELL.2022.09.022

Weaver, L. K., Hintz-Goldstein, K. A., Pioli, P. A., Wardwell, K., Qureshi, N., Vogel, S. N., & Guyre, P. M. (2006). Pivotal Advance: Activation of cell surface Toll-like receptors causes shedding of the hemoglobin scavenger receptor CD163. *Journal of Leukocyte Biology*, *80*(1), 26–35. https://doi.org/10.1189/JLB.1205756

Wicher, K. B., & Fries, E. (2004). Prohaptoglobin is proteolytically in the endoplasmic reticulum by the complement C1r-like protein. *Proceedings of the National Academy of Sciences of the United States of America*, *101*(40), 14390–14395. https://doi.org/10.1073/PNAS.0405692101/ASSET/AE4BA907-74AD-47CB-A071-01AA257EE1D9/ASSETS/GRAPHIC/ZPQ0400461160006.JPEG

Yang, H., Zhang, J., Zhang, X., Shi, J., Pan, Y., Zhou, R., Li, G., Li, Z., Cai, G., & Wu, Z. (2018). CD163 knockout pigs are fully resistant to highly pathogenic porcine reproductive and respiratory syndrome virus. *Antiviral Research*, *151*, 63–70. https://doi.org/10.1016/J.ANTIVIRAL.2018.01.004

Young, G., Hundt, N., Cole, D., Fineberg, A., Andrecka, J., Tyler, A., Olerinyova, A., Ansari, A., Marklund, E. G., Collier, M. P., Chandler, S. A., Tkachenko, O., Allen, J., Crispin, M., Billington, N., Takagi, Y., Sellers, J. R., Eichmann, C., Selenko, P., … Kukura, P. (2018). Quantitative mass imaging of single biological macromolecules. *Science*, *360*(6387), 423–427. https://doi.org/10.1126/SCIENCE.AAR5839/SUPPL_FILE/AAR5839S4.MOV

Zivanov, J., Nakane, T., Forsberg, B. O., Kimanius, D., Hagen, W. J. H., Lindahl, E., & Scheres, S. H. W. (2018). New tools for automated high-resolution cryo-EM structure determination in RELION-3. *ELife*, *7*. https://doi.org/10.7554/ELIFE.42166

Zivanov, J., Nakane, T., & Scheres, S. H. W. (2019). A Bayesian approach to beam-induced motion correction in cryo-EM single-particle analysis. *Urn:Issn:2052-2525*, *6*(1), 5–17. https://doi.org/10.1107/S205225251801463X

# Appendix: Constructs and primers

Table 9: All expression constructs used in this dissertation and the primers used to clone them. Forward and reverse primer sequence are denoted in the upper and lower cell, respectively. Letters in red indicate mutations.

| Construct | Plasmid | PCR template | 5' to 3' primer sequence |
|---|---|---|---|
| CD163ecto | pHLsec | Synthetic gene of CD163ecto | CTCCGGAAGGCTGGAAGTG |
| | | | CCTTTGTCCTGTGGCTCC |
| CD163fl-GFP fusion – fragment 1 | pHLsec | Synthetic gene of CD163ecto | GATGGGTTGCGTAGCTGAAACCG GTGGCACCGACAAAGAACTGAG AC |
| | | | ACTAGACTGTCTGCTGCTTCTGC |
| CD163fl-GFP fusion – fragment 2 | | Synthetic gene of CD163-C-terminus-GFP fusion | AGGCAGAAGCAGCAGACAGT |
| | | | GATGGTGATGGTGGTGCTTGG |
| CD163ecto with Avi-tag | pHLsec | Ectodomain of CD163 in pHLsec | CCCAGAAGATCGAGTGGCACGA GGGCGCCGCCGAGCC |
| | | | CCTCGAAGATGTCGTTCAGGCCA CTAGACTGTCTGCTGCTTCTGCCT G |
| CD163-R809T – fragment 1 | pHLsec | Synthetic gene of CD163ecto | GATGGGTTGCGTAGCTGAAACCG GTGGCACCGACAAAGAACTGAG AC |
| | | | CCAGCATCCTCTTTGTG GGTGCAATTCTGCTGT |
| CD163-R809T – fragment 2 | | CD163flGFP in pHLsec OR CD163ectoAvi-tag in pHLsec | ACAGCAGAATTGCACC CACAAAGAGGATGCTGG |
| | | | GATGGTGATGGTGGTGCTTGG |

| Construct | Plasmid | PCR template | 5’ to 3’ primer sequence |
|---|---|---|---|
| CD163-284NGT – fragment 1 | pHLsec | Synthetic gene of CD163ecto | GATGGGTTGCGTAGCTGAAACCGGT GGCACCGACAAAGAACTGAGAC |
| | | | GGTGCCCCAGGTGCCGTT GAAGCGCAC |
| CD163-284NGT – fragment 2 | | CD163flGFP in pHLsec OR CD163ectoAvi-tag in pHLsec | GTGCGCTTCAACGGCACC TGGGGCACC |
| | | | GATGGTGATGGTGGTGCTTGG |
| CD163-G351W – fragment 1 | pHLsec | Synthetic gene of CD163ecto | GATGGGTTGCGTAGCTGAAACCGGT GGCACCGACAAAGAACTGAGAC |
| | | | CAGTAGTGTTTCCACCACTCGTGG |
| CD163-G351W – fragment 2 | | CD163flGFP in pHLsec OR CD163ectoAvi-tag in pHLsec | CCACGAGTGGTGGAAACACTACTG |
| | | | GATGGTGATGGTGGTGCTTGG |
| Full-length CD163WT, R809T, 284NGT, G351W fused to GFP | pcDNA5/FRT | Corresponding CD163ecto in pHLsec | GTGGGAGGTCTATATAAGCAGAGCT CTCCTGGGCAACGTGCTG |
| | | | AGTGGATCCTTAATTAATGGCGCG CCAGCCTGCACCTGAGGAGT |